Copy
RM L54C29

RESEARCH MEMORANDUM

WIND-TUNNEL INVESTIGATION AT HIGH SUBSONIC SPEEDS OF THE STABILITY CHARACTERISTICS OF A COMPLETE MODEL HAVING SWEPTBACK-, M-, W-, AND CRANKED-WING PLAN FORMS AND SEVERAL HORIZONTAL-TAIL LOCATIONS

By Kenneth W. Goodson and Robert E. Becht

Langley Aeronautical Laboratory
Langley Field, Va.

NATIONAL ADVISORY COMMITTEE
FOR AERONAUTICS

WASHINGTON

May 14, 1954

NACA RM L54C29

NATIONAL ADVISORY COMMITTEE FOR AERONAUTICS

RESEARCH MEMORANDUM

WIND-TUNNEL INVESTIGATION AT HIGH SUBSONIC SPEEDS OF THE STABILITY CHARACTERISTICS OF A COMPLETE MODEL HAVING SWEPTBACK-, M-, W-, AND CRANKED-WING PLAN FORMS AND SEVERAL HORIZONTAL-TAIL LOCATIONS

By Kenneth W. Goodson and Robert E. Becht

SUMMARY

An investigation was made at high subsonic speeds of a complete model having a basic sweptback wing or one of three composite plan-form wings. The composite plan-form wings (M, W, and cranked) were obtained through modifications to the basic 45° swept-wing design. All wings were of aspect ratio 4.0 and taper ratio 0.3. These wings were tested through an angle-of-attack range in the Langley high-speed 7- by 10-foot tunnel at Mach numbers from 0.80 to 0.92.

The data show that all the composite plan forms alleviated the tendency toward longitudinal instability at moderate and high lift coefficients that existed for the basic swept-wing model. Of the wings investigated, the M plan form appeared to have the most desirable stability characteristics over the Mach number range tested and to allow the greatest latitude in selection of horizontal-tail position. For the tail length investigated, longitudinal instability existed at high lift coefficients for each of the wings with the horizontal tail in the highest position (0.57 semispan above wing-chord plane). The center tail (on wing chord plane) appeared to reduce the severity of the instability. Addition of a 10-percent-mean-aerodynamic-chord slat to the outboard 35 percent of the basic swept-wing semispan also appeared to improve the stability.

Positive tail-off directional stability was obtained with the model having the M-wing at high lift coefficients for all Mach numbers except 0.92; whereas negative tail-off stability was obtained with the swept wing at all lift coefficients and Mach numbers investigated. The vertical-tail contribution to directional stability decreased with increasing lift coefficients up to a Mach number of 0.90 for the M-wing model but was essentially constant for the swept-wing model through the Mach number range tested.

INTRODUCTION

The use of thin swept wings to improve the high-speed-performance characteristics of airplanes has resulted in abrupt reductions in longitudinal stability that have been described as "pitch-up." Results of an intensive study of means for alleviating the pitch-up tendency on configurations having a 45° sweptback wing of aspect ratio 4.0 and taper ratio 0.3 have been reported in references 1 to 4. Of the various wing modifications and tail positions previously studied, it appeared that satisfactory high-lift stability (particularly at Mach numbers near 0.9) could be obtained only by combining one of the most effective leading-edge modifications with a tail position well below the wing-chord plane. The present investigation was undertaken to determine conditions under which satisfactory stability might be obtained when the basic swept-wing plan form is modified by more extreme measures than those considered in references 1 to 4. The modifications to the basic swept wing were made by shearing the airfoil sections to form composite wing plan forms described as the M-, W-, and cranked types. Longitudinal characteristics were determined for a model equipped with each of these wings (including the basic sweptback wing) and with the horizontal-tail located at various heights. Some lateral stability characteristics were determined for two of these wings.

COEFFICIENTS AND SYMBOLS

All data are presented about the stability axes as shown in figure 1. The pitching-moment coefficients are referred to the quarter-chord of the mean aerodynamic chord, except where otherwise noted.

C_L lift coefficient, $\frac{\text{Lift}}{qS}$

C_D drag coefficient, $\frac{\text{Drag}}{qS}$

C_m pitching-moment coefficient, $\frac{\text{Pitching moment}}{qS\bar{c}}$

C_l rolling-moment coefficient, $\frac{\text{Rolling moment}}{qSb}$

C_n yawing-moment coefficient, $\frac{\text{Yawing moment}}{qSb}$

[redacted]

C_Y	lateral-force coefficient, $\frac{\text{Lateral force}}{qS}$
L/D	lift-drag ratio
q	dynamic pressure, $\rho V^2/2$, lb/sq ft
ρ	mass density of air, slugs/cu ft
V	free-stream velocity, fps
M	Mach number
S	wing area, 2.250 sq ft
c	local chord parallel to plane of symmetry, ft
$\bar{c}$	wing mean aerodynamic chord, $\frac{2}{S}\int_0^{b/2} c^2 dy$, 0.822 ft
$\bar{c}_H$	horizontal-tail mean aerodynamic chord, 0.338 ft
$\bar{c}_V$	vertical-tail mean aerodynamic chord, 0.757 ft
b	wing span, 3.000 ft
y	spanwise distance from plane of symmetry, ft
z	horizontal tail height from fuselage center line, positive upward, ft
α	angle of attack, deg
β	angle of sideslip, deg

Subscript:

β	denotes partial derivative of a coefficient with respect to sideslip angle; for example, $C_{l_\beta} = \frac{\partial C_l}{\partial \beta}$

[redacted]

MODEL AND APPARATUS

A three-view drawing of the complete research model with the basic 45° sweptback wing of aspect ratio 4.0 and taper ratio 0.3 is shown in figure 2(a). The composite wing plan forms (fig. 2(b)) were designed by shearing the basic 45° swept wing in a chordwise direction while holding the aspect ratio and taper ratio constant. The swept wing was constructed of solid aluminum whereas the composite wings were made of fiber-glass—plastic composition over steel spars. A sketch of the vertical locations of the horizontal tail is shown in figure 2(c). The construction of the tail assembly limited the incidence of the horizontal tail to zero degrees for all tail heights. The dimensions of the fuselage, which had a fineness ratio of 10.94, are presented in figure 2(d). A photograph of the complete model with the M-wing plan form mounted on the sting in the Langley high-speed 7- by 10-foot tunnel is shown in figure 3.

For some tests the outboard 35 percent of the swept-wing semispan was fitted with a leading-edge slat (auxiliary airfoil). (See fig. 4). This particular slat configuration was used as an expedient device for determining the general effects of leading-edge slats or auxiliary airfoils.

TESTS

The sting-supported model was tested in the Langley high-speed 7- by 10-foot tunnel through a Mach number range of 0.80 to 0.92 and through an angle-of-attack range that varied with loading conditions (the maximum range being about -2° to 24°). The lateral parameters were determined by pitching the model through the angle-of-attack range at sideslip angles of ±4°. The Reynolds number (based on the mean aerodynamic chord) varied with Mach number from about 2.5×10^6 to 3.0×10^6. Note that the horizontal tail was removed for the tail-off pitch tests and that both the horizontal and vertical tails were removed for the lateral-stability tail-off tests.

CORRECTIONS

Blockage corrections were applied to the results by the method of reference 5. Jet-boundary corrections to the angle of attack and drag were applied in accordance with reference 6. Corrections for the longitudinal pressure gradient have been applied to the data.

[redacted]

Model support tares have not been applied except for a fuselage base pressure correction to the drag. The corrected drag data represent a condition of free-stream static pressure at the fuselage base. From past experience, it is expected that the influence of the sting support on the model characteristics is negligible with regard to lift and pitching moment.

The angle of attack and angle of sideslip have been corrected for deflection of the balance and sting support. No attempt has been made to correct the data for aeroelastic distortion of the model.

PRESENTATION OF RESULTS

The results of the investigation are presented in the figures listed as follows:

DISCUSSION

Longitudinal Characteristics

Effect of wing plan form and tail height.- Characteristics of the fuselage alone are compared in figure 5 with characteristics of the swept-wing—fuselage combination. These results show that the nonlinearities of the wing-fuselage pitching-moment curves apparently result from the wing-alone characteristics or possibly from interference effects.

[redacted]

The tail-off data presented in figures 6 to 9 show that the tail-off stability near $\alpha = 0^\circ$ varies considerably for the different wing plan forms in spite of the fact that the quarter-chord point of the mean aerodynamic chord was held at essentially the same fuselage station for all wings. This is illustrated by the results of the following table which compares values of $\left(\frac{\partial C_m}{\partial \alpha}\right)_{\alpha=0}$ for the fuselage-alone configuration and the wing-fuselage configurations:

Configuration	$\left(\frac{\partial C_m}{\partial \alpha}\right)_{\alpha=0}$ at M = 0.80
Fuselage alone	0.0070
Swept wing and fuselage	-.0041
M-wing and fuselage	.0114
W-wing and fuselage	-.0009
Cranked wing and fuselage	.0055

Although the angle-of-attack range that could be obtained during the tail-on tests was somewhat limited (particularly when the tail was in the low position), it is believed that most of the important characteristics of the various complete-model configurations are shown by the test data obtained. In order to provide a reasonable basis for comparing shapes of the pitching-moment curves, some of the data obtained at Mach numbers of 0.80 and 0.90 have been recomputed with the assumed position of the center of gravity adjusted to give a static margin of $0.05\bar{c}$ at a Mach number of 0.80 for each configuration. Results for tail-off, center-tail, and high-tail configurations are shown in figure 10. The tail-off results show that although any of the composite wings provide improved characteristics over those of the swept wing at a Mach number of 0.80, only the M-type composite wing provided a substantial improvement at M = 0.90. With the center-tail position, a tendency toward pitch-up is indicated for the swept and cranked wings at lift coefficients of from 0.4 to 0.6, but there appears to be no such tendency for the M- and W-wings. With the tail in the high position, a pitch-up existed for any of the wings tested where sufficiently high angles of attack were reached. Such a condition is indicated at M = 0.80; however, at M = 0.90, pitch-up occurred only for the swept wing within the limited angle-of-attack range that could be obtained.

It should be pointed out that the degree of pitch-up for the tail-on configurations might have been somewhat different if the incidence of the horizontal tail had been set for trim in the high angle-of-attack range

[redacted]

rather than the arbitrary value of zero degrees tested. The pitch-up might be less abrupt for the trimmed condition because of loss in tail effectiveness at the higher angles of attack caused by possible reduction in dynamic pressure at the tail.

Values of the pitching-moment-curve slope $\frac{\partial C_m}{\partial C_L}$ of the various tail-on and tail-off configurations are presented in figure 11 for the zero-lift condition. It is of interest to note that over the test Mach number range, the rearward shift in aerodynamic center for the various tail-on configurations generally is about the same as or less than the shift with tail off. The increment of pitching-moment-curve slope near $C_L = 0$ due to addition of the tail is plotted against tail height in figure 12. Although wing plan form apparently has quite an appreciable effect on the tail contribution to the pitching moment, the greatest tail contribution invariably is obtained with the highest tail.

The untrimmed lift-drag ratios of the various wing-fuselage combinations are compared at Mach numbers of 0.80 and 0.90 in figure 13. At either Mach number, the L/D values for the W-wing are considerably lower than those of the other wings - mainly because of high values of drag due to lift. These trends were indicated for another W-wing configuration at low Mach numbers above lift coefficients of about 0.4. (See ref 7.) The cranked wing also shows considerable reduction in L/D at M = 0.90. Values of L/D for the M-wing compare favorably with the values for the swept wing at both of the selected Mach numbers; in fact, at lift coefficients below that for $(L/D)_{max}$, the M-wing is superior to the swept wing. This results in part from the higher lift-curve slopes for the M-wing at low lift coefficients; for example:

Configuration	C_{L_α} at -	
	M = 0.80	M = 0.90
Swept wing	0.067	0.076
M-wing	.074	.090

The drag data presented in figures 5 to 9 indicate, in general, that the minimum drag of the composite-wing configurations is slightly higher than that of the basic swept-wing configuration, with the greatest difference indicated at the highest test Mach number.

[redacted]

Swept wing with leading-edge slat.- The effect of adding a $0.10\bar{c}$ slat (fig. 4) to the outboard 35 percent of the swept-wing semispan is shown in figure 14. Also shown for comparison are results from tail-off tests of a somewhat similar model (ref. 4) with one of the better drooped-leading-edge chord-extension configurations along with the clean undrooped wing configuration. For the configuration of reference 4, the entire wing leading edge, including a $0.10\bar{c}$ chord-extension located on the outboard 35 percent of the semispan, was drooped 6°. The pitching-moment curves of the tail-off configuration with slats appear to be somewhat more linear than those of the basic swept wing or the swept wing with drooped leading edge and chord-extensions. With a horizontal tail located in the center position, addition of the slat generally made the variation of pitching moment with angle of attack more linear, except at a Mach number of 0.92.

Addition of the slat to the swept wing increased the lift coefficient at the higher angles of attack and also reduced the drag due to lift; however, the maximum L/D was not appreciably affected by addition of the slat. The drooped-nose chord-extension configuration of reference 4 showed a considerable reduction in drag due to lift and an appreciable increase in L/D values, probably because of the improved flow over the wing associated with the leading-edge droop. The effect of drooping the nose-slat configuration was not investigated. The slat generally increased the minimum drag at all Mach numbers tested.

Lateral Characteristics

Lateral stability characteristics of the model with the swept and M plan forms are shown in figures 15 and 16, respectively, for several tail configurations. Both the horizontal and vertical tails were removed for the tail-off configuration.

Positive tail-off directional stability was obtained with the model having the M-wing at high lift coefficients for all Mach numbers except 0.92, whereas negative tail-off stability was obtained with the swept wing at all lift coefficients and Mach numbers investigated. The positive tail-off values of directional stability obtained with the M-wing plan form increase with increasing negative values of C_{Y_β}. (See fig. 16.)

The contribution of the vertical tail to the directional stability of the M-wing model decreased with increasing lift coefficient up to a Mach number of 0.90, but became essentially constant at $M = 0.92$. Contrary to this, however, the tail contribution to the directional stability of the swept wing model was essentially constant at all lift coefficients for the lower Mach numbers, but showed an increase at high lifts at Mach numbers of 0.90 and 0.92. The vertical-tail contribution

to directional stability of the model with either wing plan form and with the high horizontal tail was considerably larger than that obtained with the horizontal tail in the center position.

A reduction of effective dihedral at intermediate and high lift coefficients was noted at all test Mach numbers for the complete swept-wing model. With the M-wing, the effective dihedral was not as great as with the swept wing.

CONCLUSIONS

An investigation at high subsonic speeds of a complete model having a sweptback wing and various composite plan-form wings (including M, W, and cranked plan forms) indicates the following conclusions:

1. All of the composite plan forms alleviated the tendency toward longitudinal instability at moderate and high lift coefficients that generally existed for the basic swept-wing model. Of the wings investigated, the M-wing appeared to have the most desirable stability characteristics over the test range of Mach numbers (0.80 to 0.92) and also to allow the greatest latitude for selection of horizontal-tail position.

2. For the one tail length investigated, and for the highest horizontal-tail position (0.57 semispan above wing-chord plane), longitudinal instability occurred at intermediate lift coefficients for each of the wings, whereas the center tail (on wing chord plane) appeared to alleviate the severity of the stability reduction in the angle-of-attack range investigated.

3. Over the test range of Mach number, the lift-drag ratios of the M-wing were almost the same as those of the swept wing; however, each of the other composite wings showed inferior drag characteristics at a Mach number of 0.90.

4. Addition of a fixed leading-edge slat to the outboard 35 percent of the basic swept-wing semispan appeared to provide a somewhat larger stability improvement than devices reported on previously; however, the slat investigated did not improve the maximum lift-drag ratio of the basic wing.

5. Positive tail-off directional stability was obtained with the model having the M-wing at high lift coefficients for all Mach numbers except 0.92; whereas negative tail-off stability was obtained with the swept wing at all lift coefficients and Mach numbers investigated.

[redacted]

The vertical-tail contribution to directional stability decreased with increasing lift coefficient up to a Mach number of 0.90 for the M-wing model but remained essentially constant for the swept-wing model.

Langley Aeronautical Laboratory,
National Advisory Committee for Aeronautics,
Langley Field, Va., March 17, 1954.

REFERENCES

1. Goodson, Kenneth W., and Few, Albert G., Jr.: Effect of Leading-Edge Chord-Extensions on Subsonic and Transonic Aerodynamic Characteristics of Three Models Having 45° Sweptback Wings of Aspect Ratio 4. NACA RM L52K21, 1953.

2. Weil, Joseph, and Morrison, William D., Jr.: A Study of the Use of Leading-Edge Notches as a Means for Improving the Low-Speed Pitching-Moment Characteristics of a Thin 45° Swept Wing of Aspect Ratio 4. NACA RM L53J27a, 1953.

3. Morrison, William D., Jr., and Alford, William J., Jr.: Effects of Horizontal-Tail Height and a Wing Leading-Edge Modification Consisting of a Full-Span Flap and a Partial-Span Chord-Extension on the Aerodynamic Characteristics in Pitch at High Subsonic Speeds of a Model with a 45° Sweptback Wing. NACA RM L53E06, 1953.

4. Spreemann, Kenneth P., and Alford, William J., Jr.: Investigation of the Effects of Wing Leading-Edge Chord-Extension and Fences in Combination With Leading-Edge Flaps on the Aerodynamic Characteristics at Mach Numbers From 0.40 to 0.93 of a 45° Sweptback Wing of Aspect Ratio 4. NACA RM L53A09a, 1953.

5. Herriot, John G.: Blockage Correction for Three-Dimensional-Flow Closed-Throat Wind Tunnels, With Consideration of the Effect of Compressibility. NACA Rep. 995, 1950. (Supersedes NACA RM A7B28.)

6. Gillis, Clarence L., Polhamus, Edward C., and Gray, Joseph L., Jr.: Charts for Determining Jet-Boundary Corrections for Complete Models in 7- by 10-Foot Closed Rectangular Wind Tunnels. NACA WR L-123, 1945. (Formerly NACA ARR L5G31.)

7. Polhamus, Edward C., and Becht, Robert E.: Low-Speed Stability Characteristics of a Complete Model With a Wing of W Plan Form. NACA RM L52A25, 1952.

[redacted]

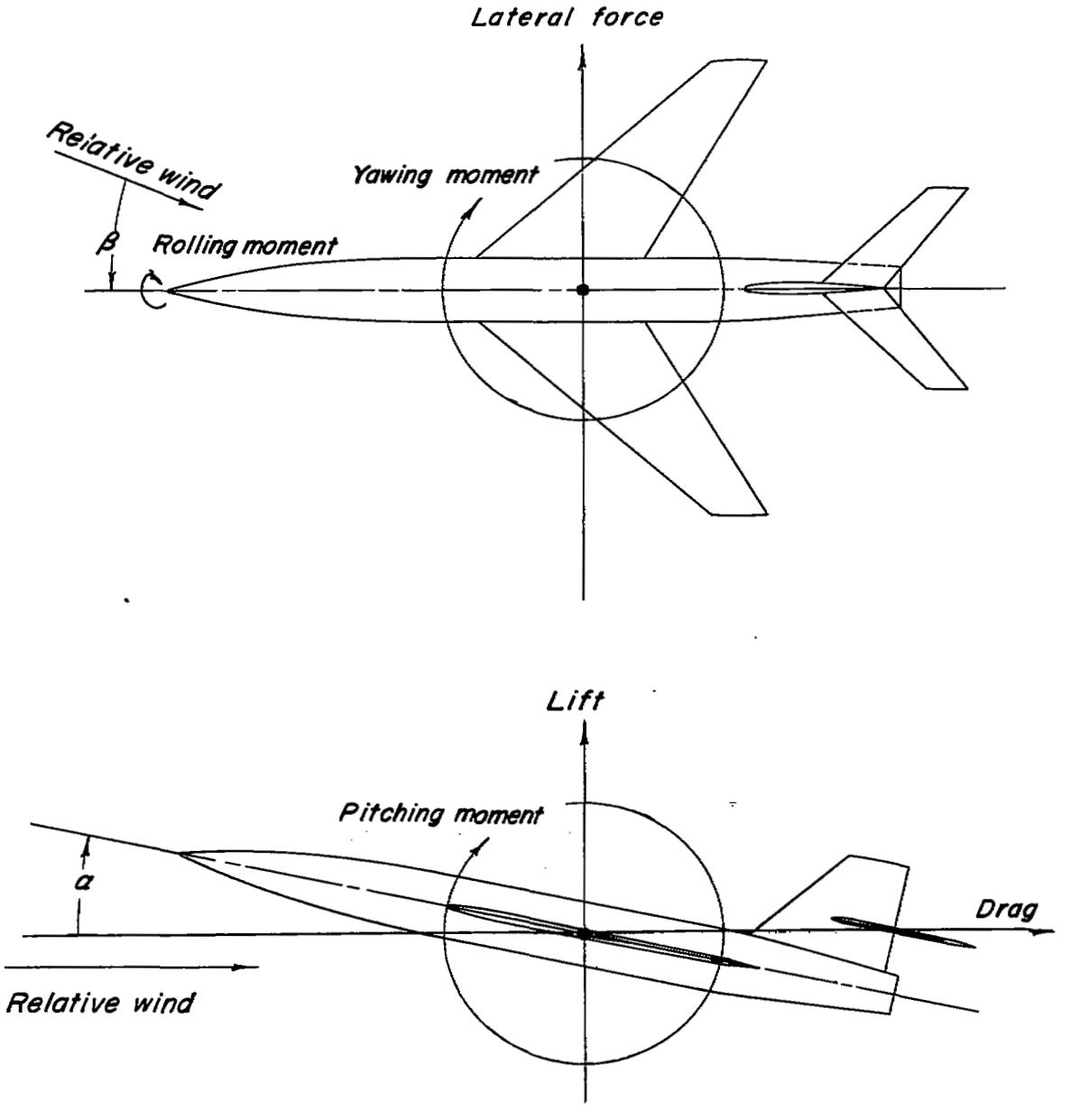

Figure 1.- System of axes. Positive values of forces, moments, and angles are indicated by arrows.

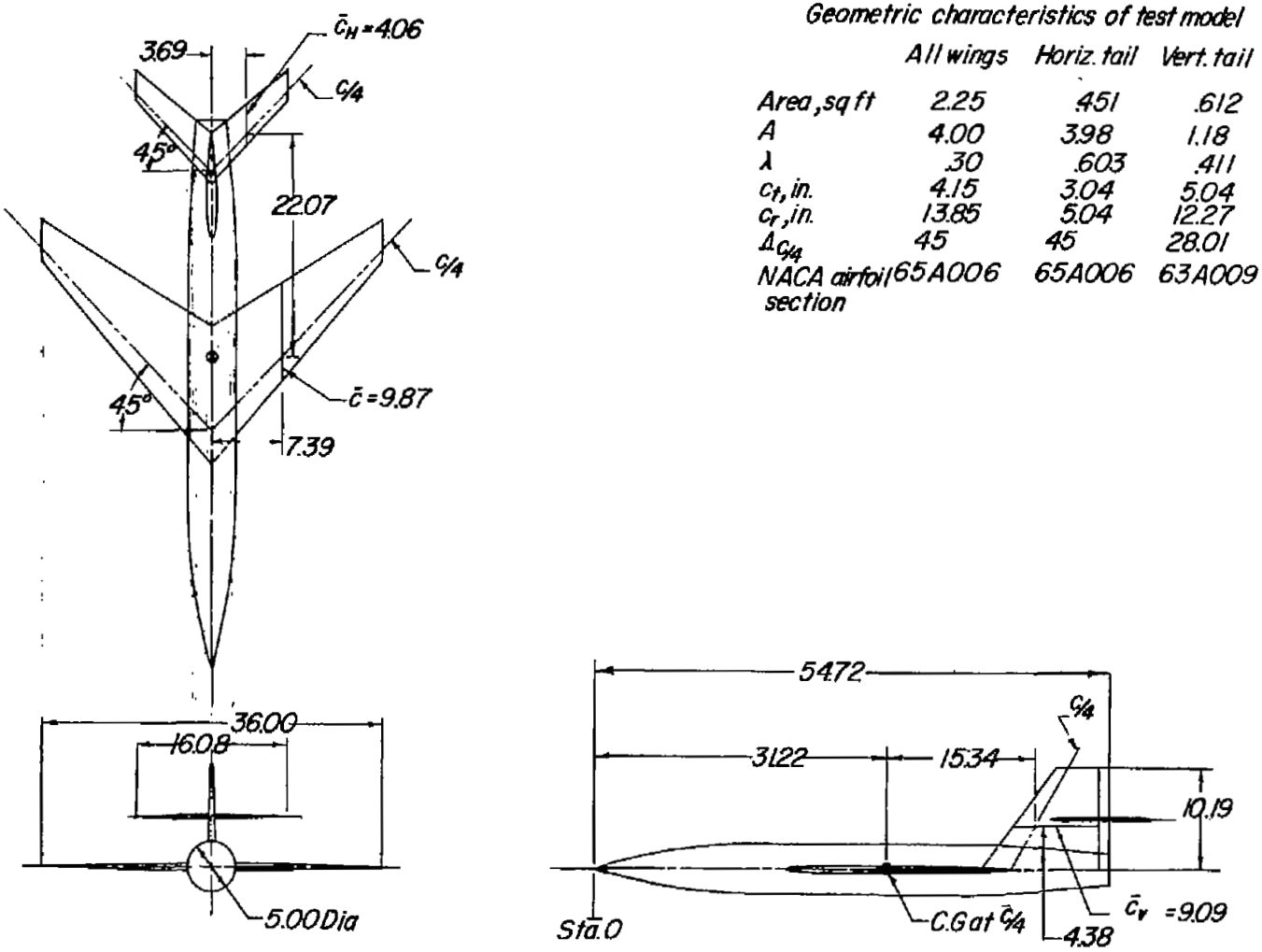

Geometric characteristics of test model

	All wings	Horiz. tail	Vert. tail
Area, sq ft	2.25	.451	.612
A	4.00	3.98	1.18
λ	.30	.603	.411
c_t, in.	4.15	3.04	5.04
c_r, in.	13.85	5.04	12.27
$\Lambda_{c/4}$	45	45	28.01
NACA airfoil section	65A006	65A006	63A009

(a) Three-view drawing of model with the swept wing.

Figure 2.- Geometric characteristics of model.

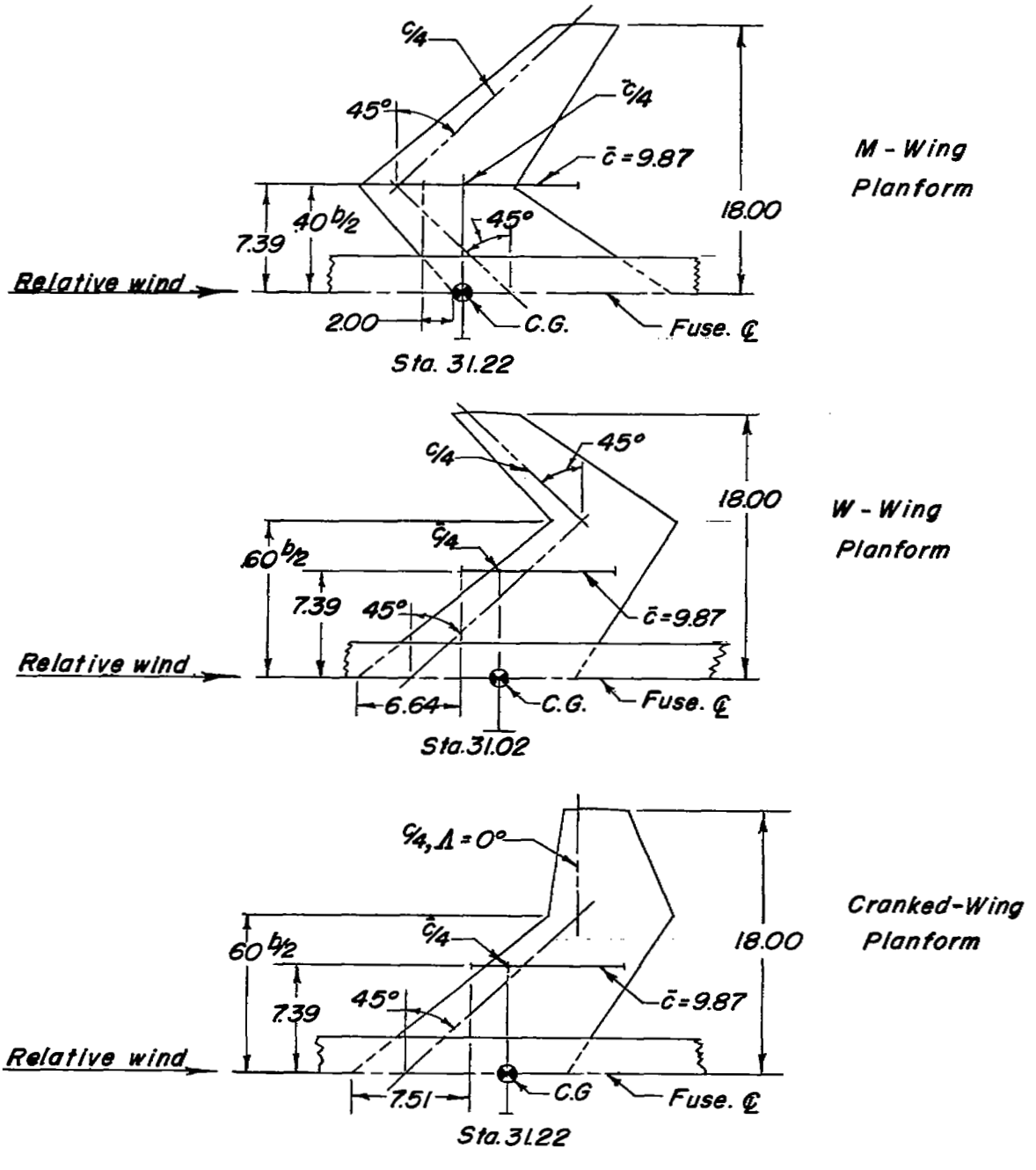

(b) Composite wing plan forms.

Figure 2.- Continued.

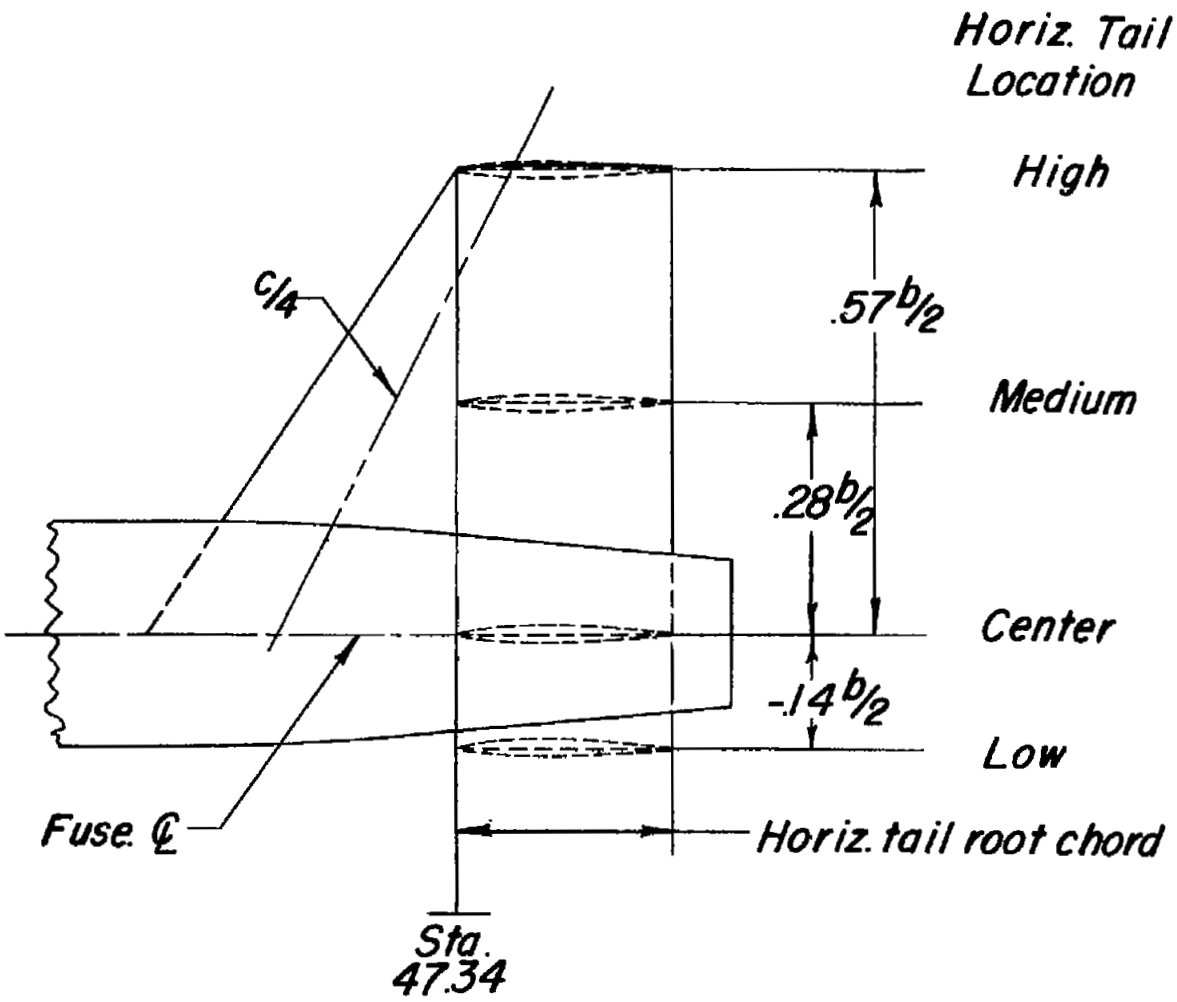

(c) Horizontal-tail locations.

Figure 2.- Continued.

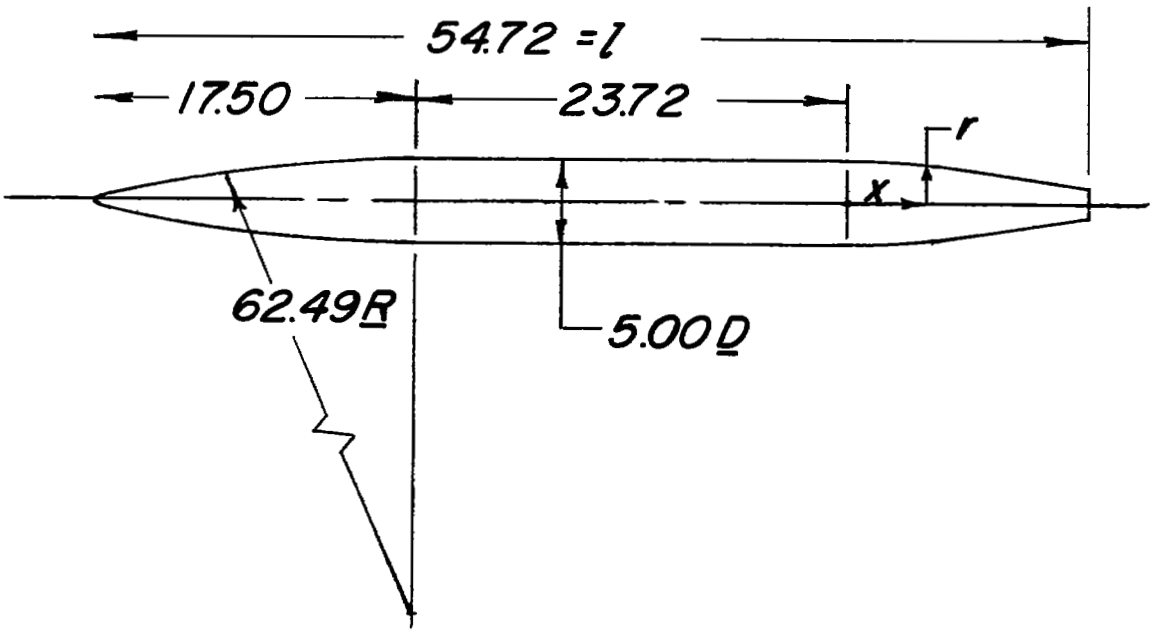

Afterbody Coordinates

x/l	r/l
0	.0456
.0320	.0445
.0639	.0427
.1187	.0390
Straight line taper	
.2460	.0301

(d) Fuselage dimensions.

Figure 2.- Concluded.

[redacted]

L-79954

Figure 3.- Photograph of test model in Langley high-speed 7- by 10-foot tunnel.

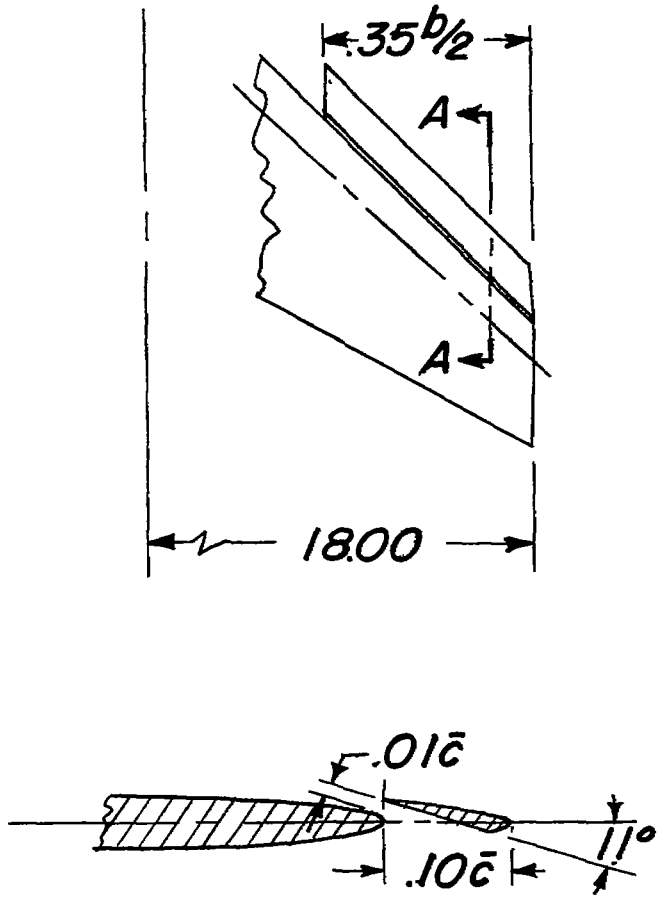

Figure 4.- Detail of leading-edge slat tested on the swept wing.

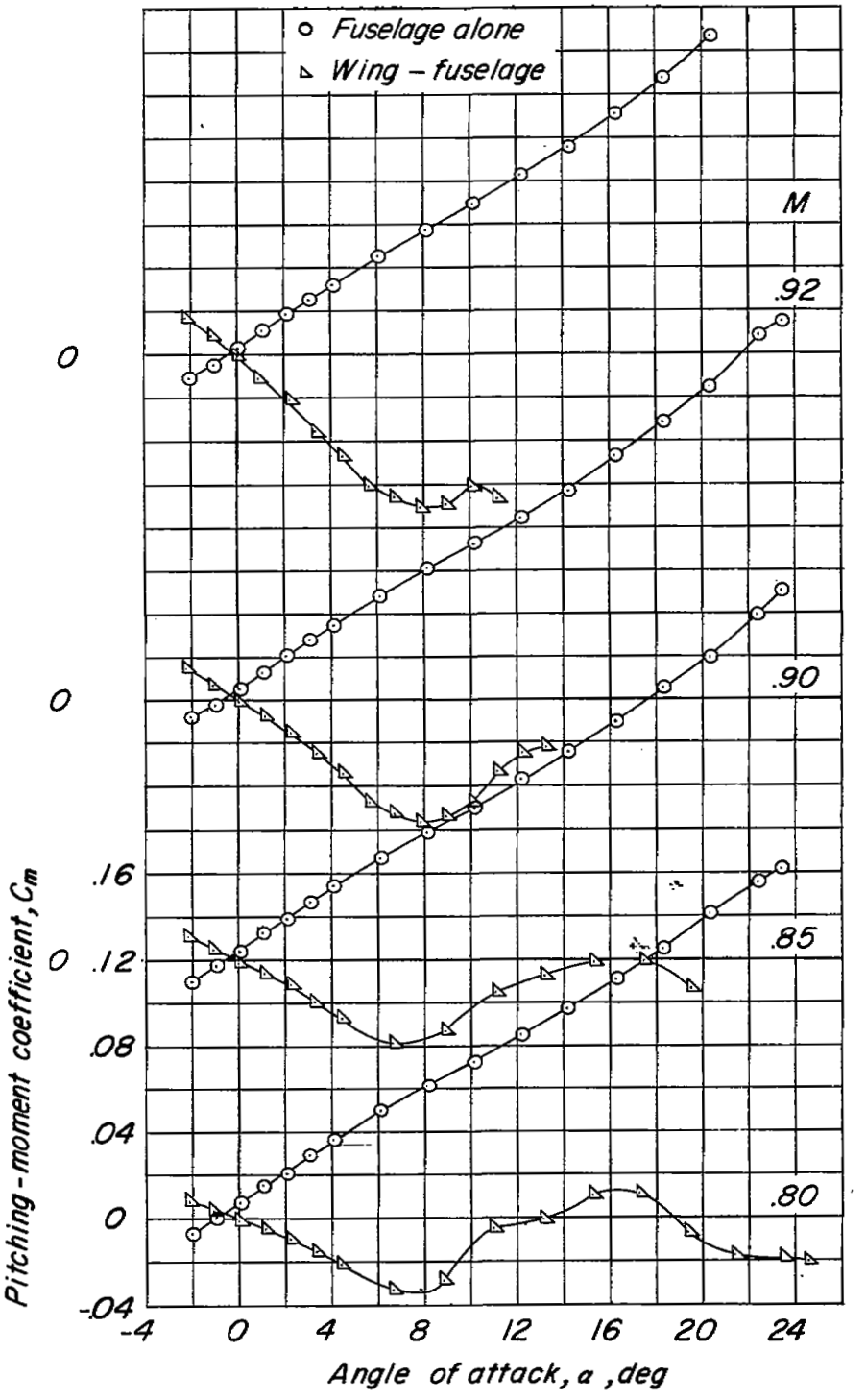

Figure 5.- Comparison of fuselage alone and swept-wing—fuselage characteristics.

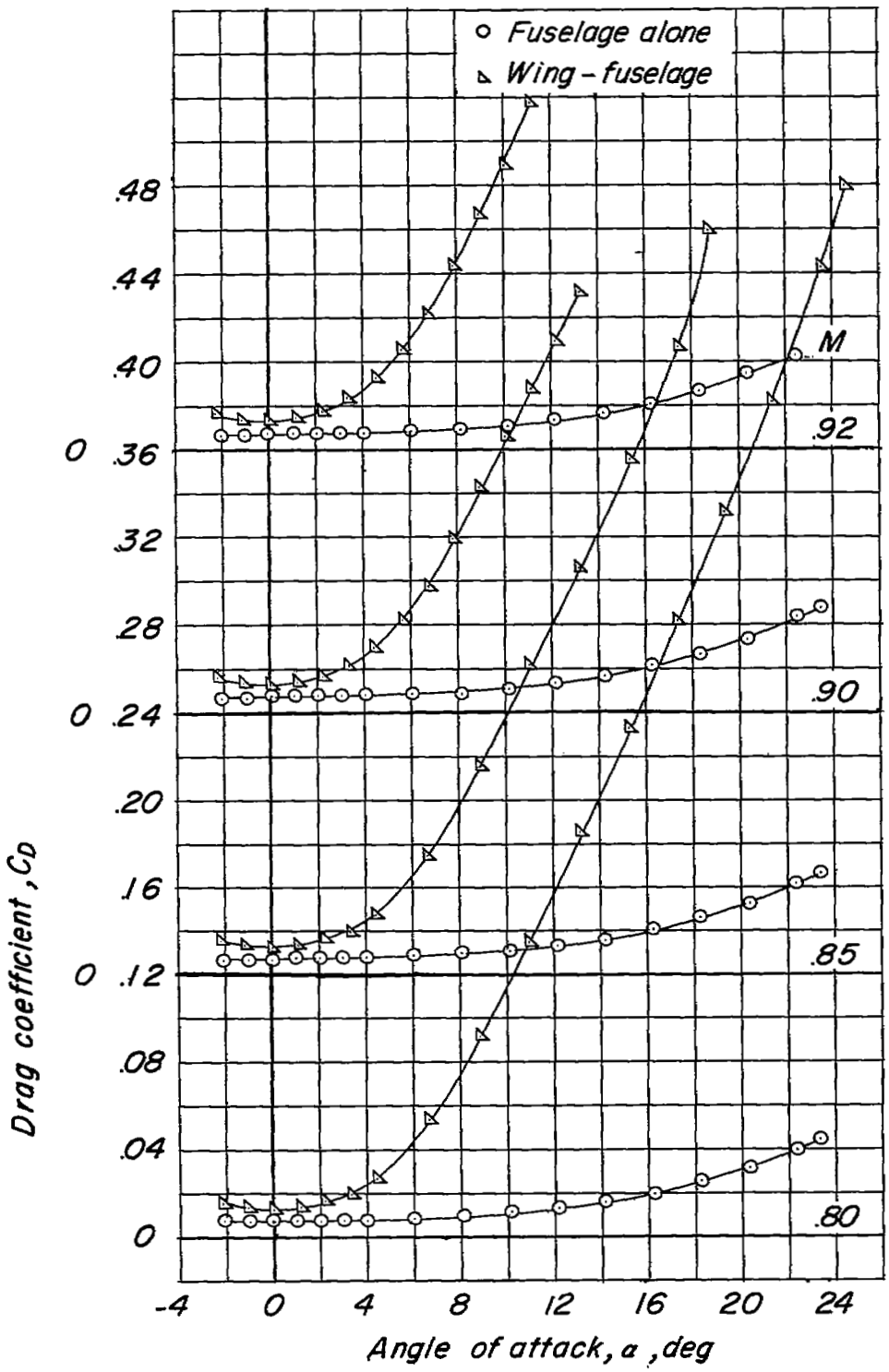

Figure 5.- Continued.

[redacted]

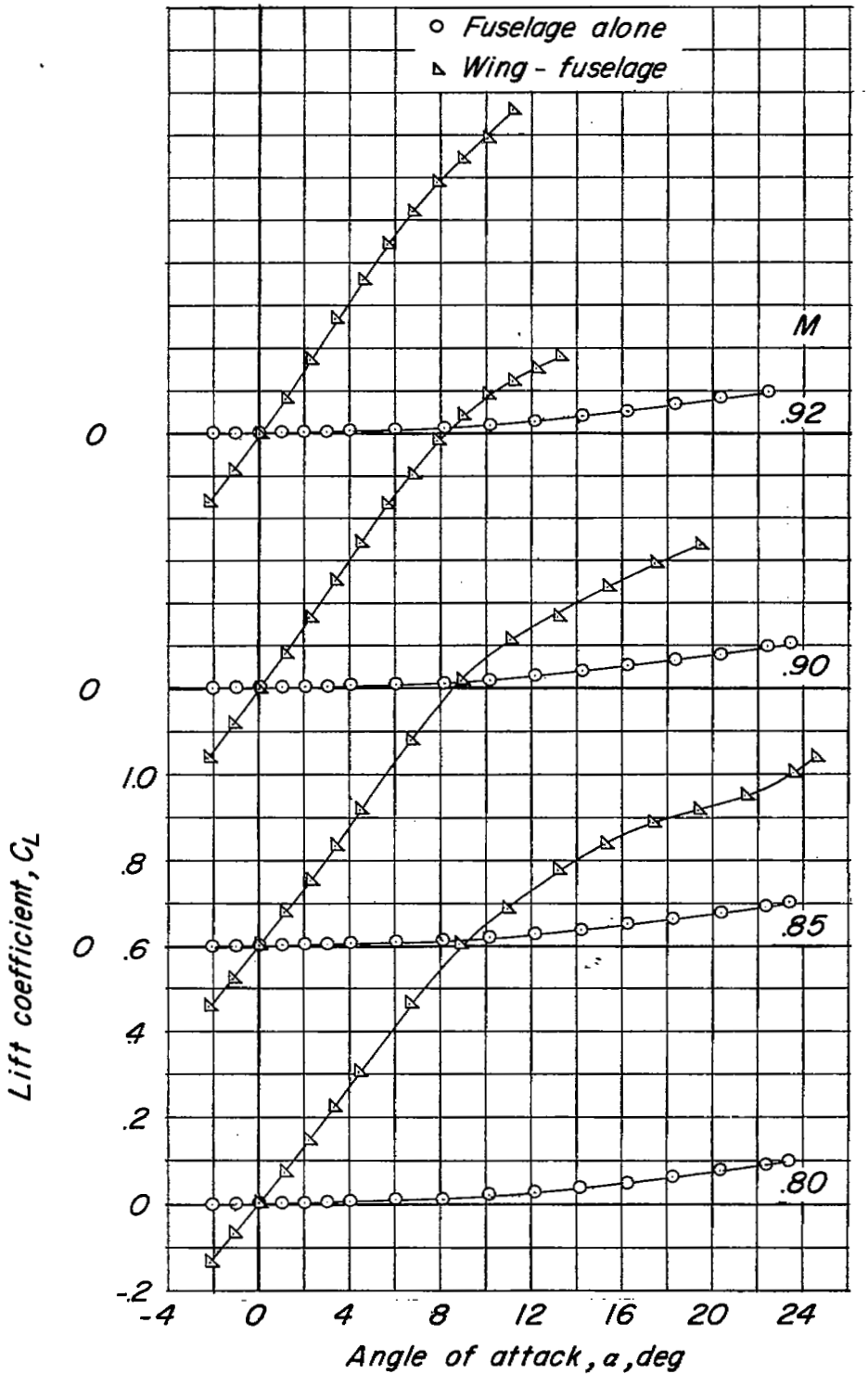

Figure 5.- Concluded.

[redacted]

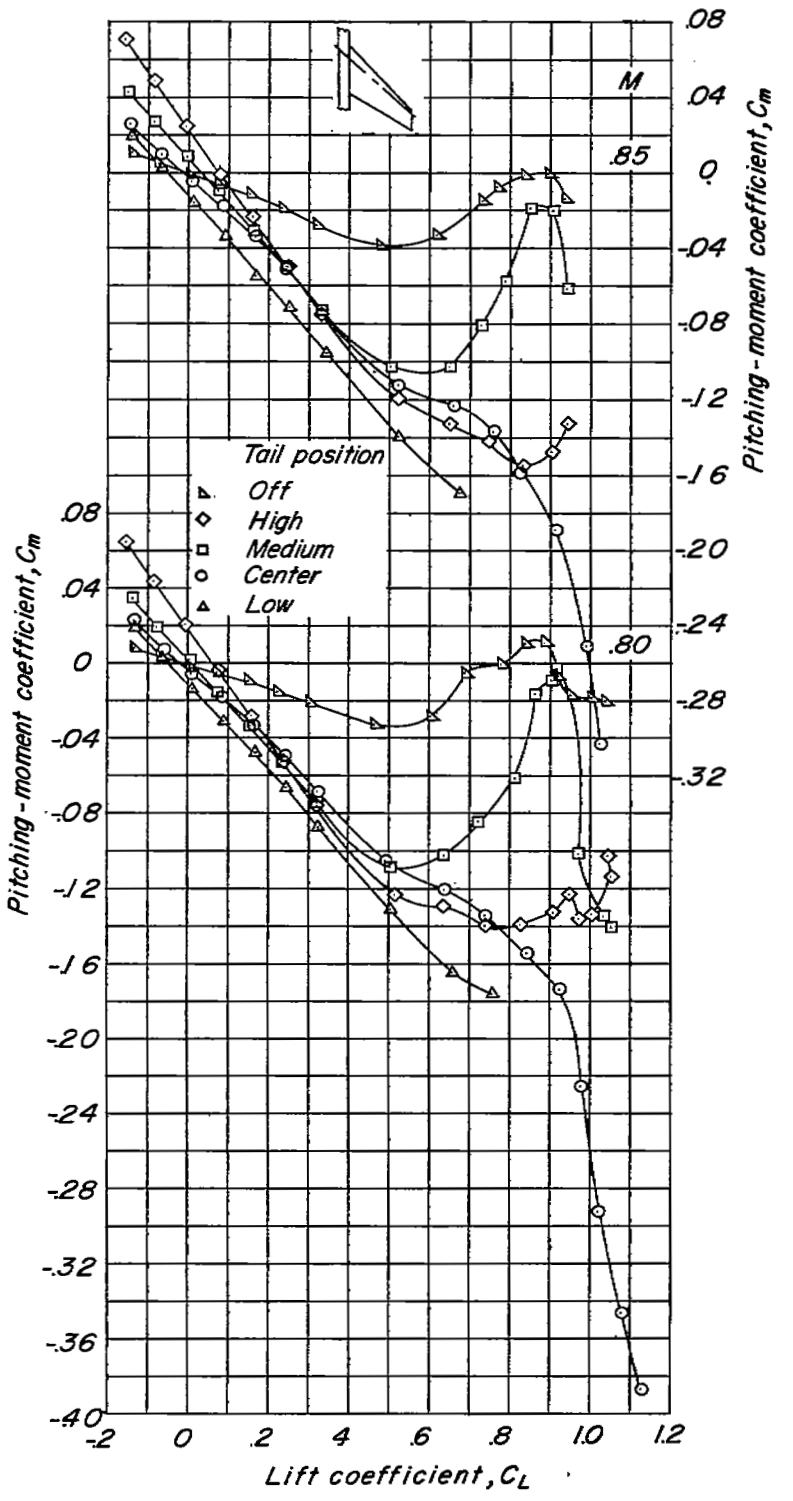

Figure 6.- Longitudinal characteristics of model with swept-wing plan form.

[redacted]

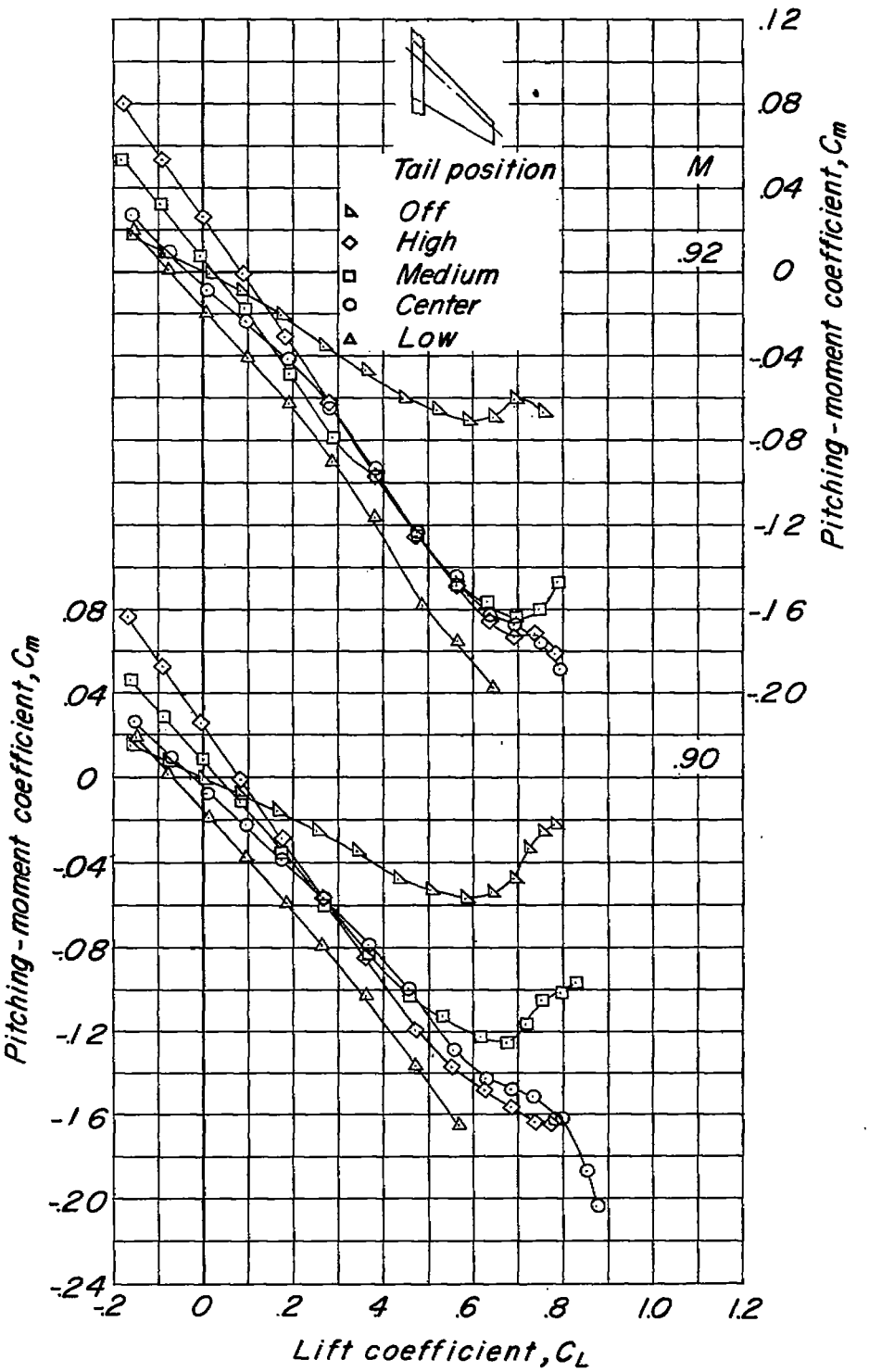

Figure 6.- Continued.

[redacted]

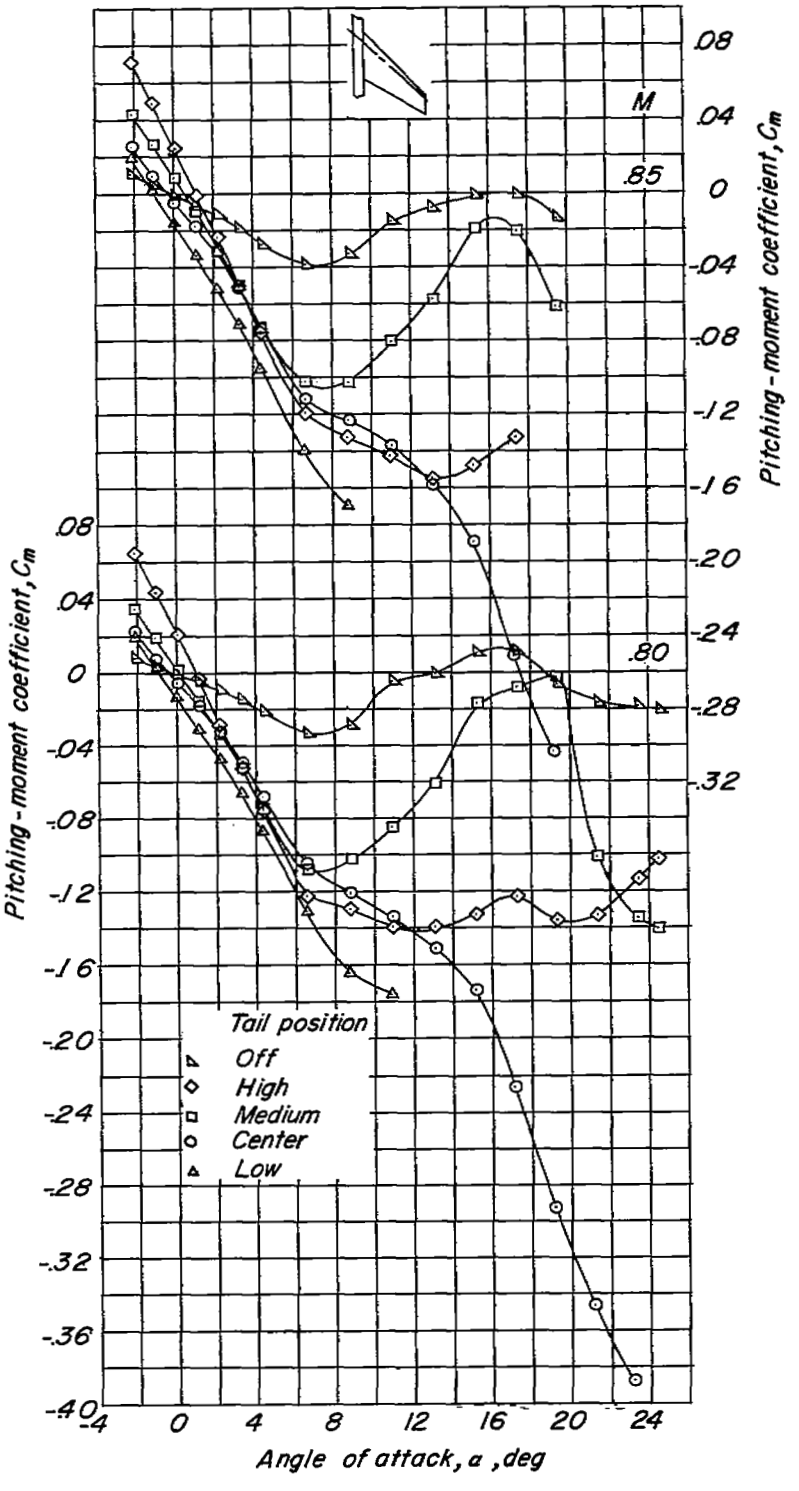

Figure 6.- Continued.

[redacted]

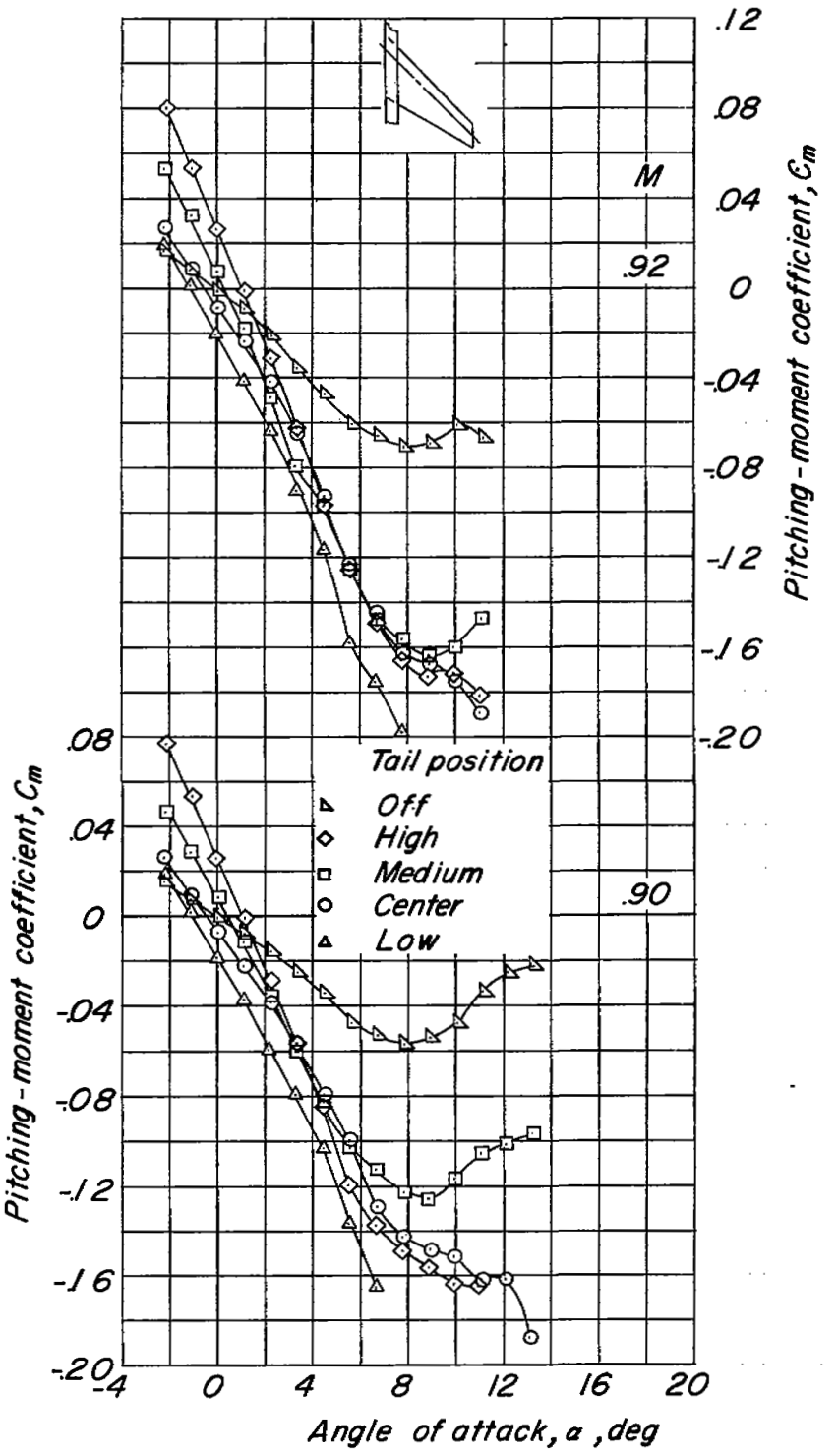

Figure 6.- Continued.

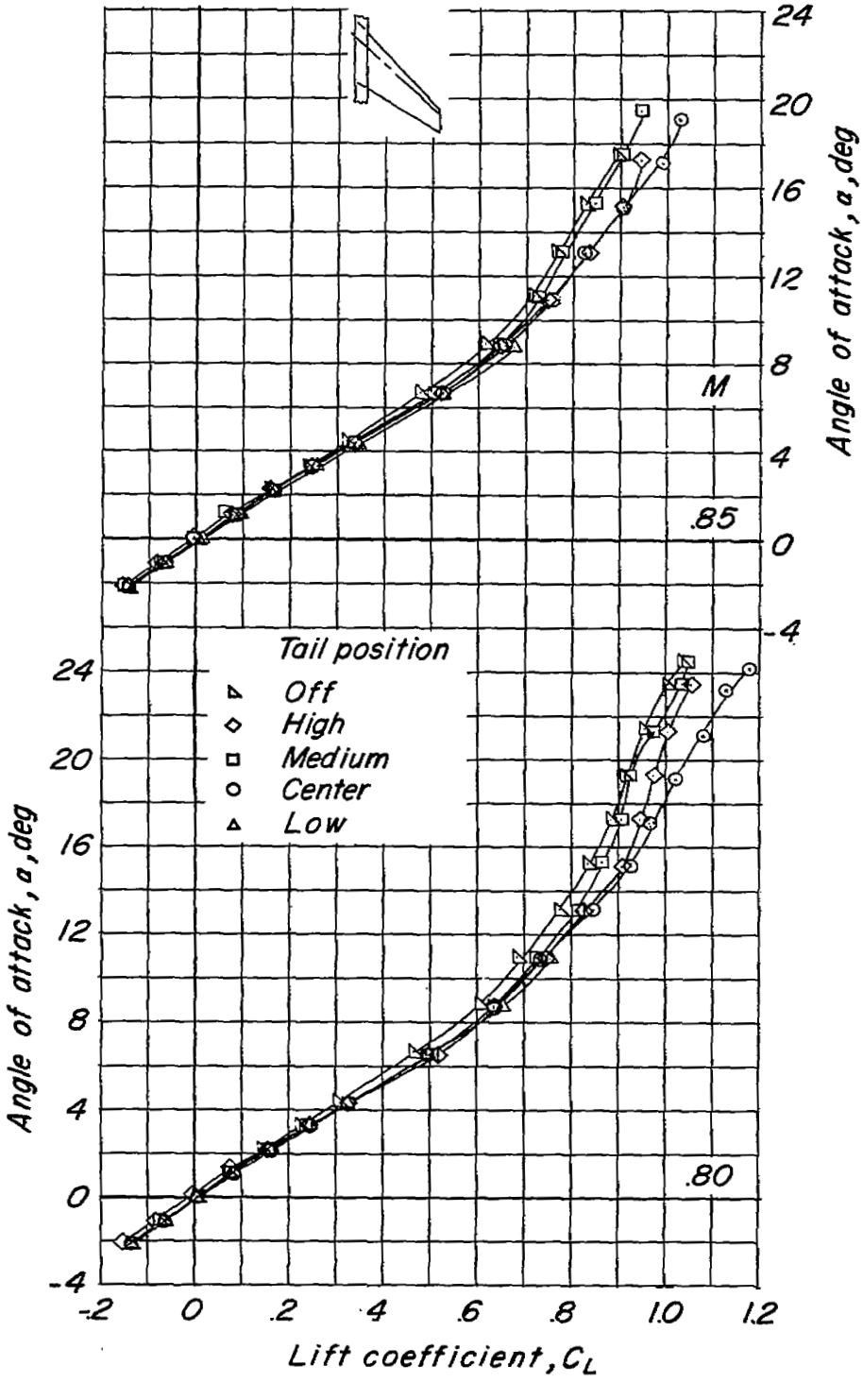

Figure 6.- Continued.

[redacted]

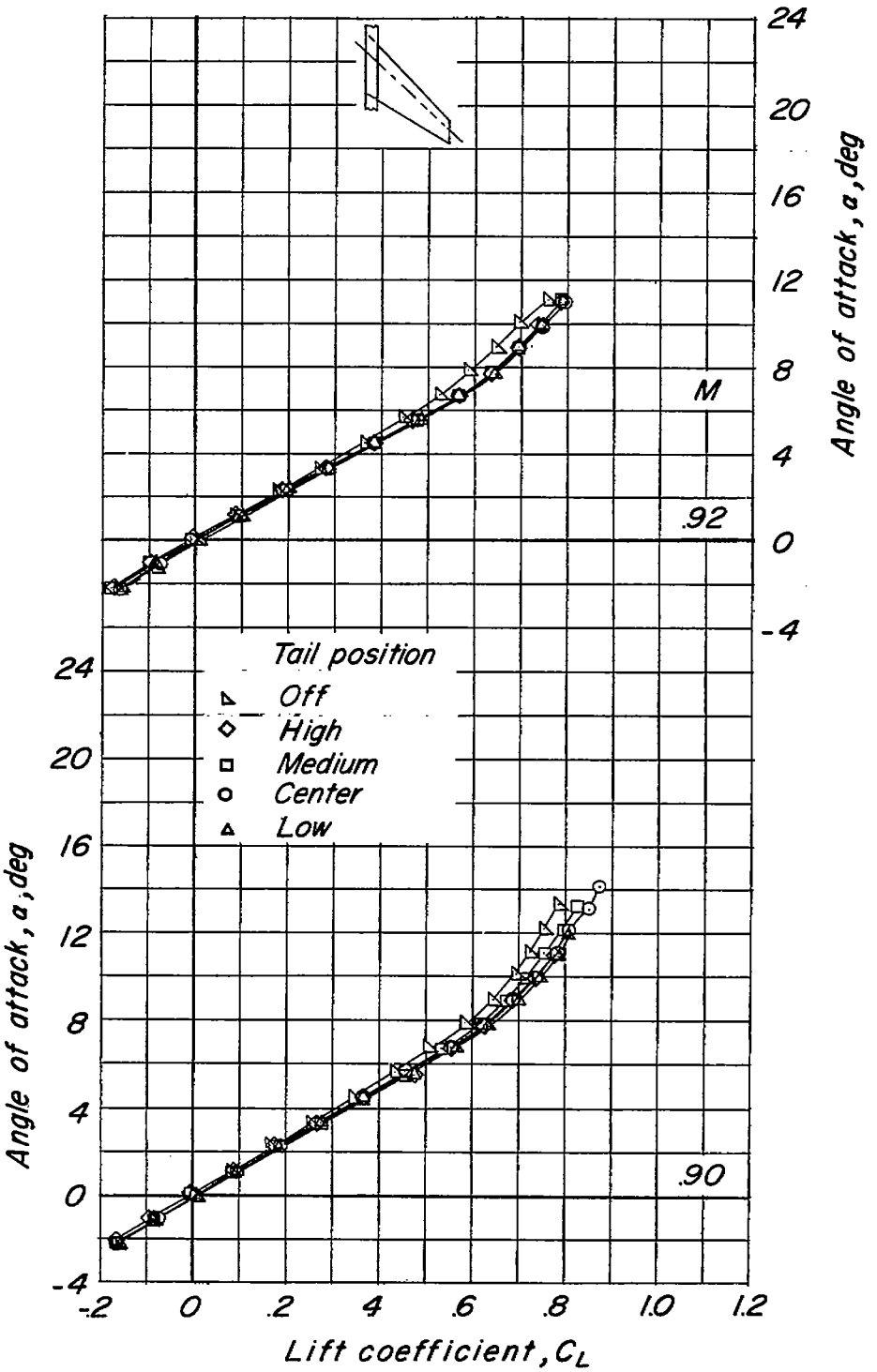

Figure 6.- Continued.

[redacted]

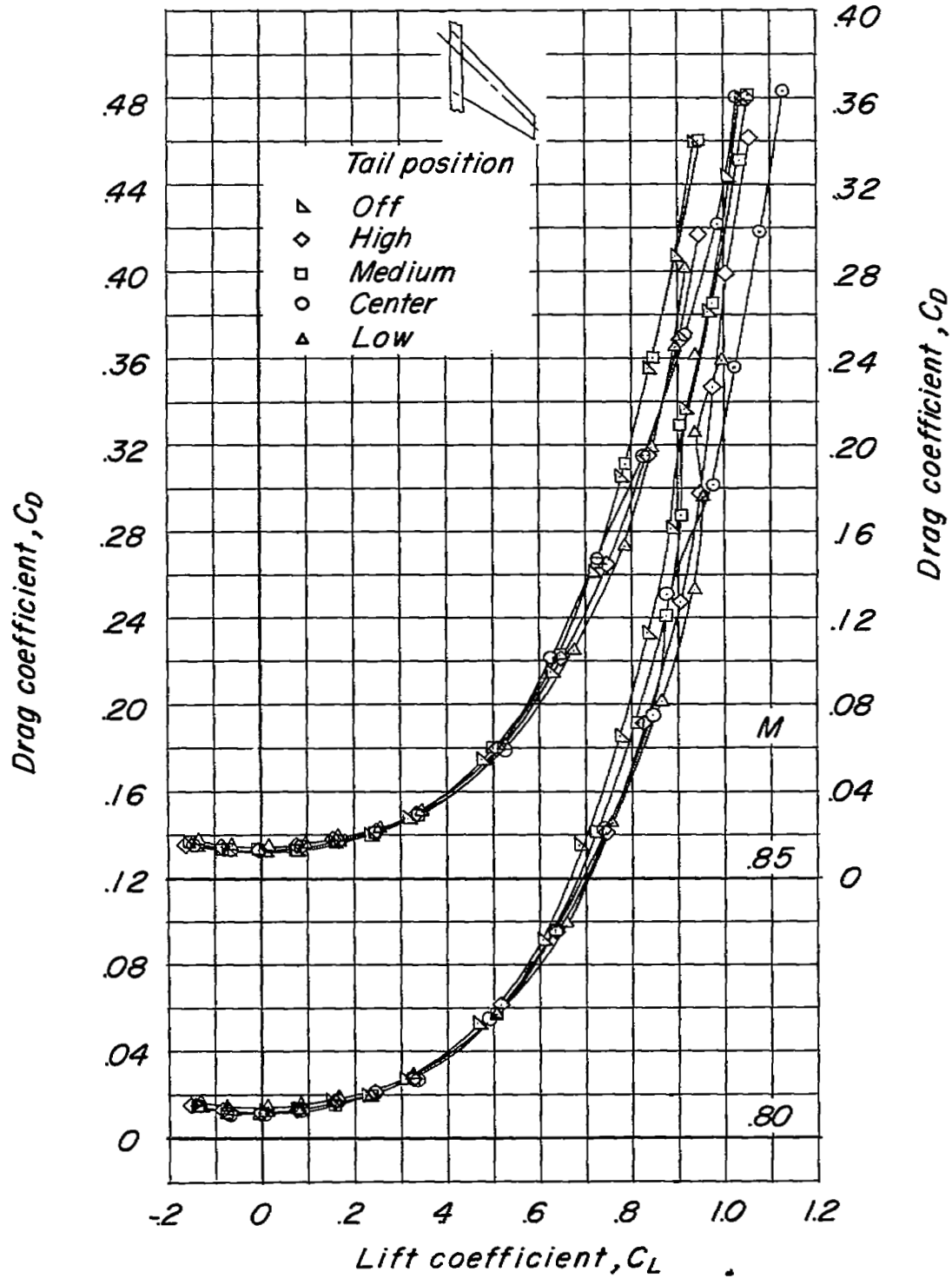

Figure 6.- Continued.

[redacted]

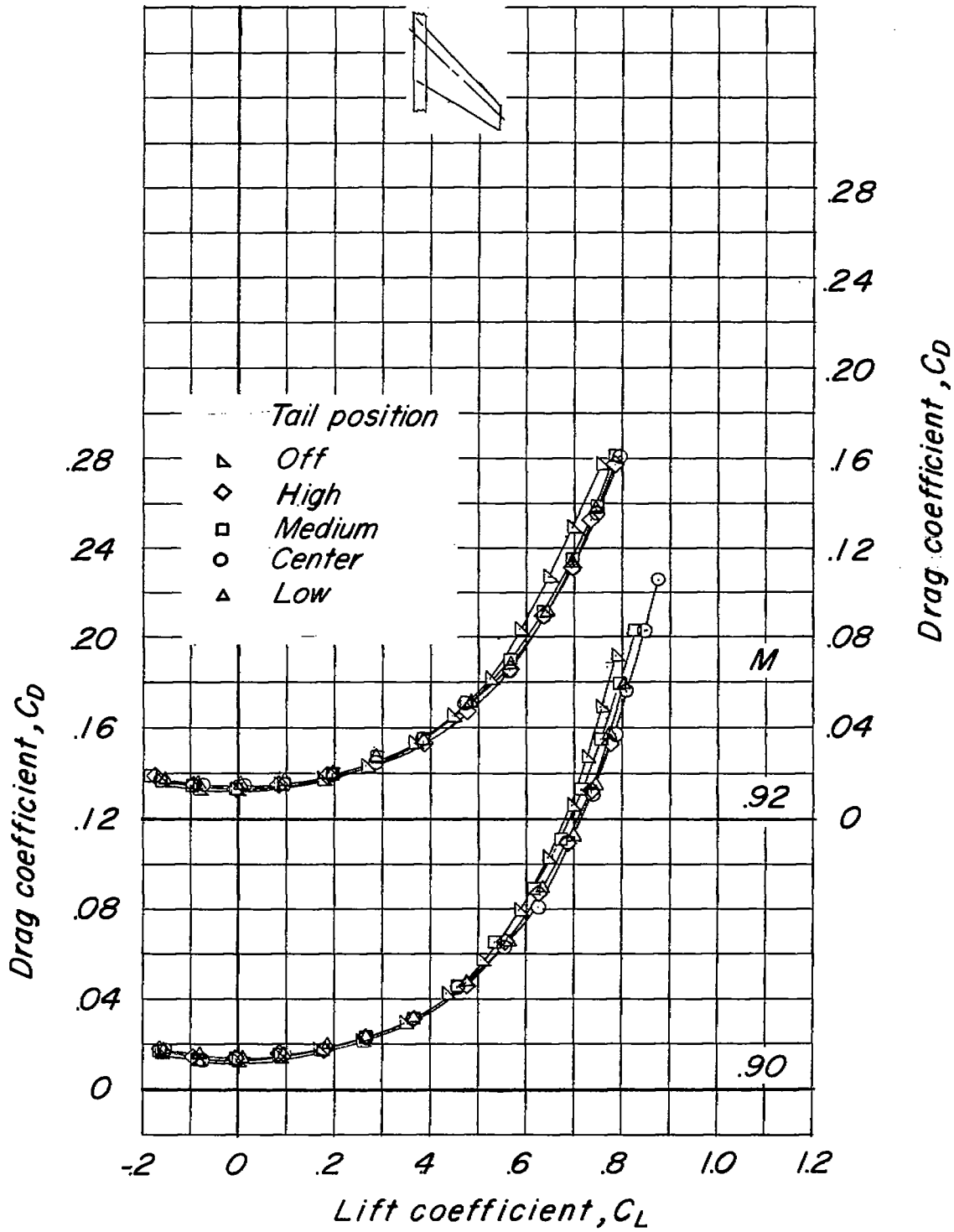

Figure 6.- Concluded.

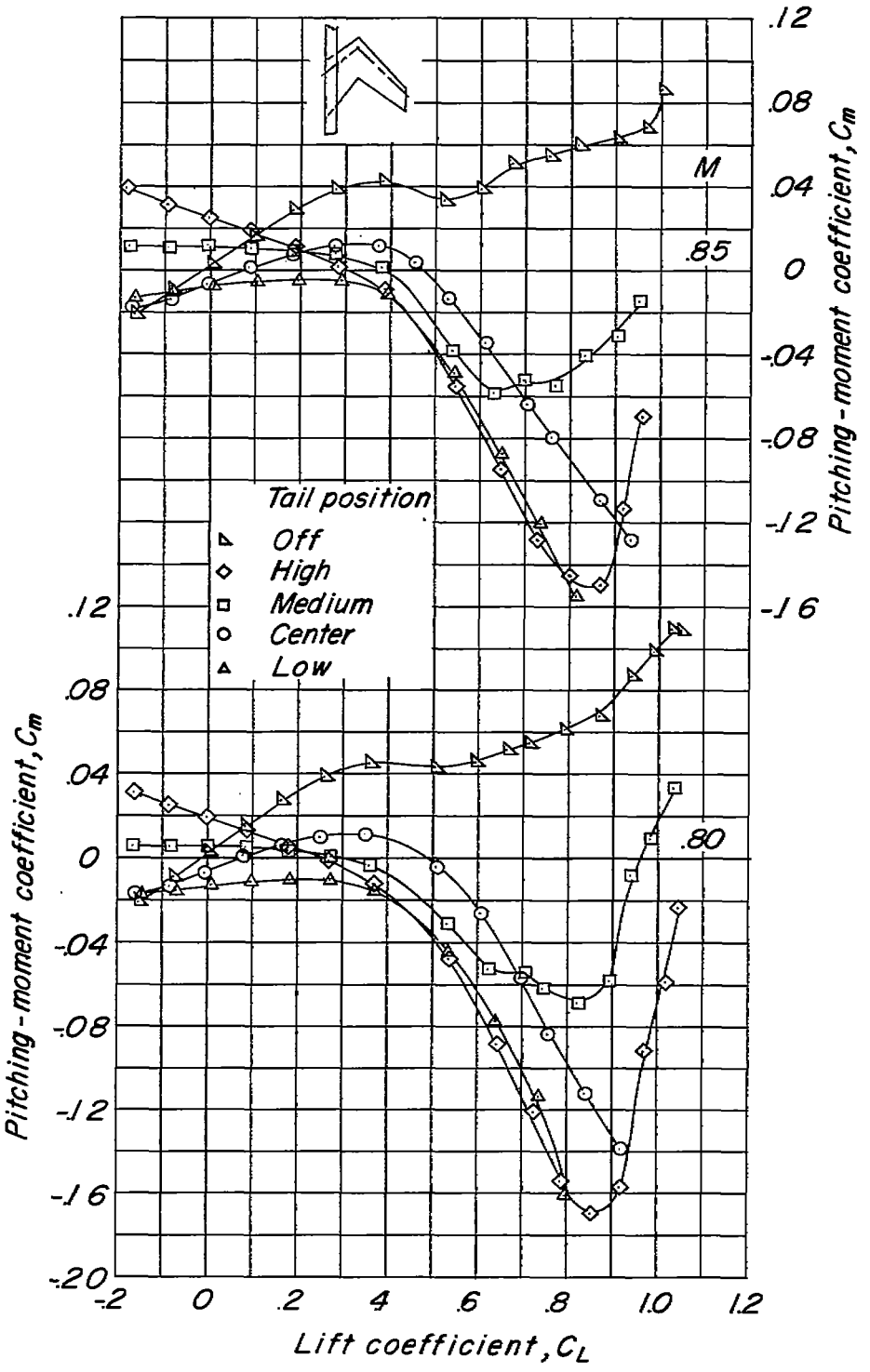

Figure 7.- Longitudinal characteristics of model with M-wing plan form.

[redacted]

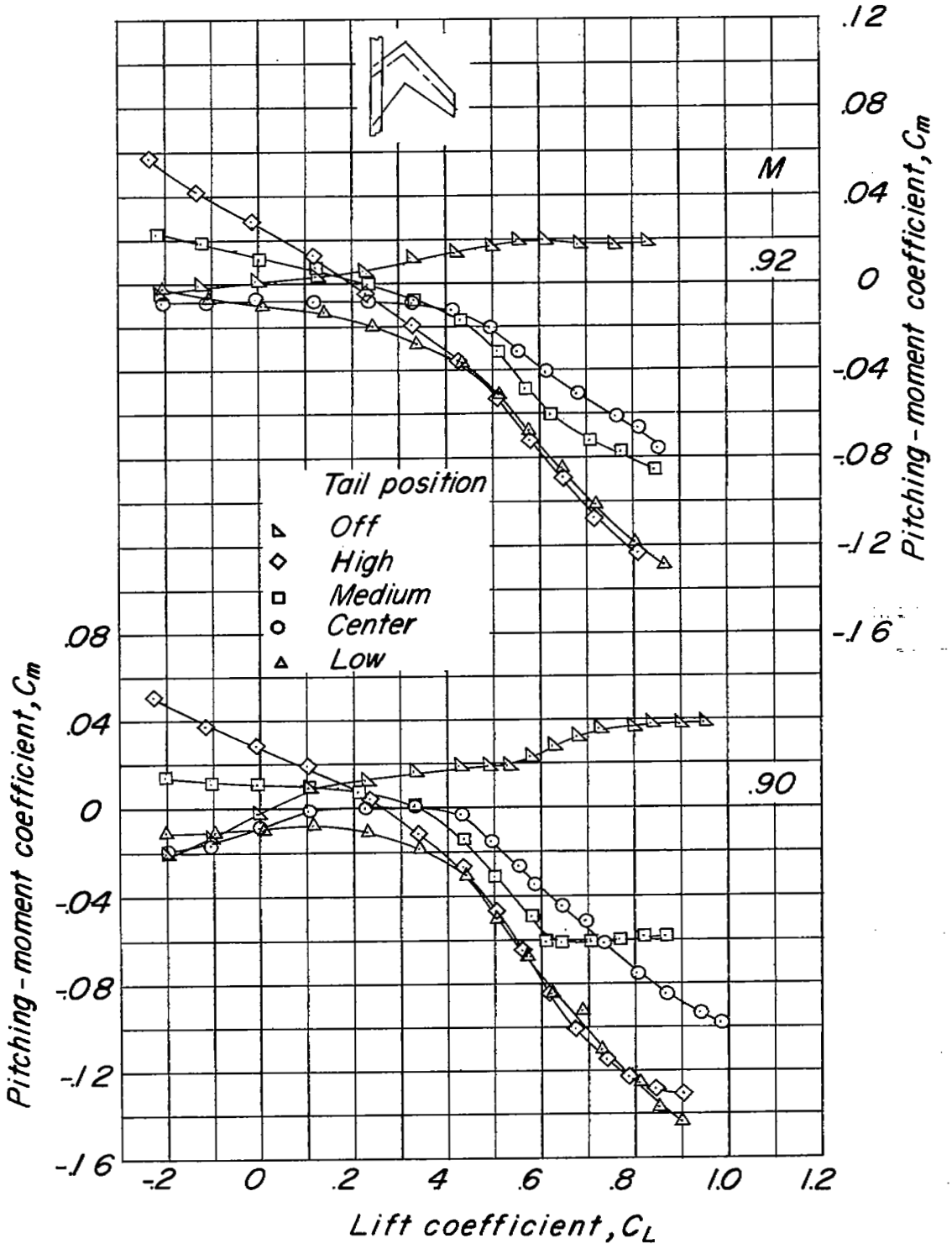

Figure 7.- Continued.

[redacted]

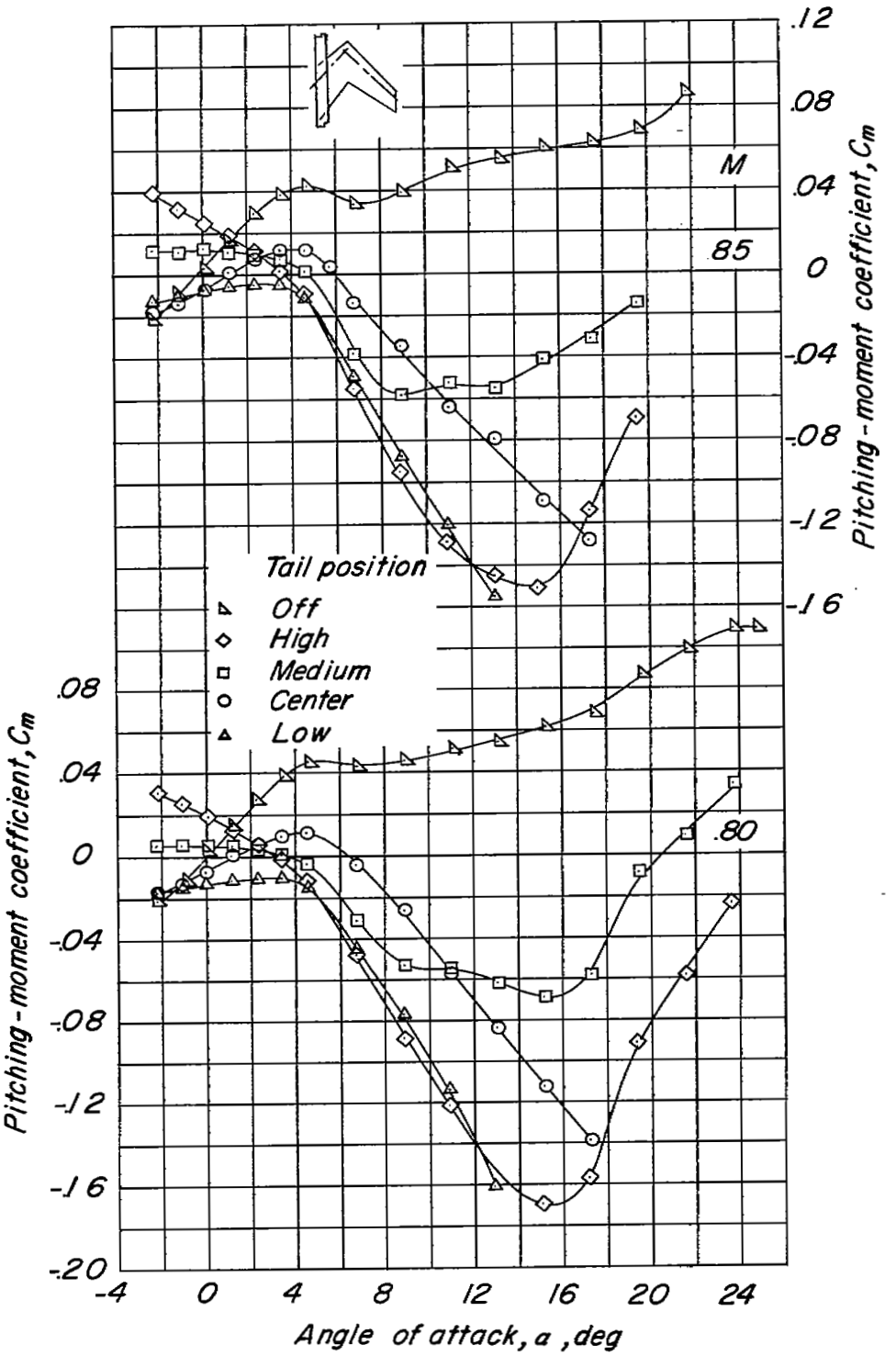

Figure 7.- Continued.

[redacted]

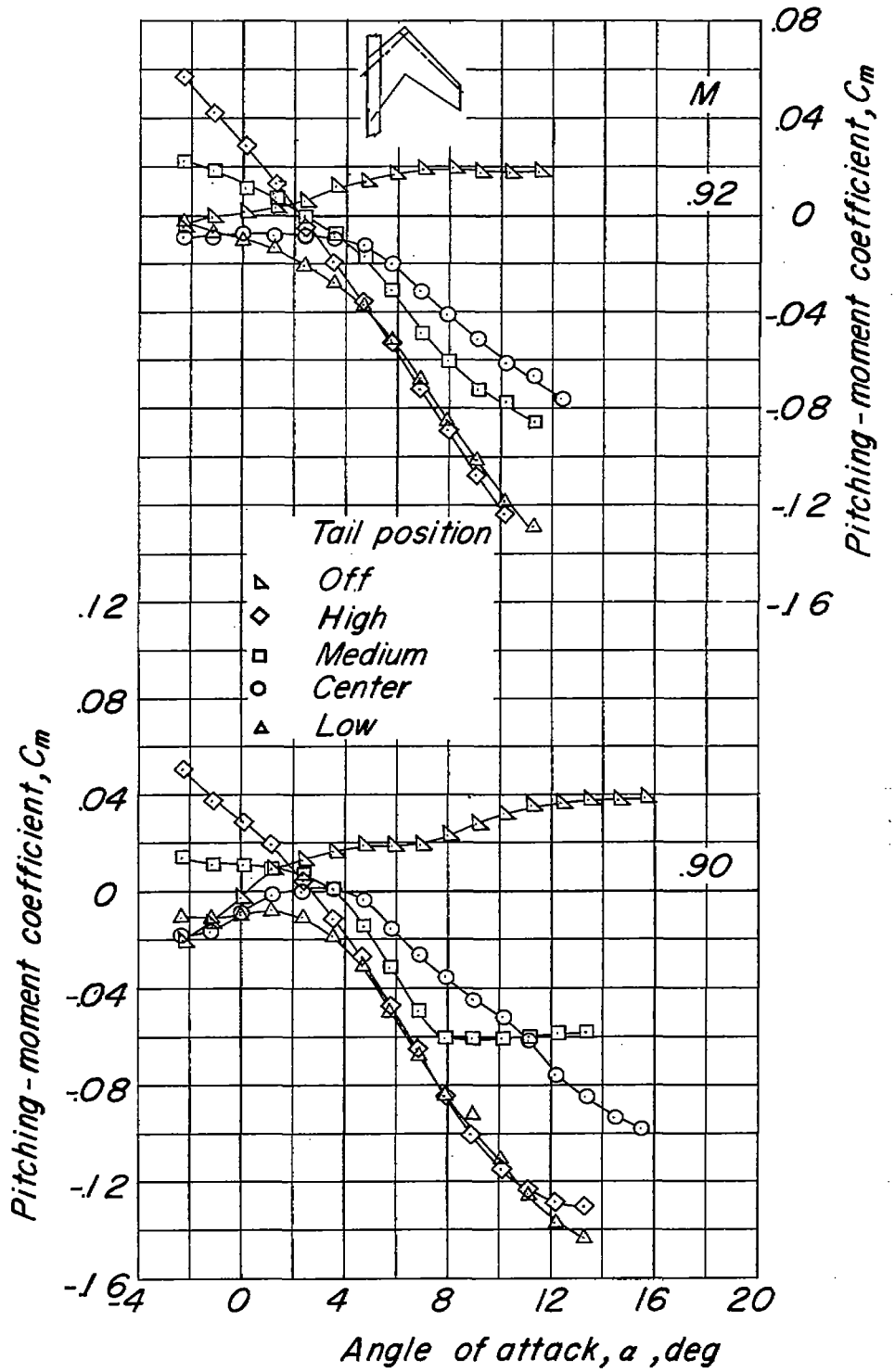

Figure 7.- Continued.

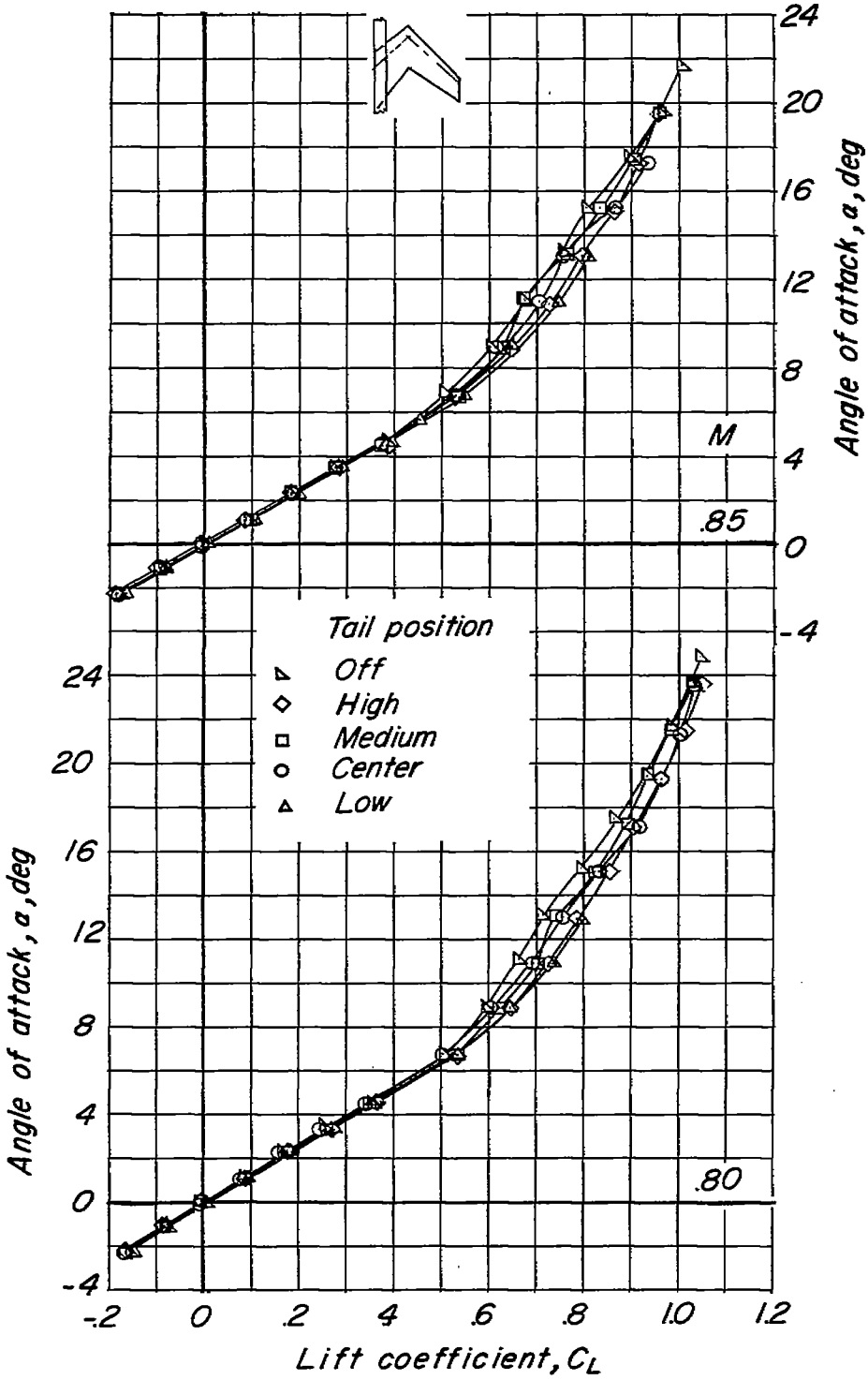

Figure 7.- Continued.

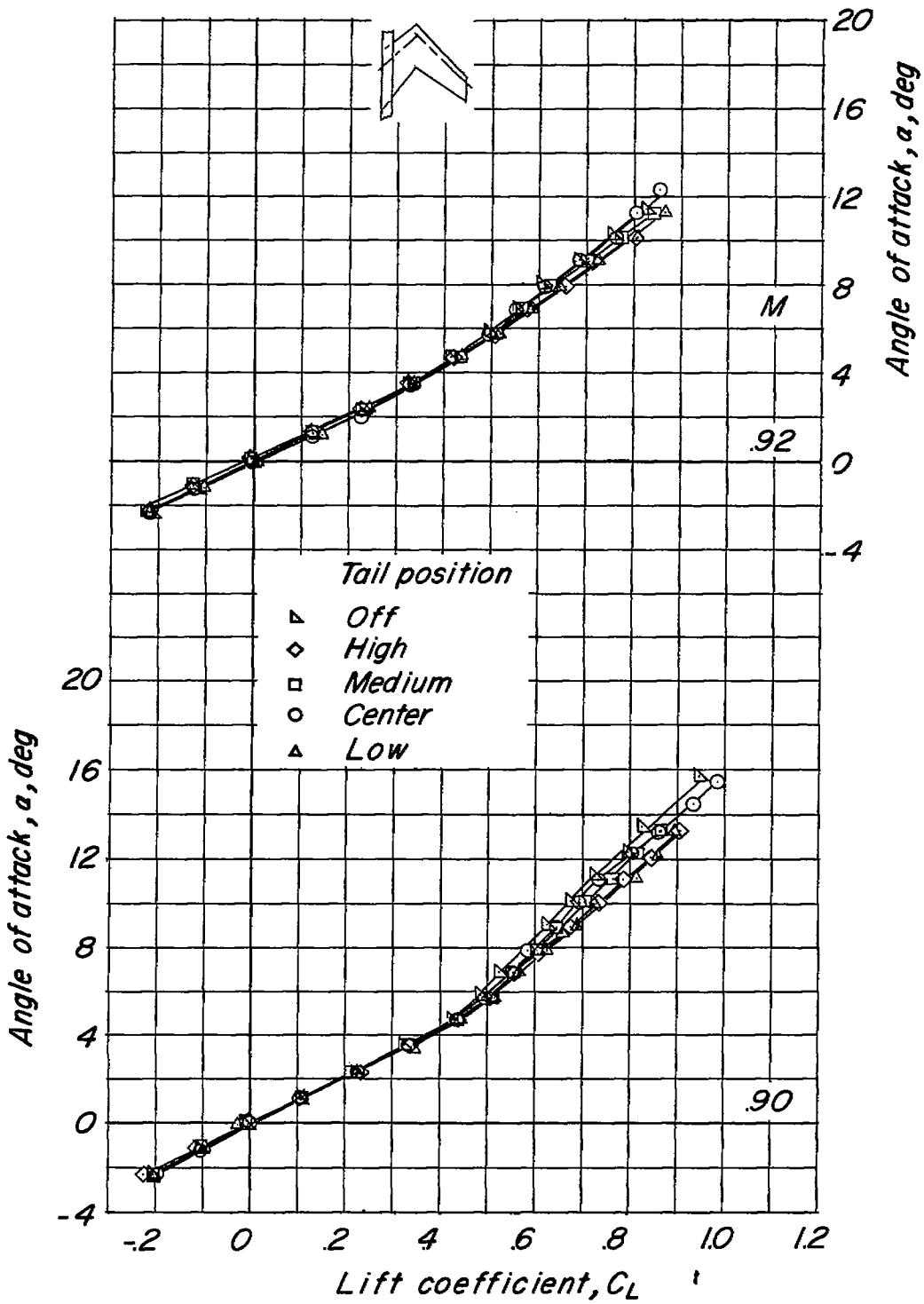

Figure 7.- Continued.

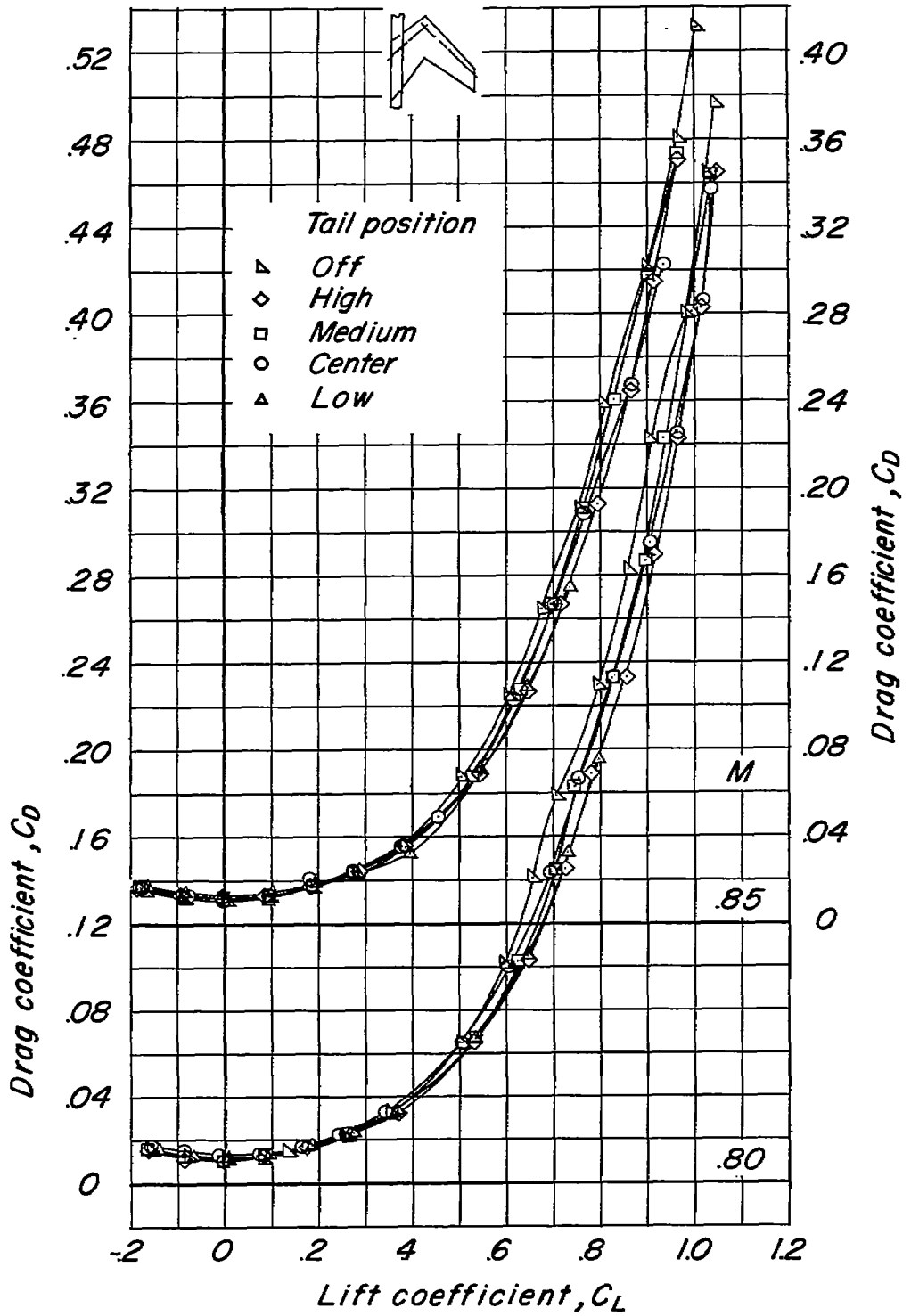

Figure 7.- Continued.

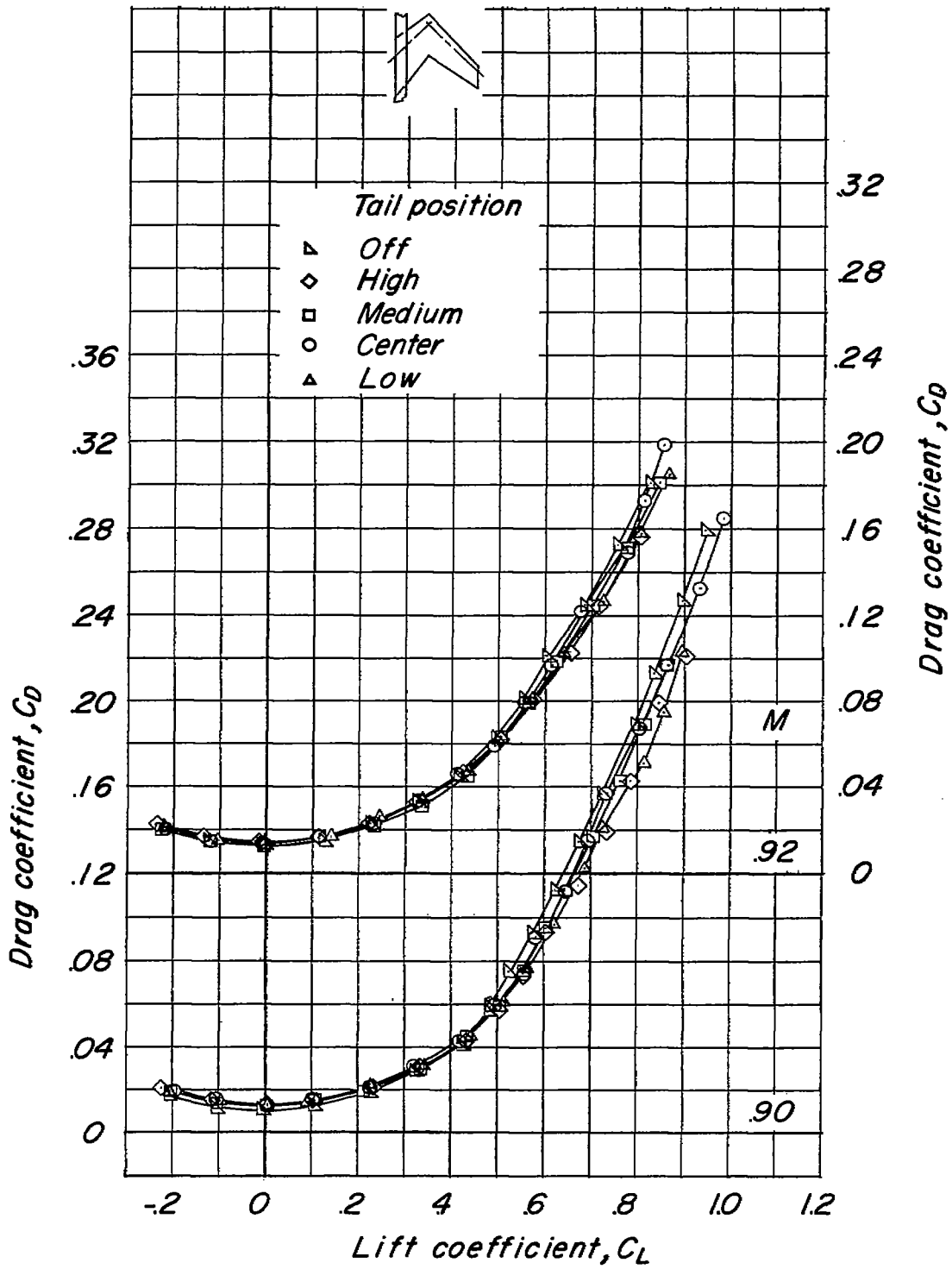

Figure 7.- Concluded.

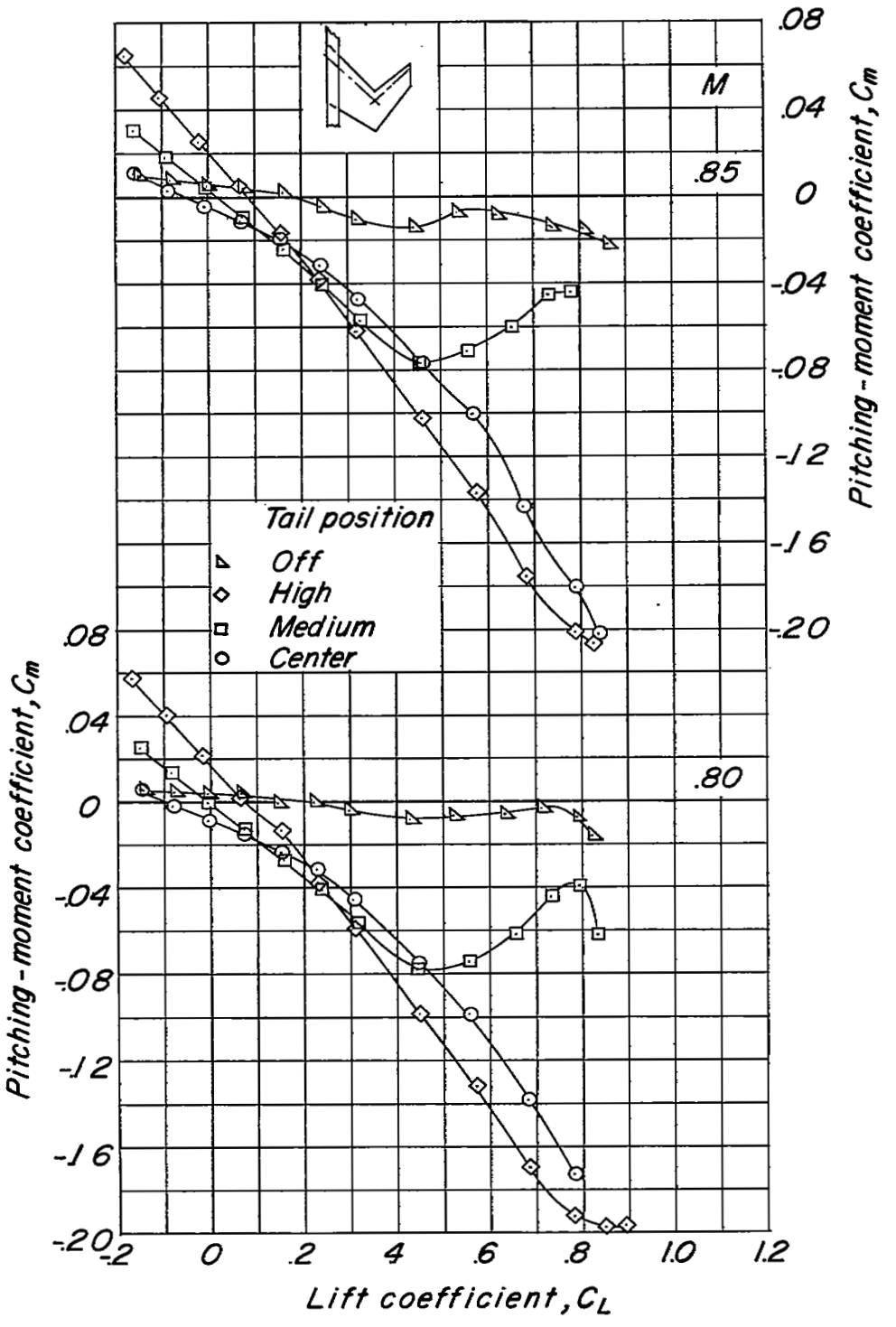

Figure 8.- Longitudinal characteristics of model with W-wing plan form.

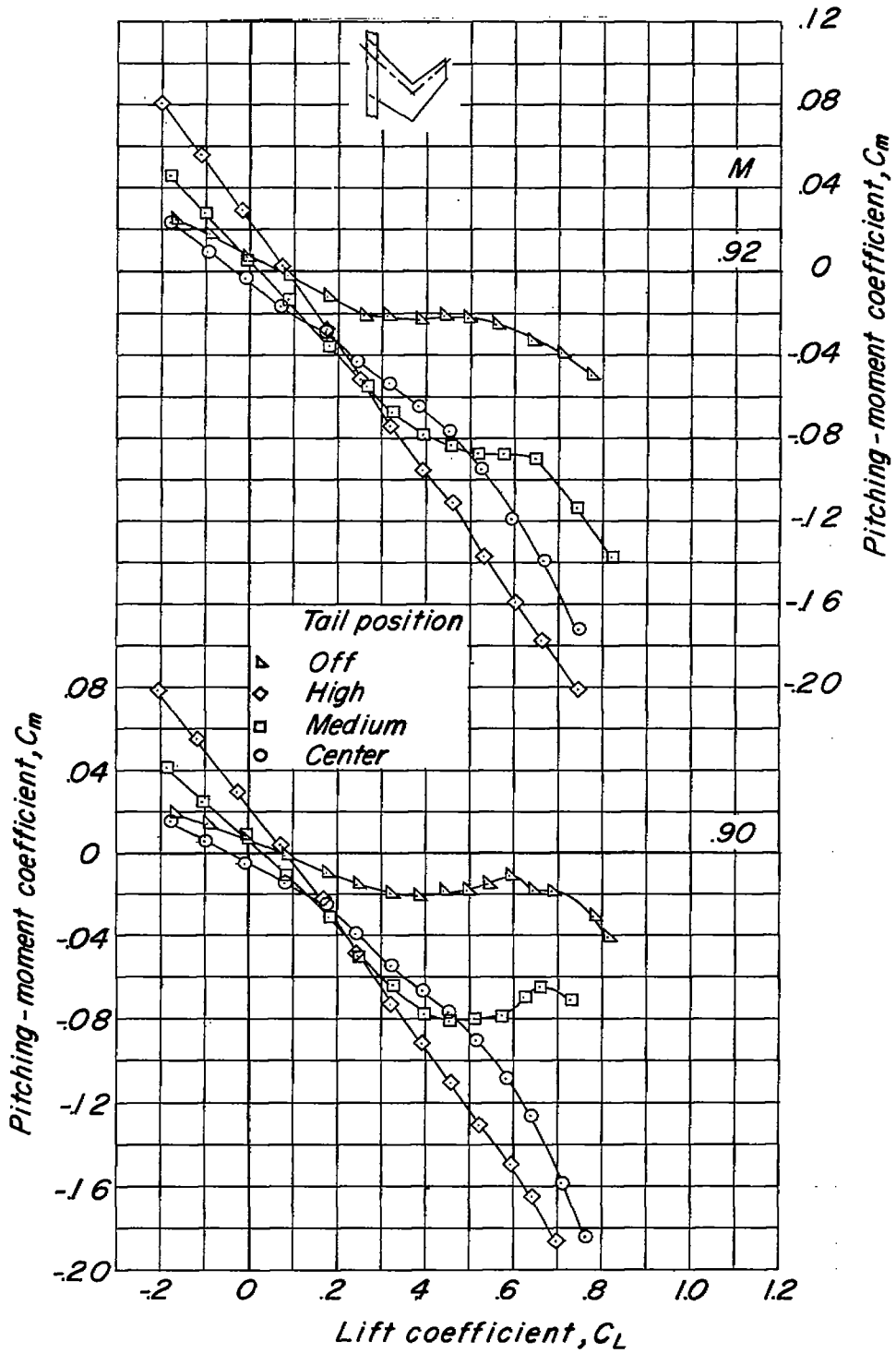

Figure 8.- Continued.

[redacted]

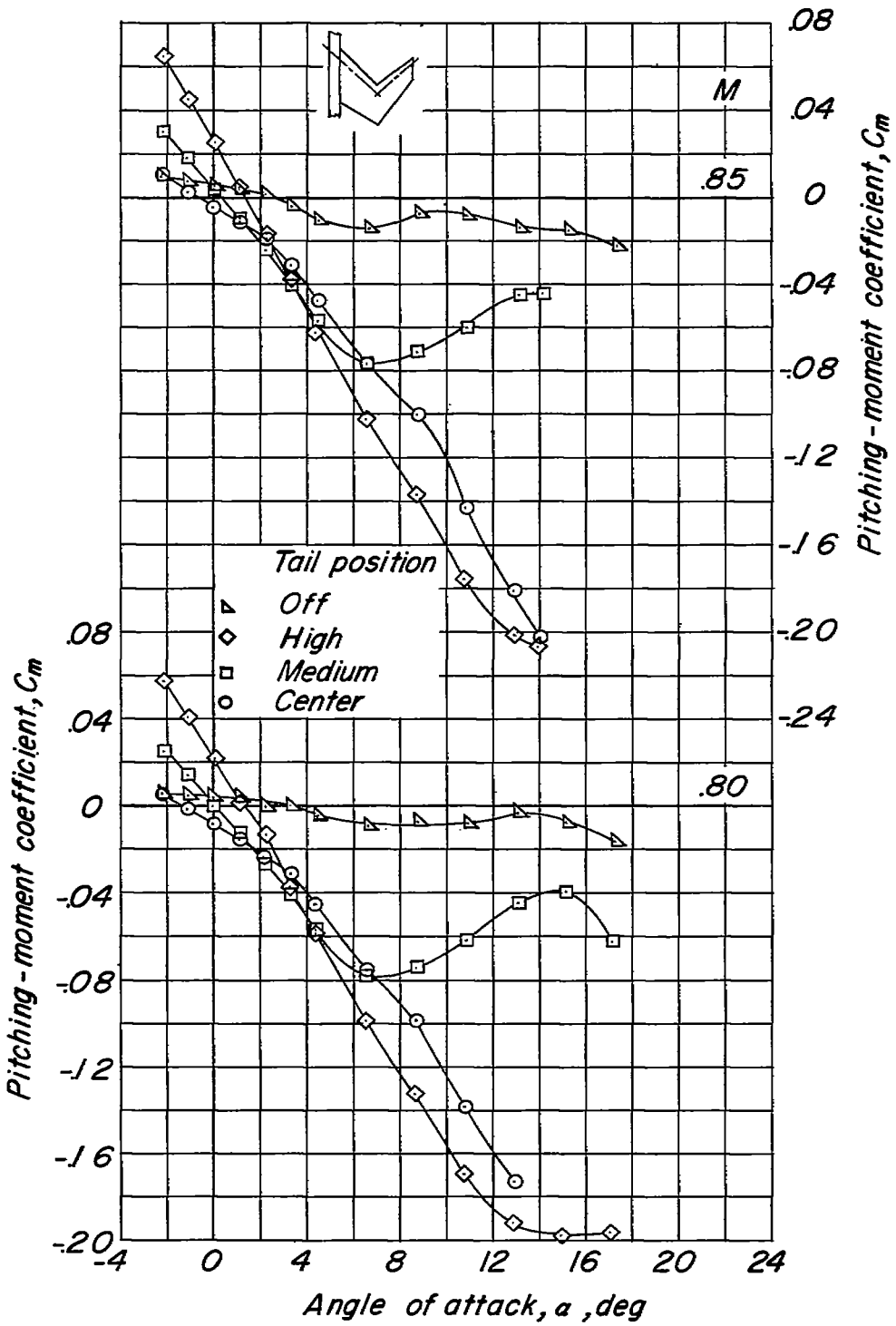

Figure 8.- Continued.

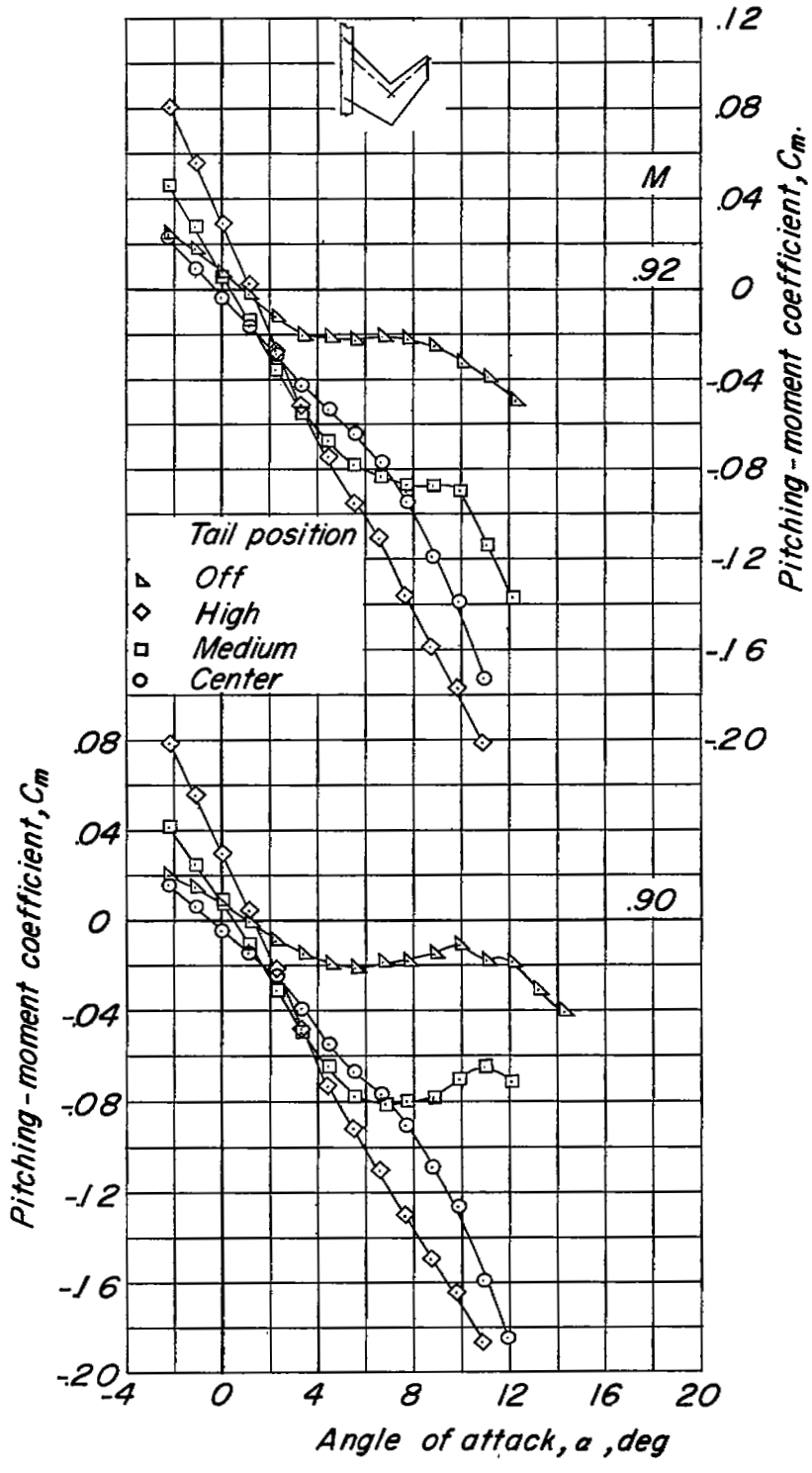

Figure 8.- Continued.

[redacted]

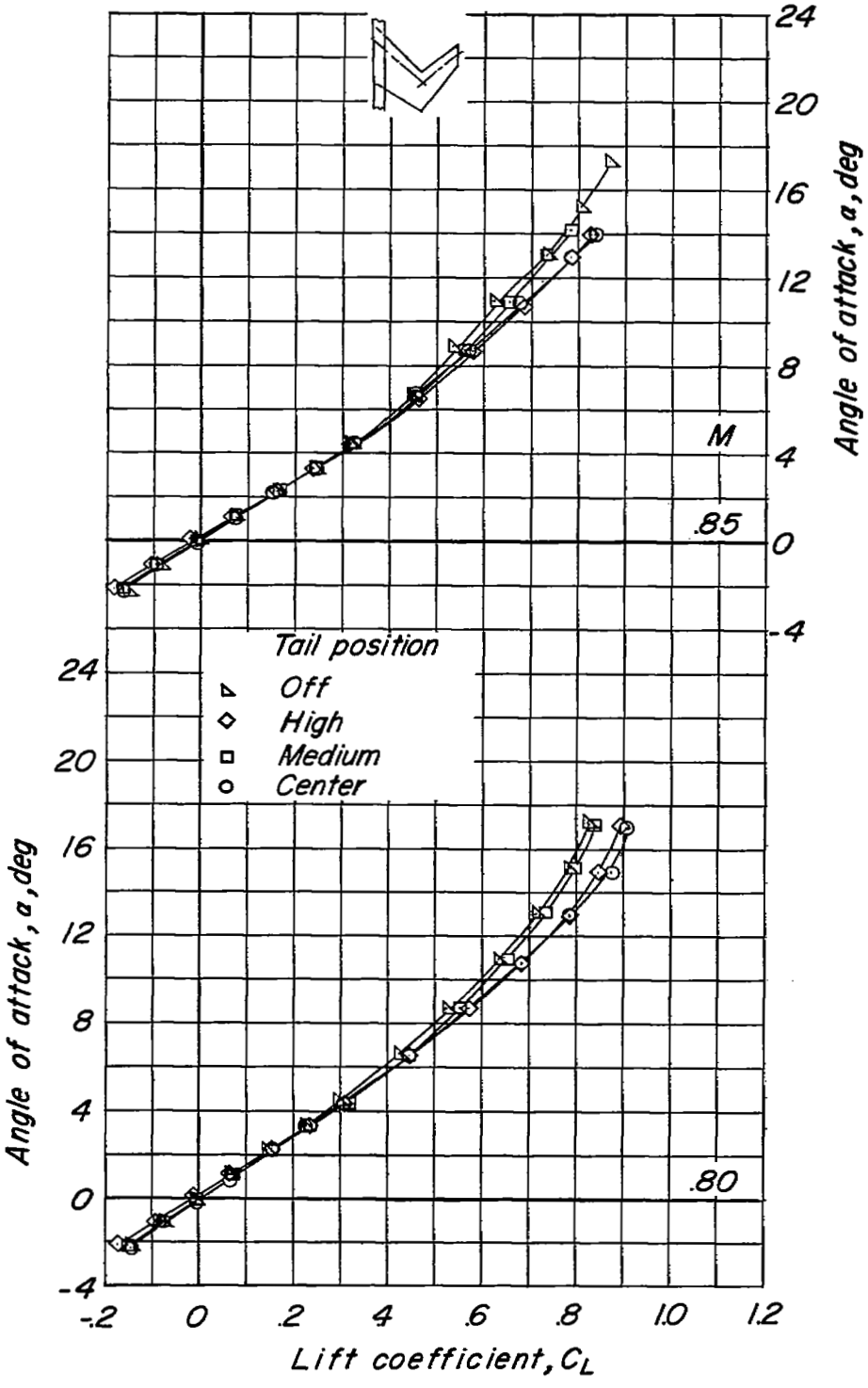

Figure 8.- Continued.

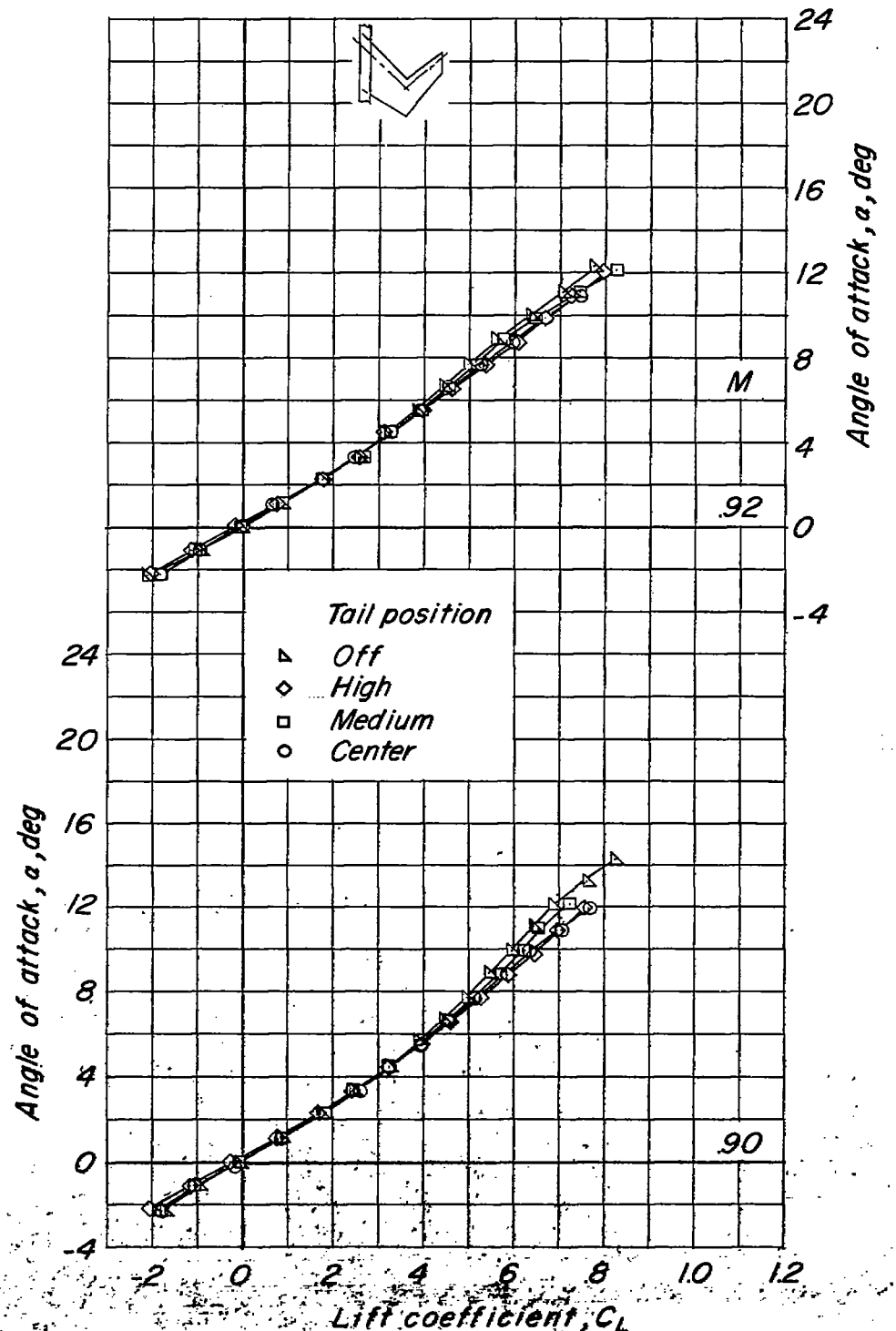

Figure 8.- Continued.

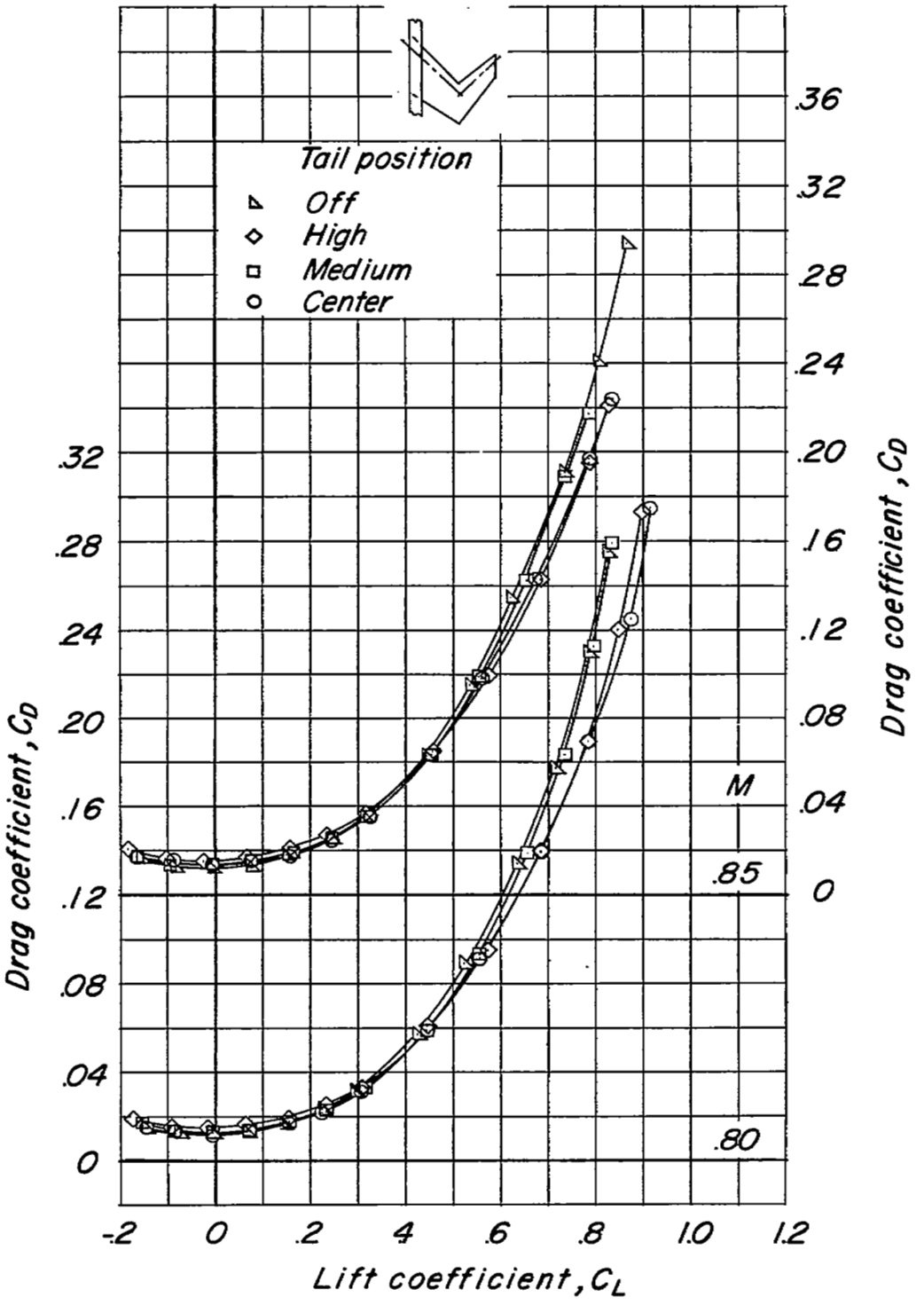

Figure 8.- Continued.

[redacted]

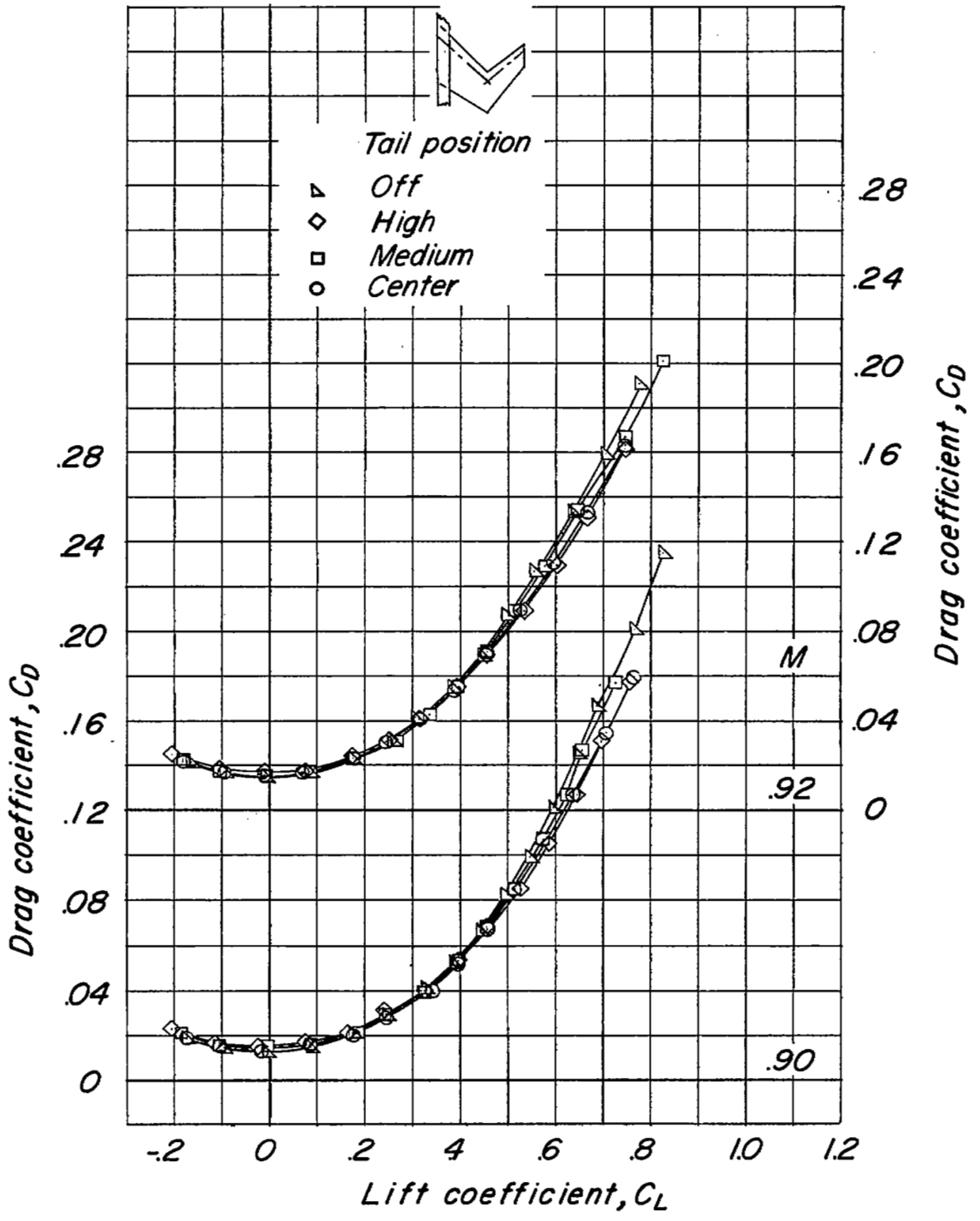

Figure 8.- Concluded.

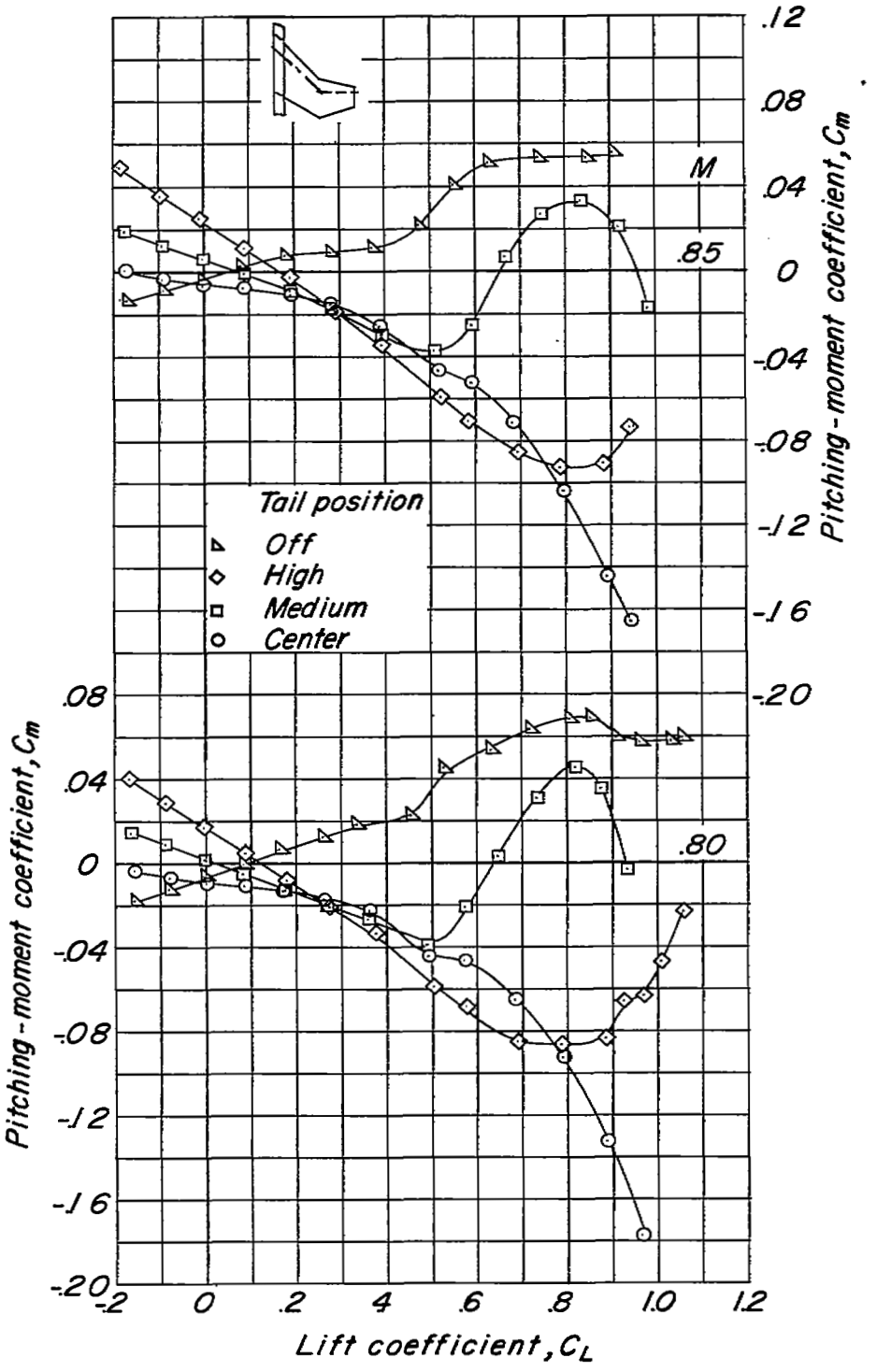

Figure 9.- Longitudinal characteristics of model with cranked-wing plan form.

[redacted]

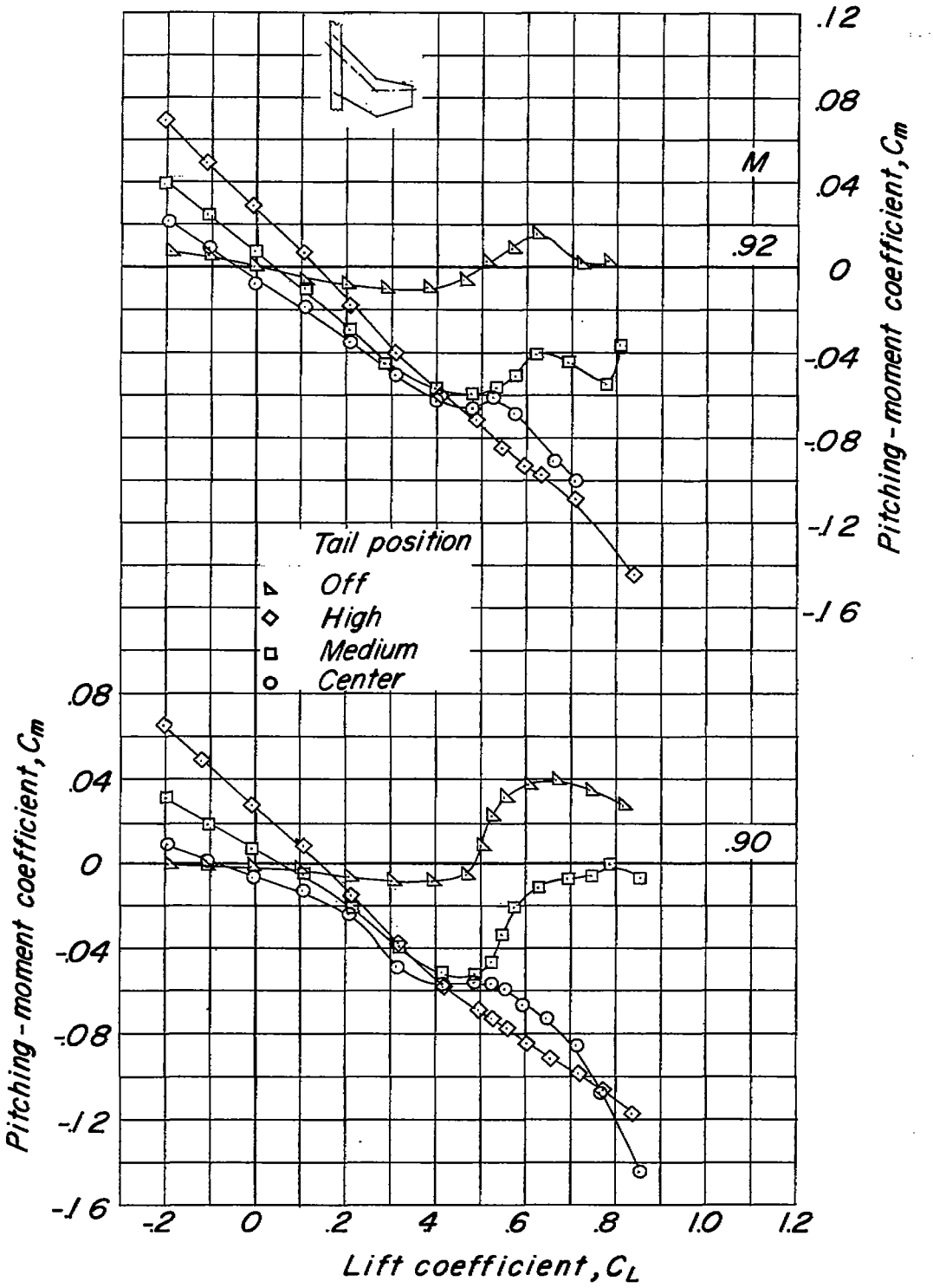

Figure 9.- Continued.

[redacted]

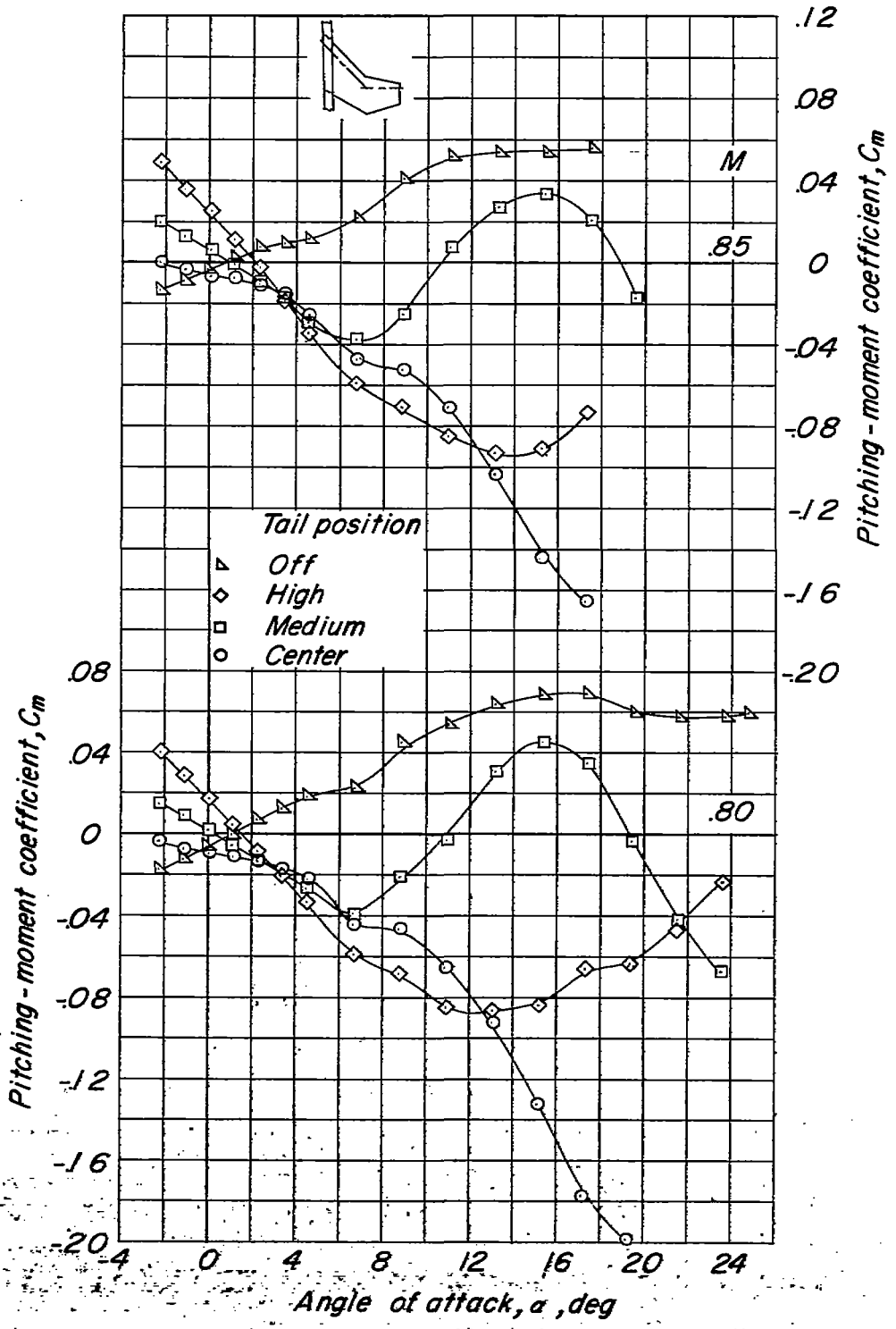

Figure 9.- Continued.

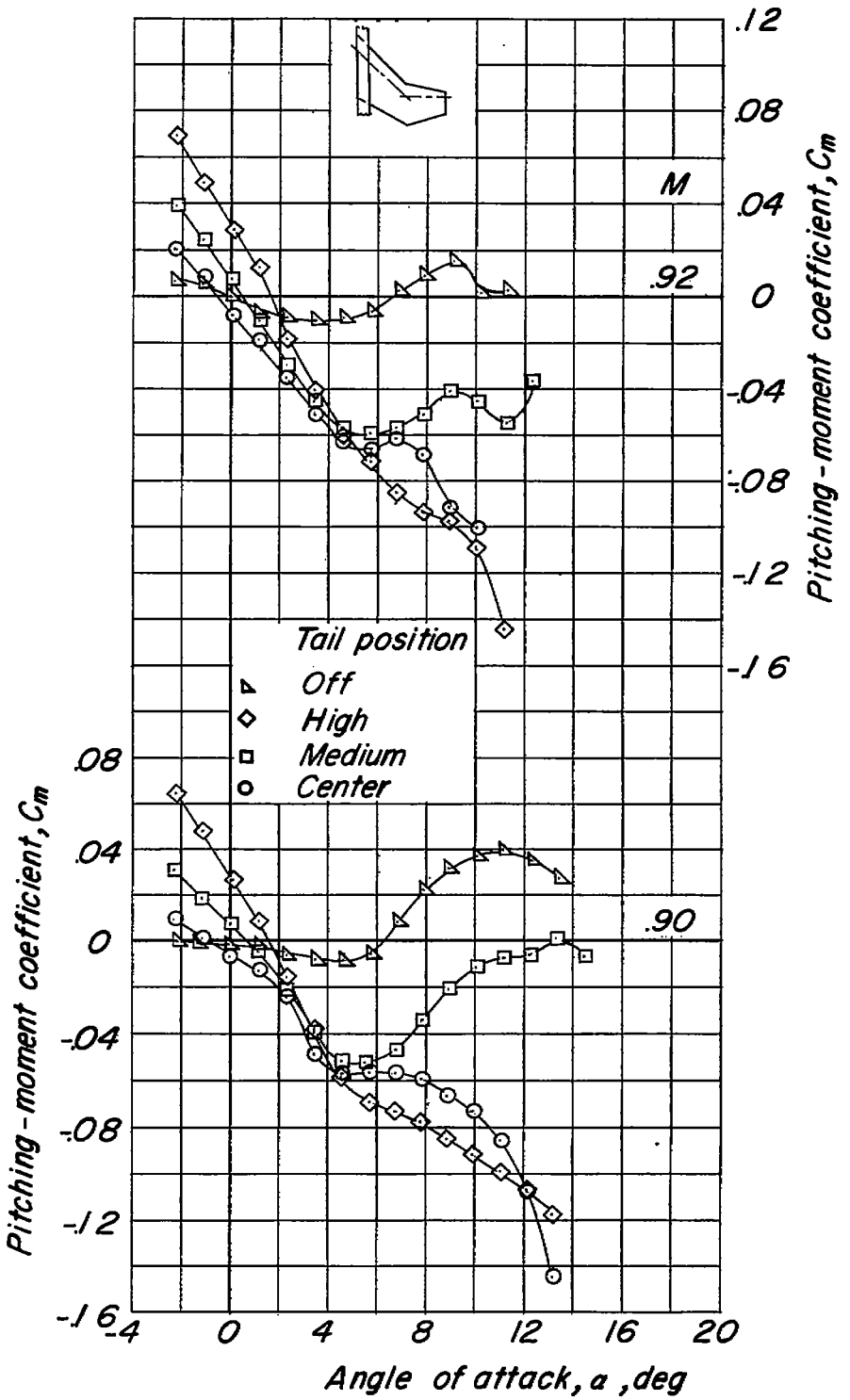

Figure 9.- Continued.

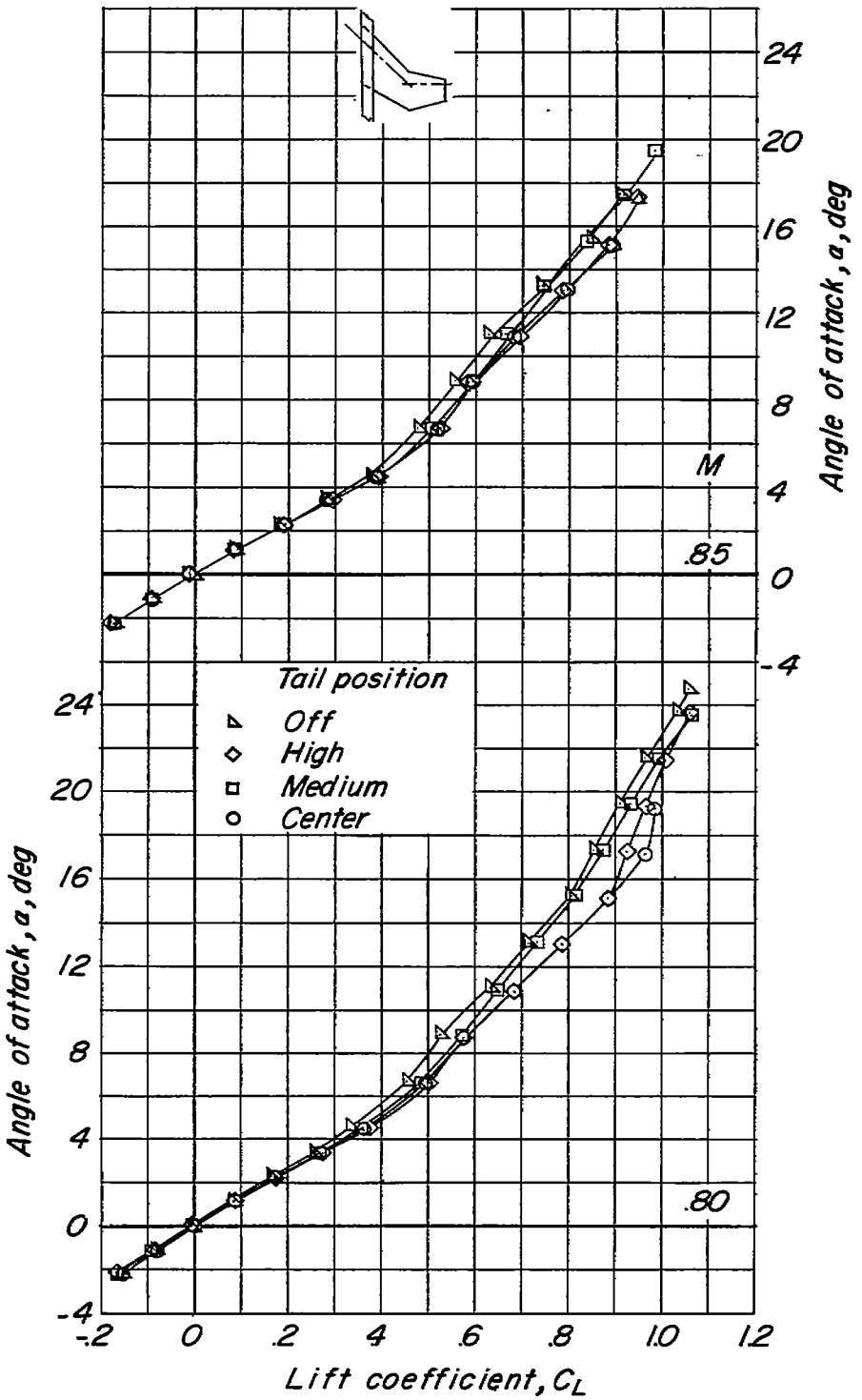

Figure 9.- Continued.

[redacted]

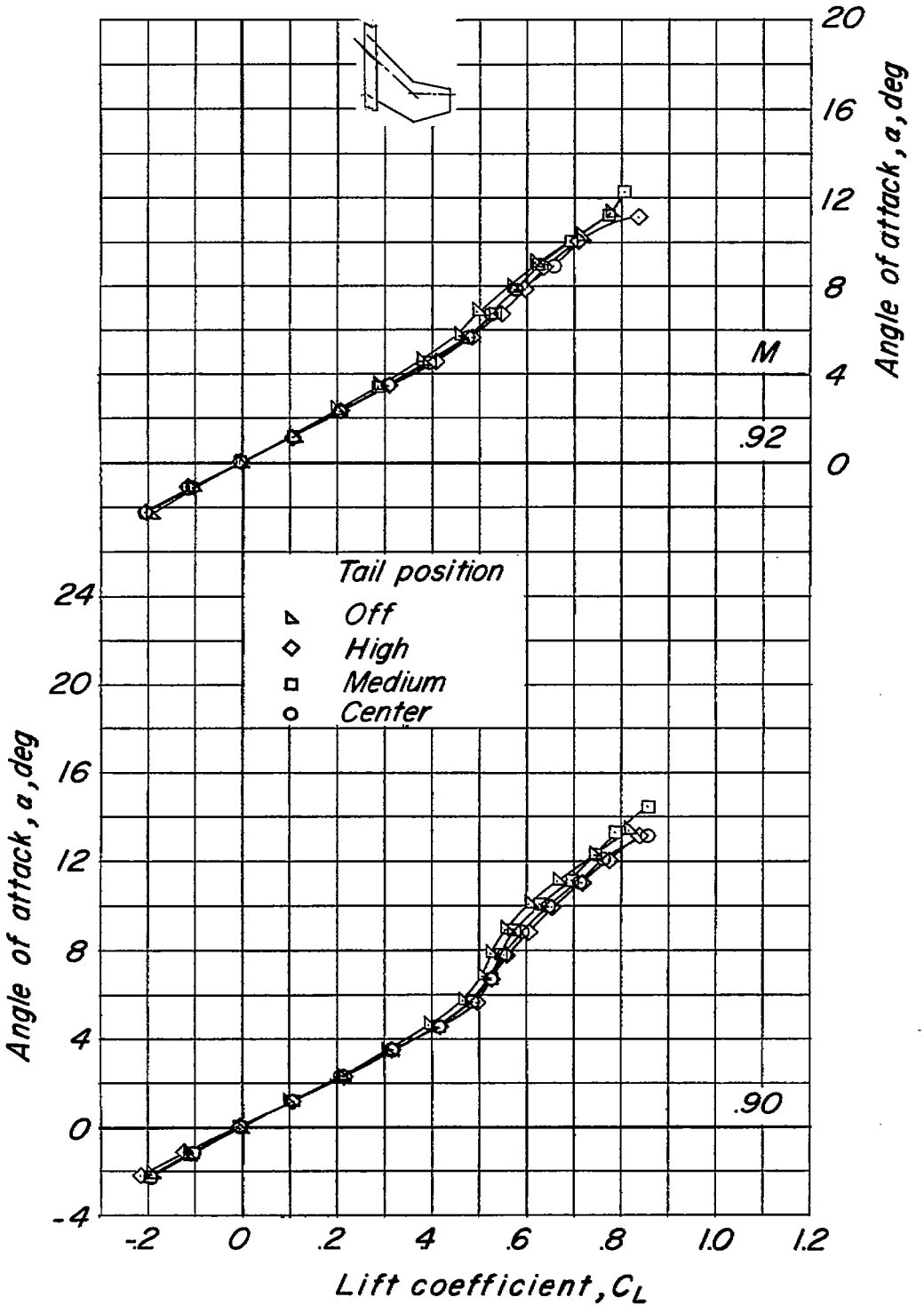

Figure 9.- Continued.

[redacted]

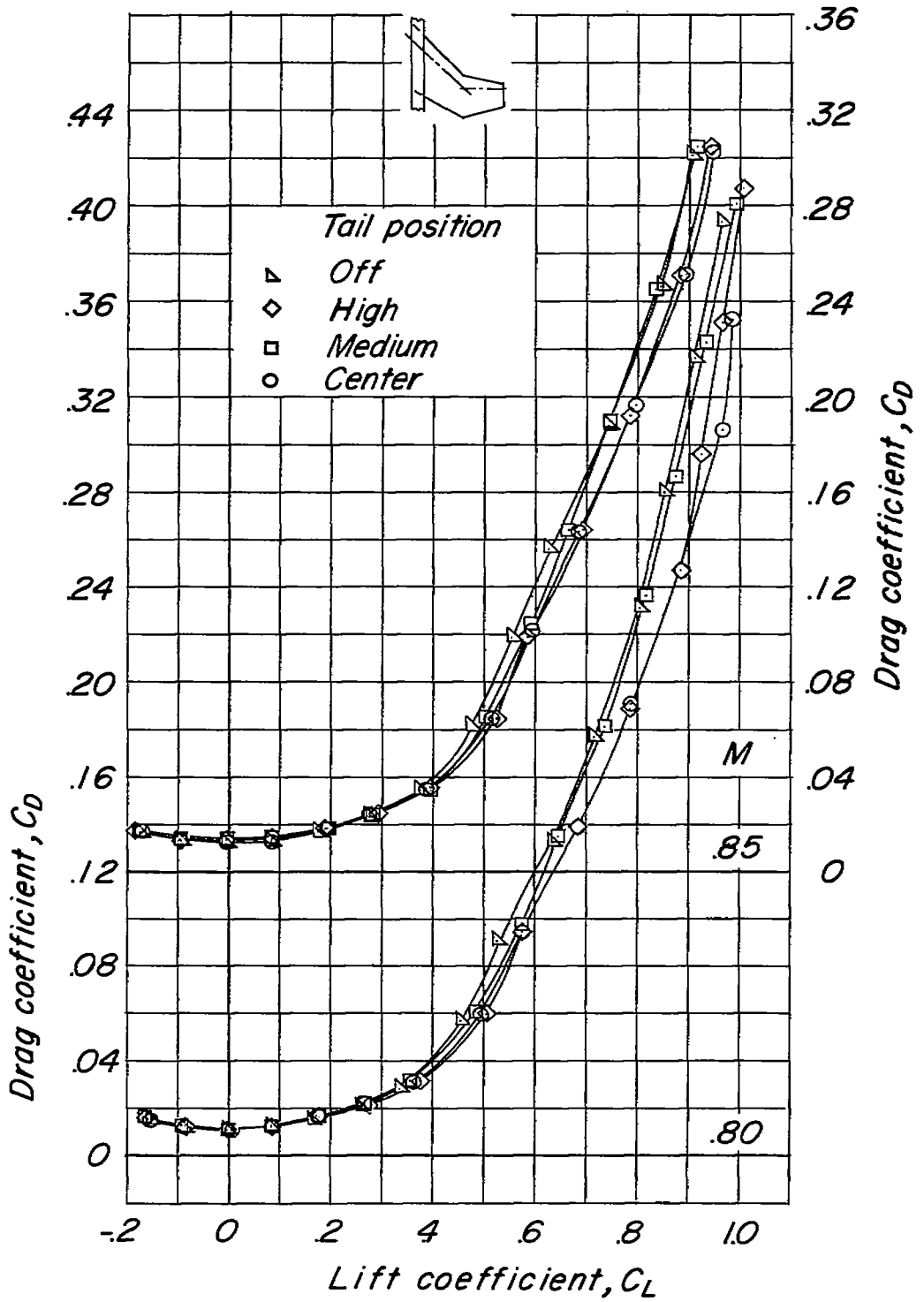

Figure 9.- Continued.

[redacted]

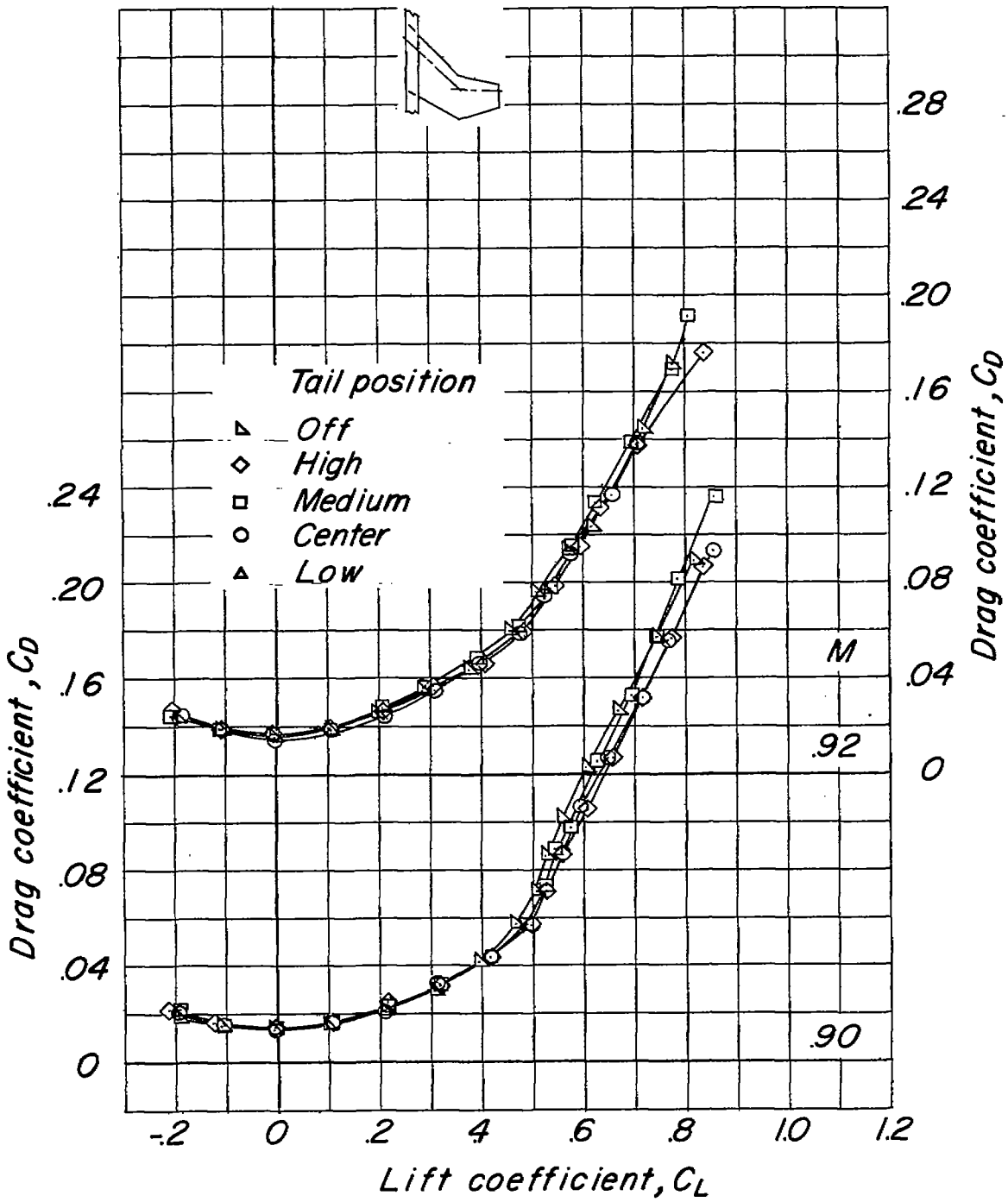

Figure 9.- Concluded.

[redacted]

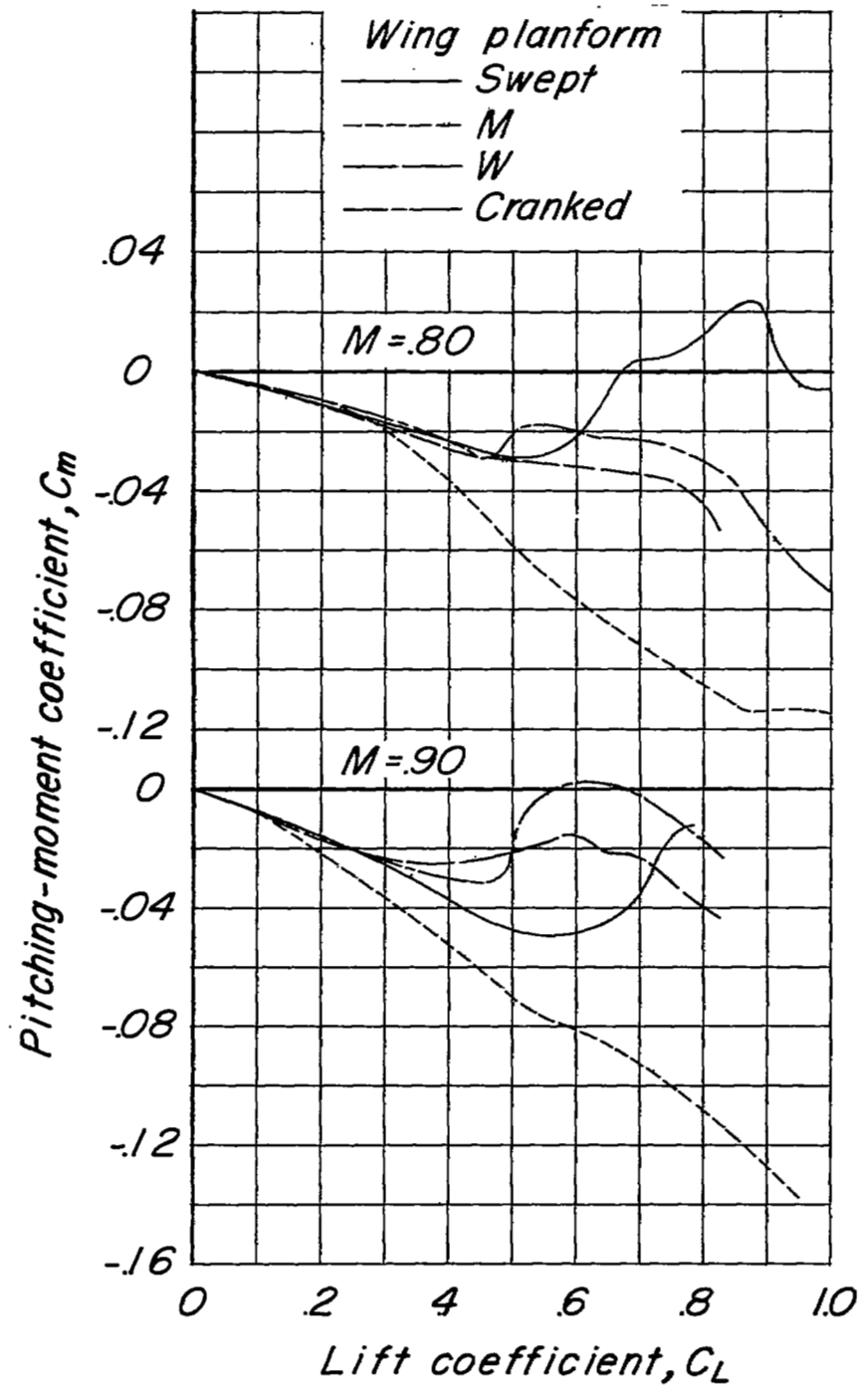

(a) Horizontal tail off.

Figure 10.- Longitudinal stability characteristics of the test model with various wing plan forms adjusted to a $0.05\bar{c}$ static margin at M = 0.80.

[redacted]

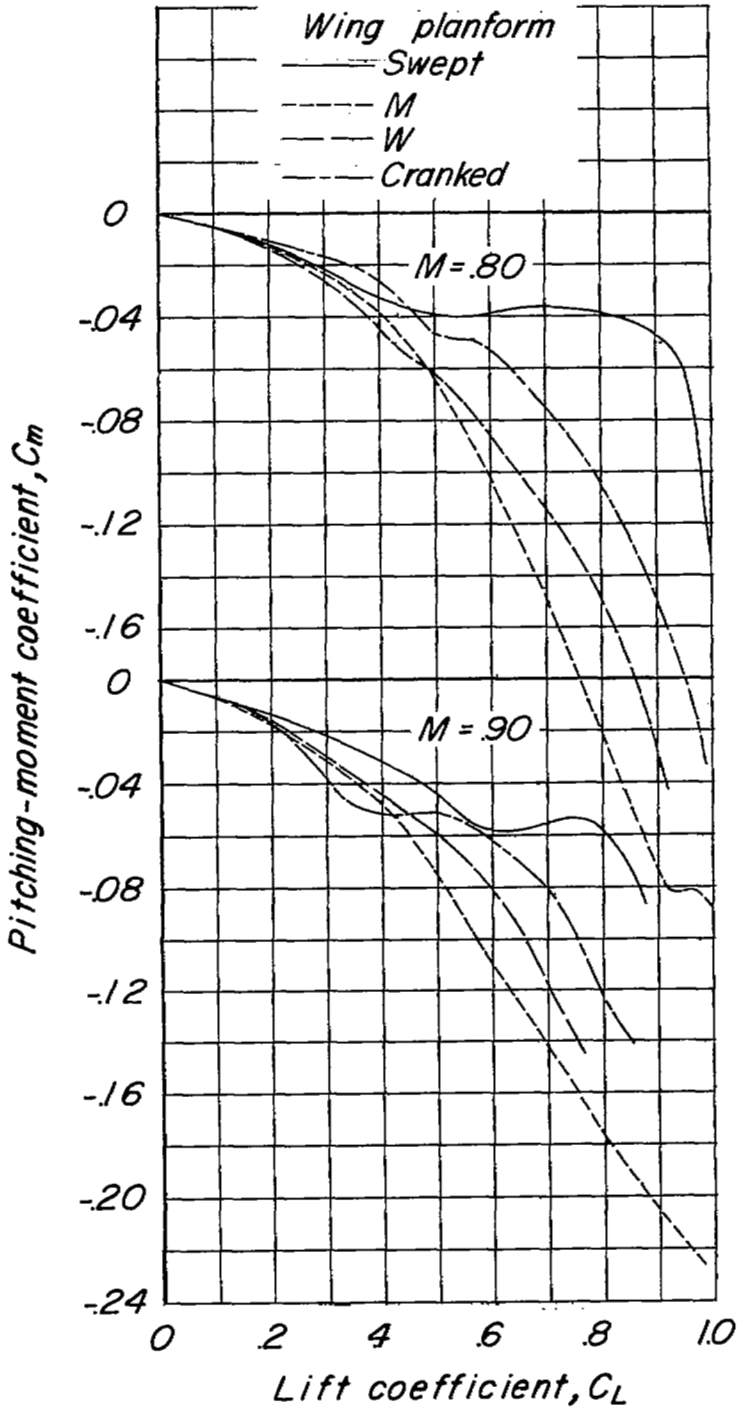

(b) Center tail.

Figure 10.- Continued.

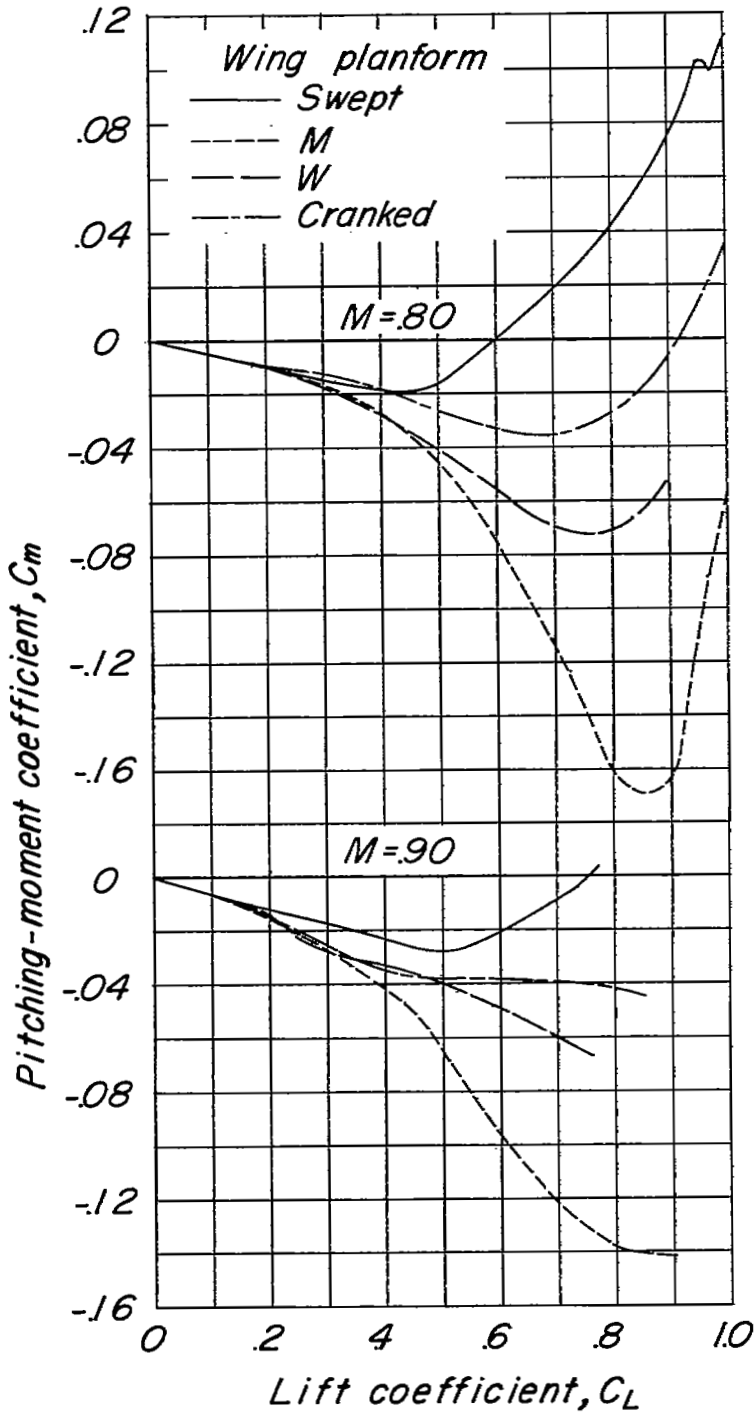

(c) High tail.

Figure 10.- Concluded.

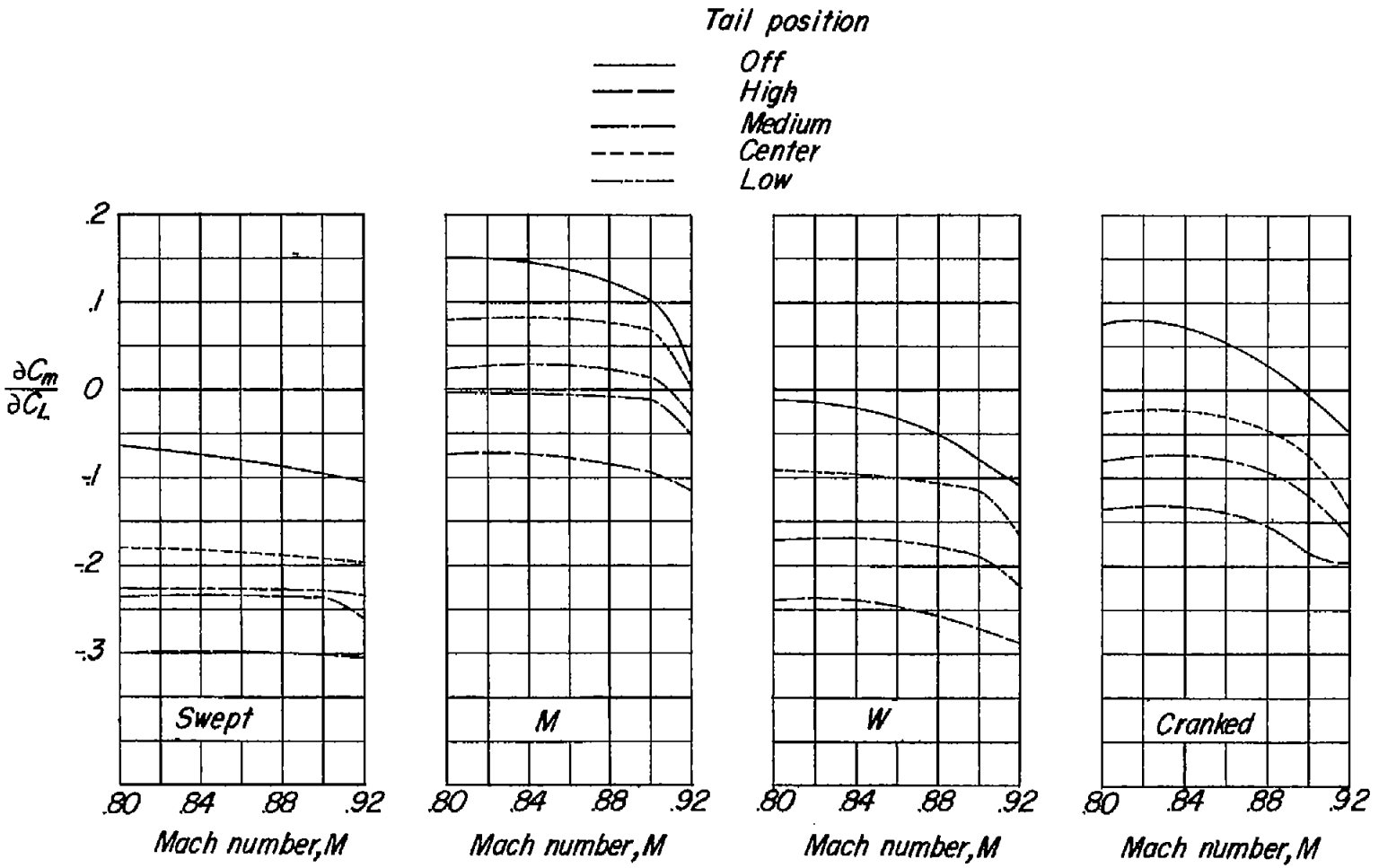

Figure 11.- Variation of $\partial C_m/\partial C_L$ with Mach number for the composite-wings model with various horizontal-tail locations. $C_L = 0$.

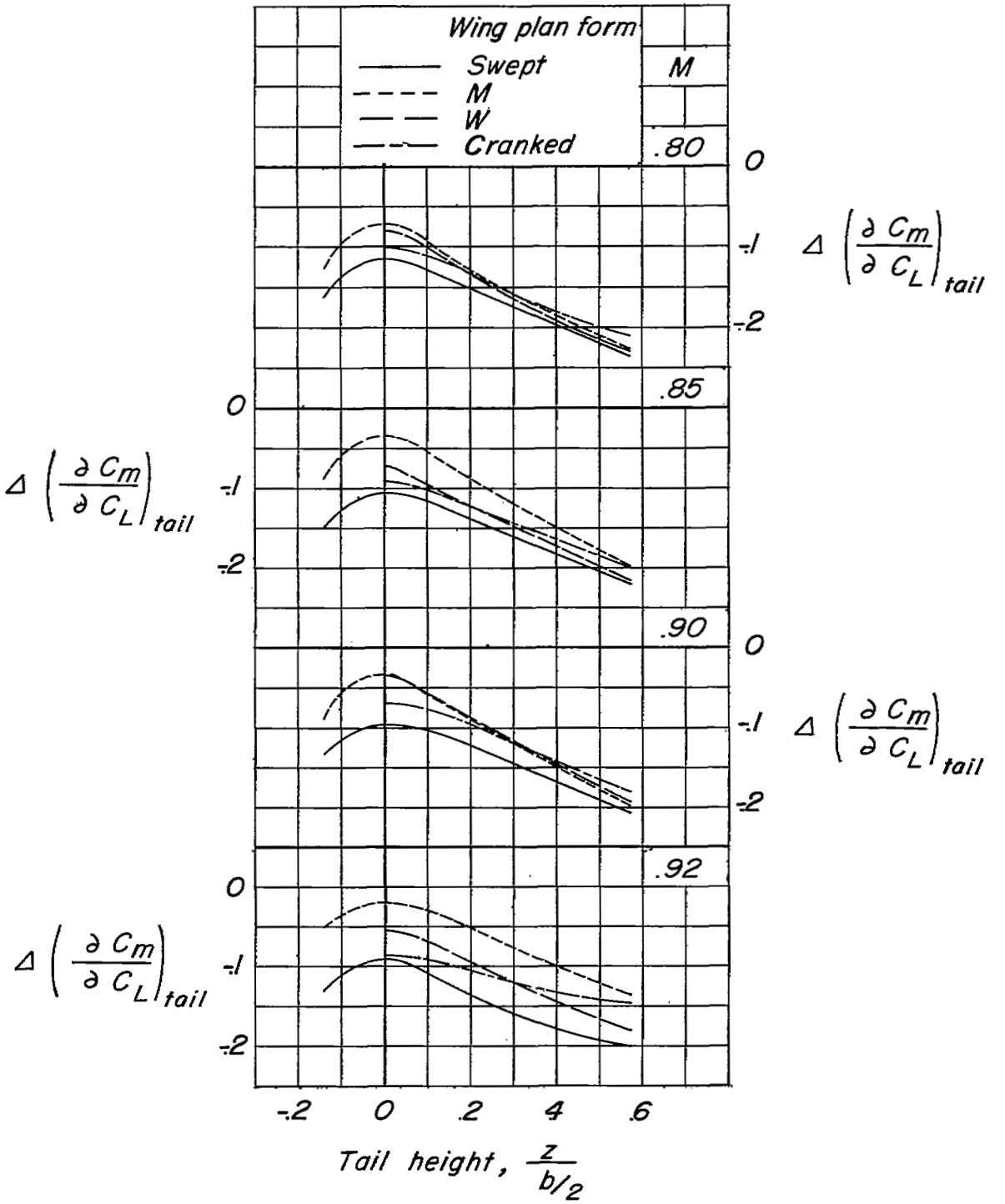

Figure 12.- Effect of tail height on the horizontal-tail contribution to the stability parameter of the composite-wing models. $C_L = 0$.

[redacted]

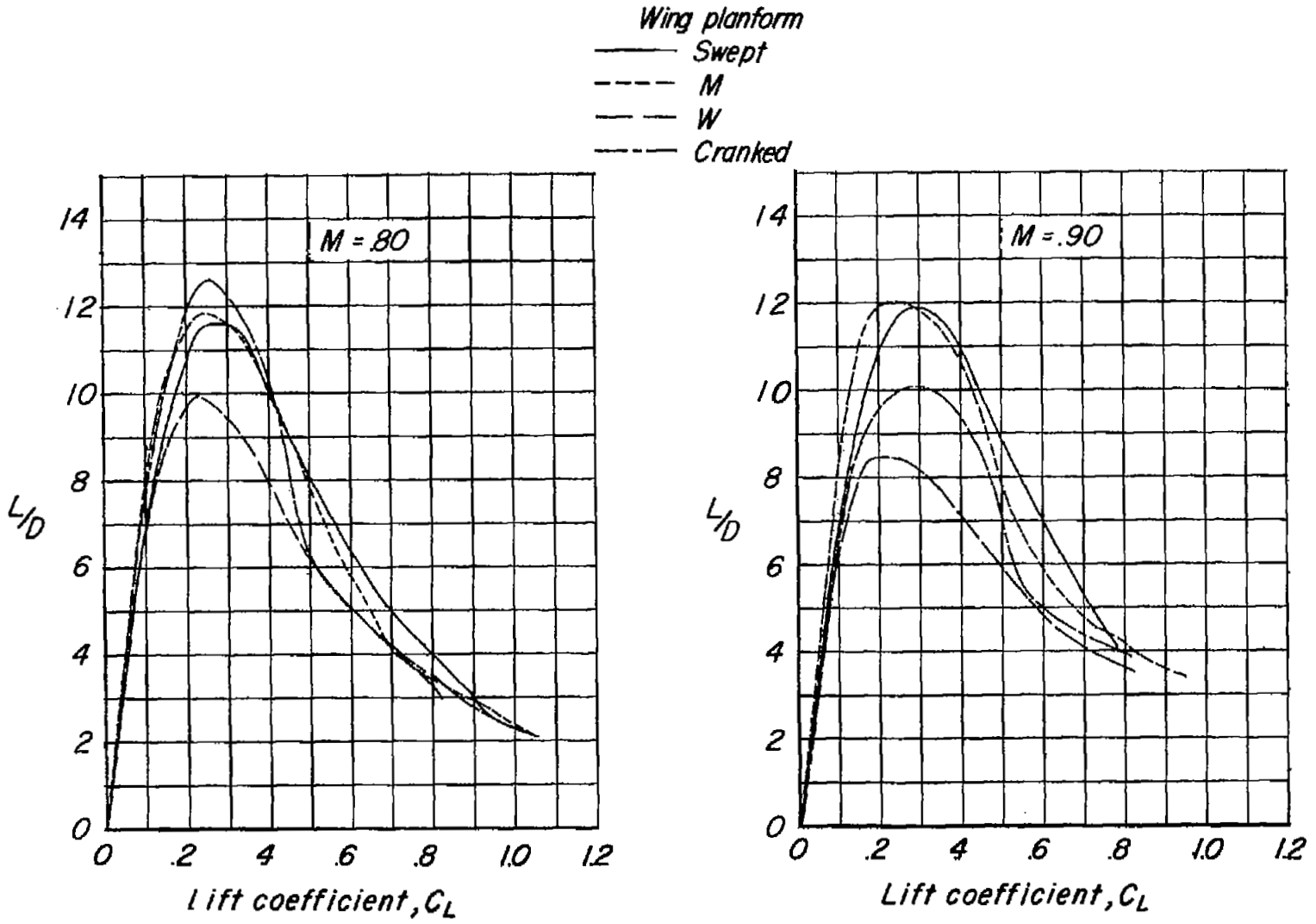

Figure 13.- Lift-drag ratios of the test model with various wing plan forms. Horizontal tail off.

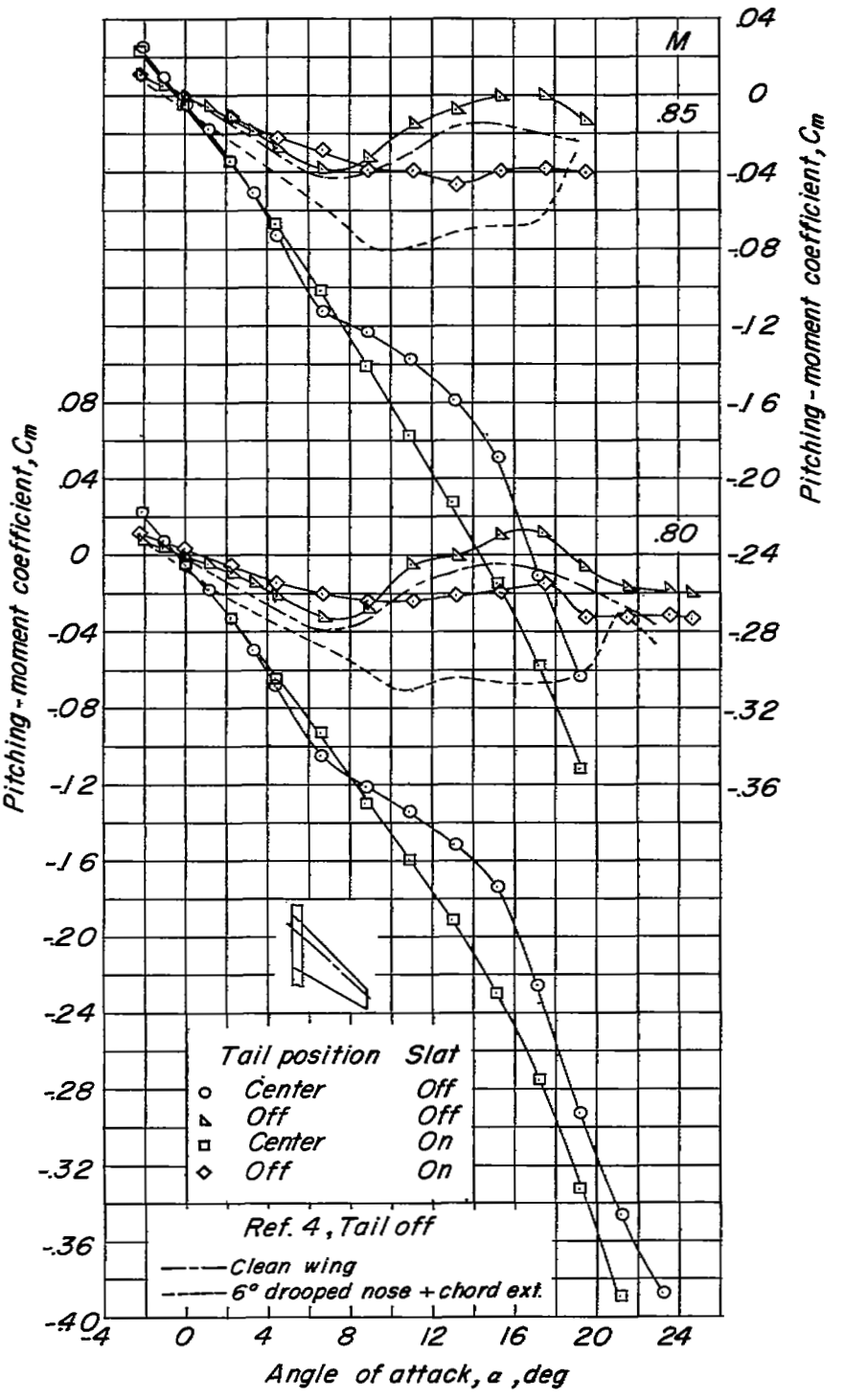

Figure 14.- Longitudinal characteristics of the swept wing with a 0.10$\bar{c}$ slat located on the outboard 35 percent of the swept-wing semispan.

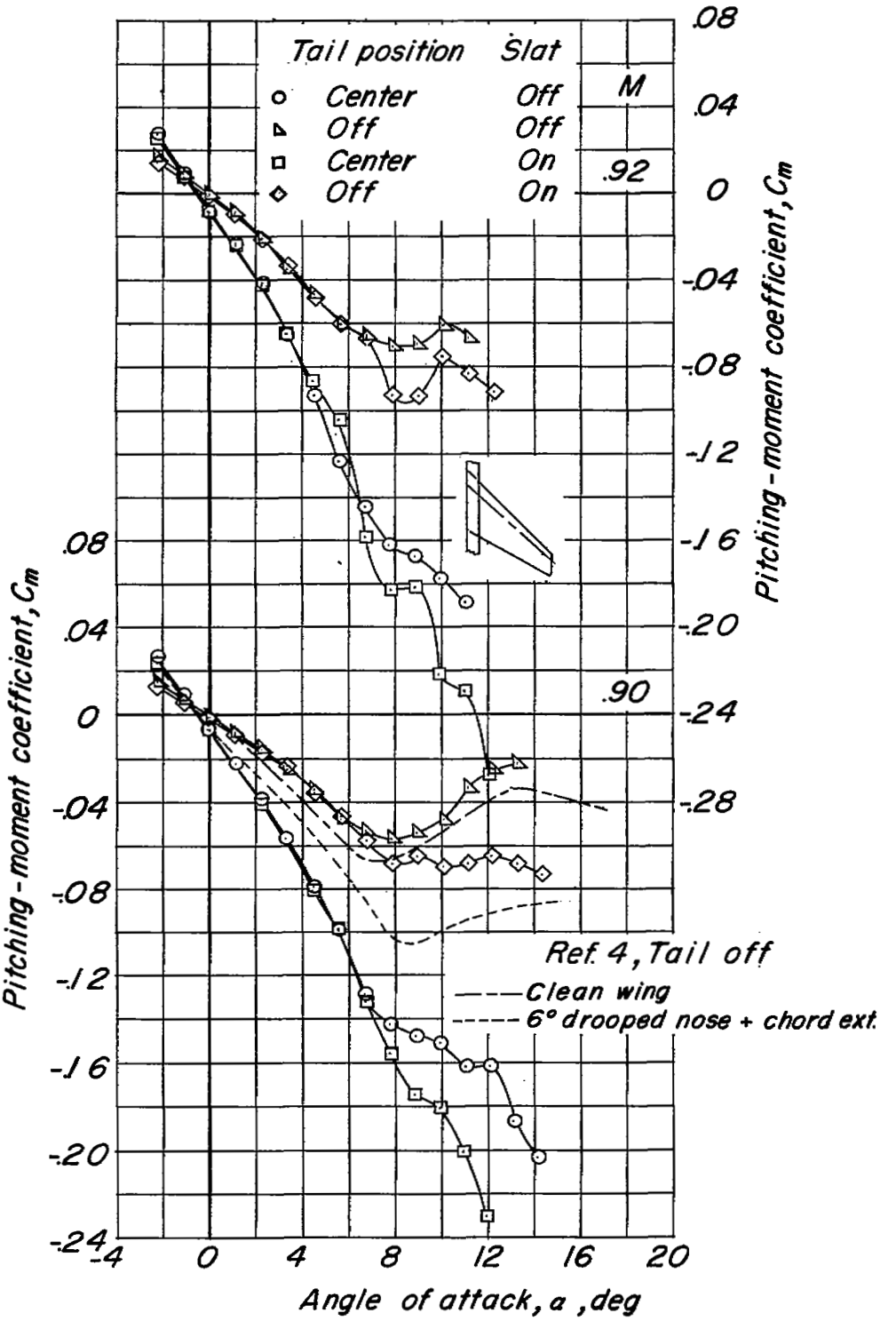

Figure 14.- Continued.

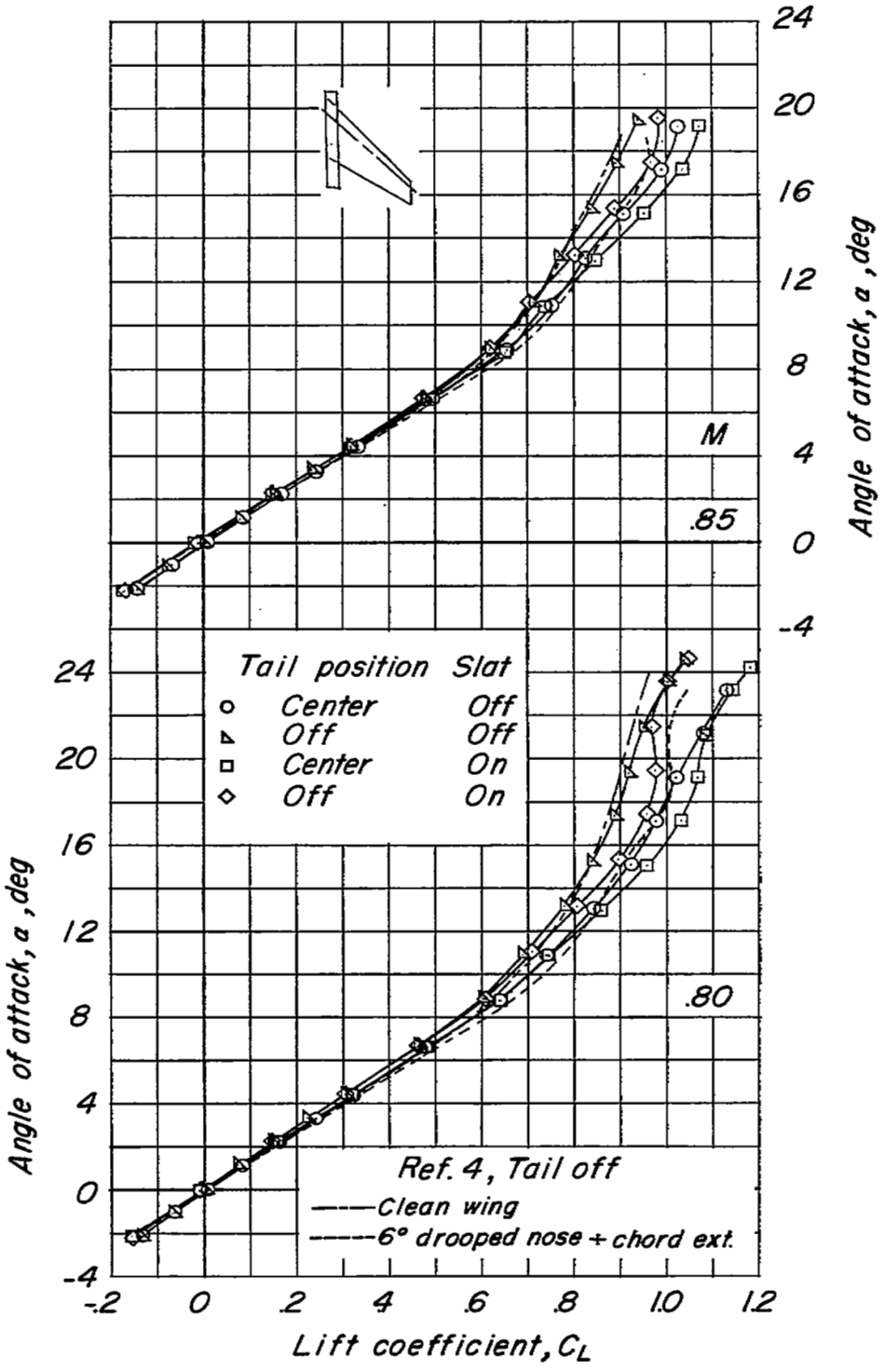

Figure 14.- Continued.

[redacted]

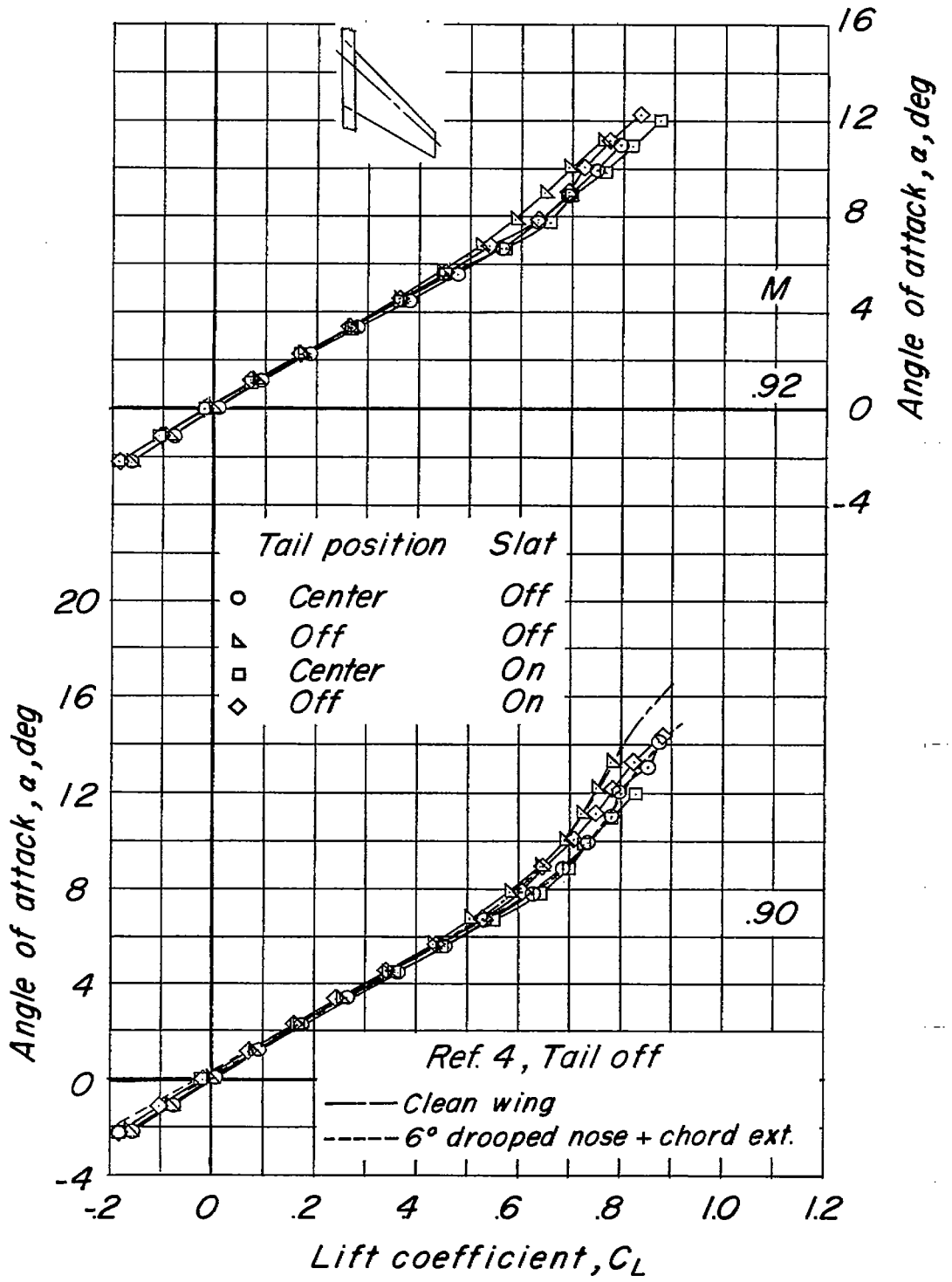

Figure 14.- Continued.

[redacted]

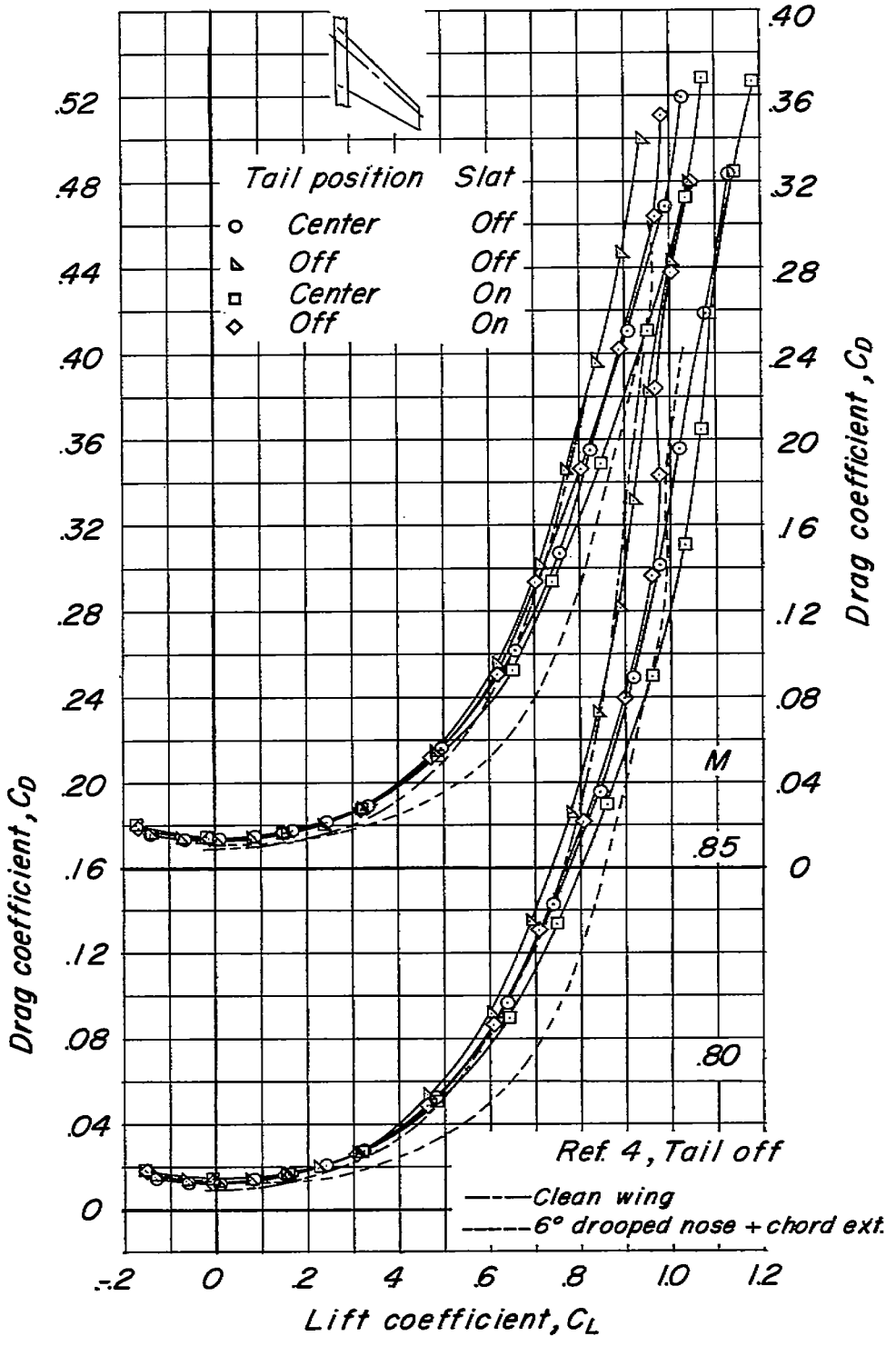

Figure 14.- Continued.

[redacted]

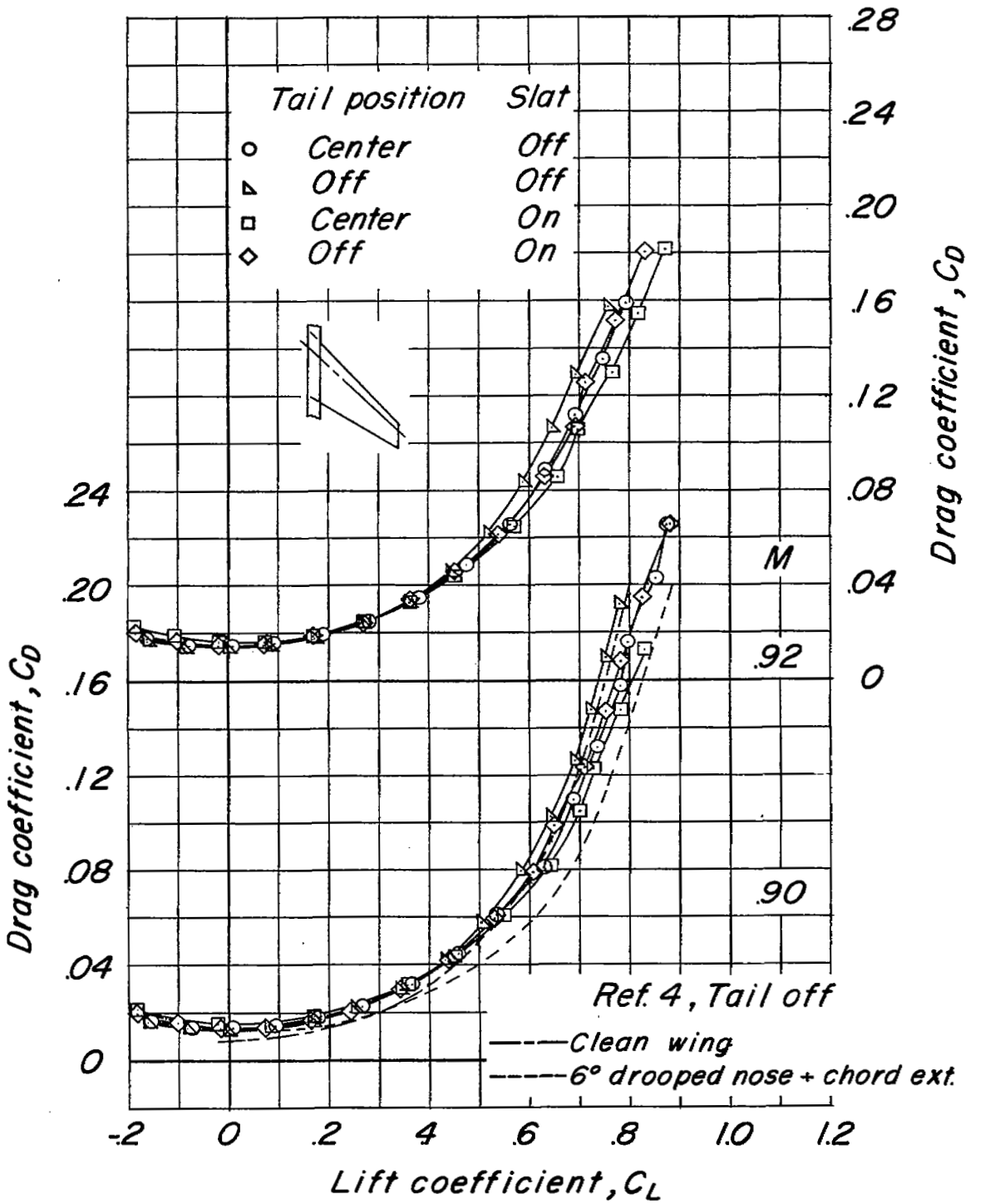

Figure 14.- Concluded.

[redacted]

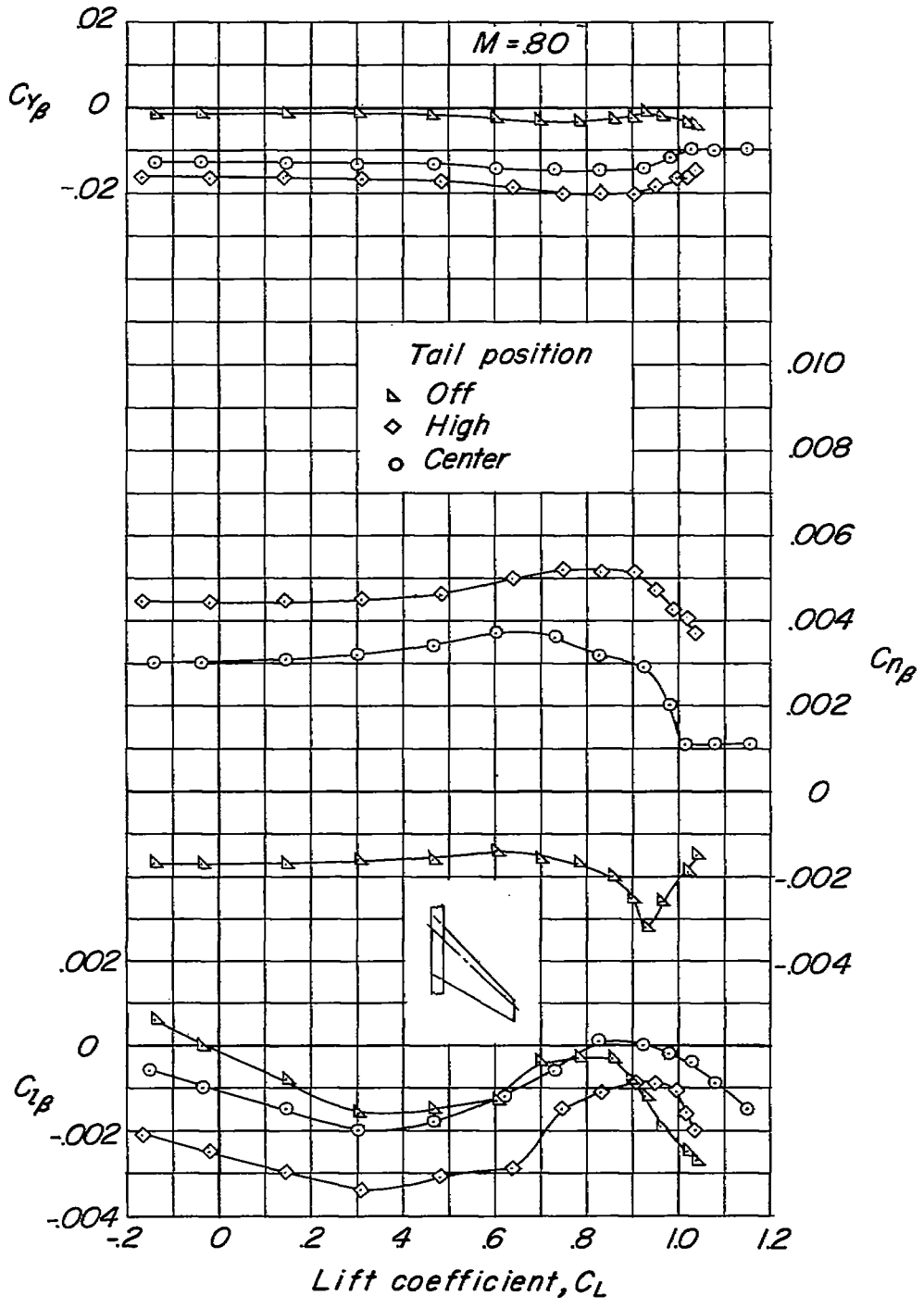

(a) M = 0.80.

Figure 15.- Lateral parameter characteristics of the swept-wing model.

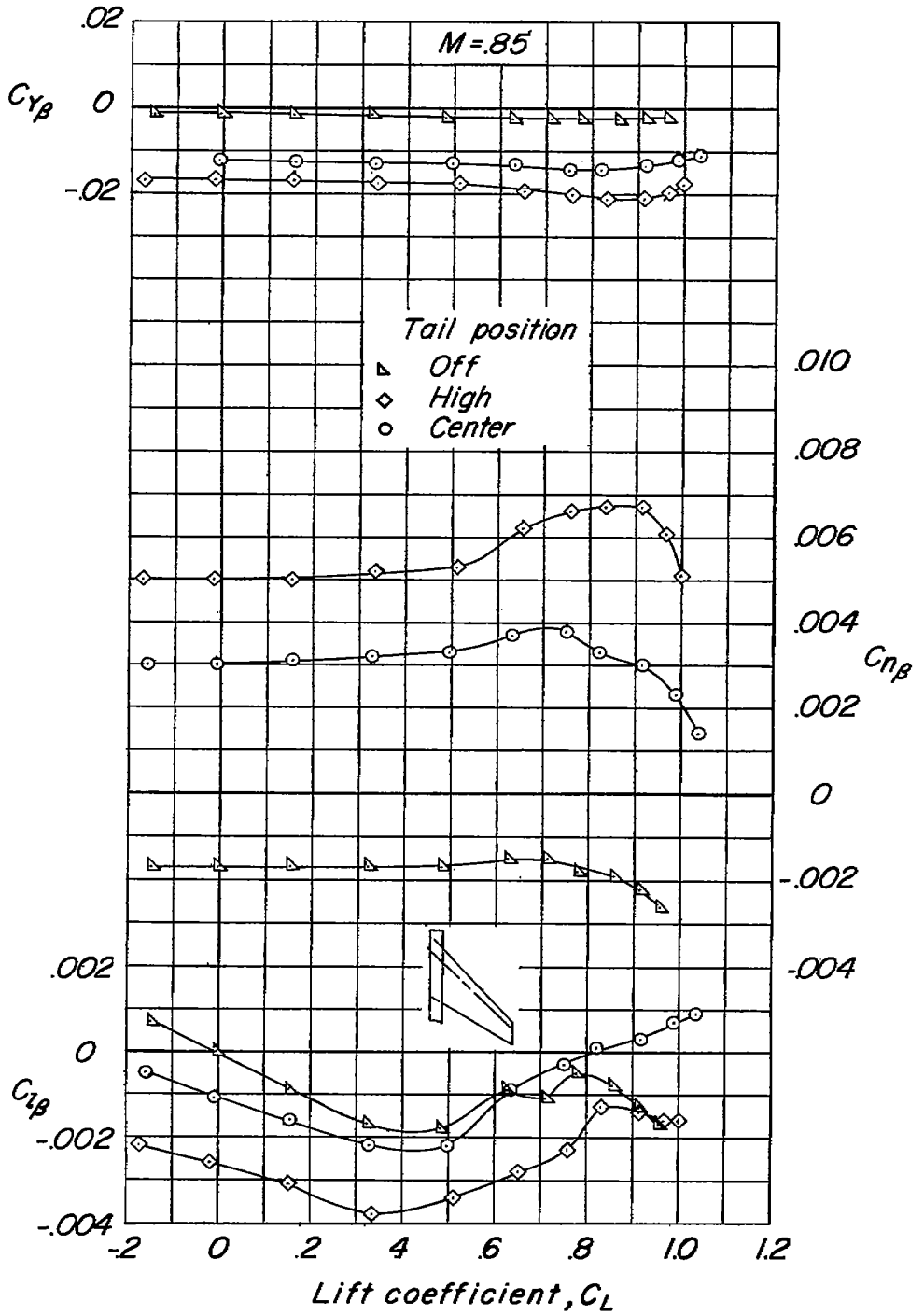

(b) M = 0.85.

Figure 15.- Continued.

[redacted]

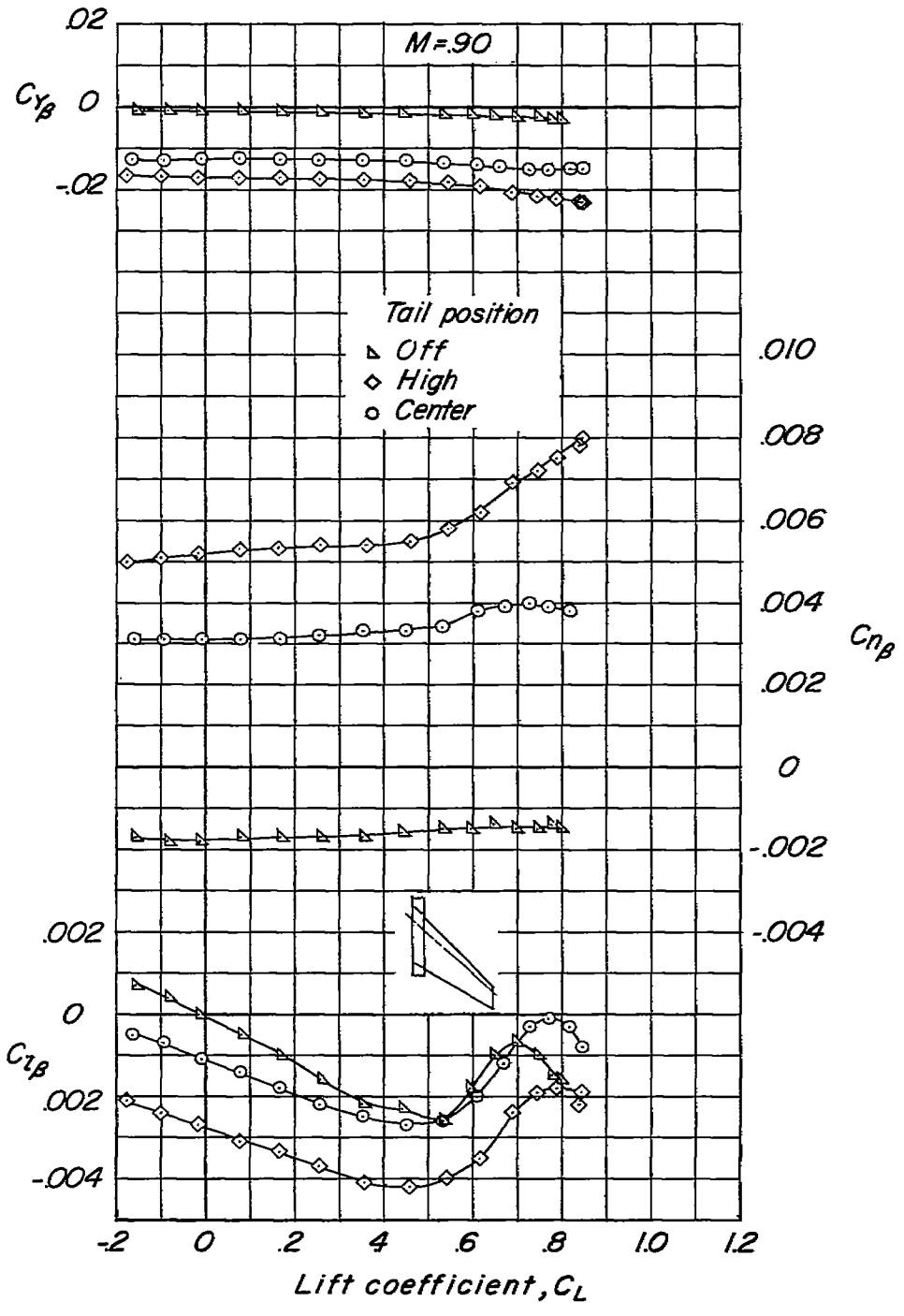

(c) M = 0.90.

Figure 15.- Continued.

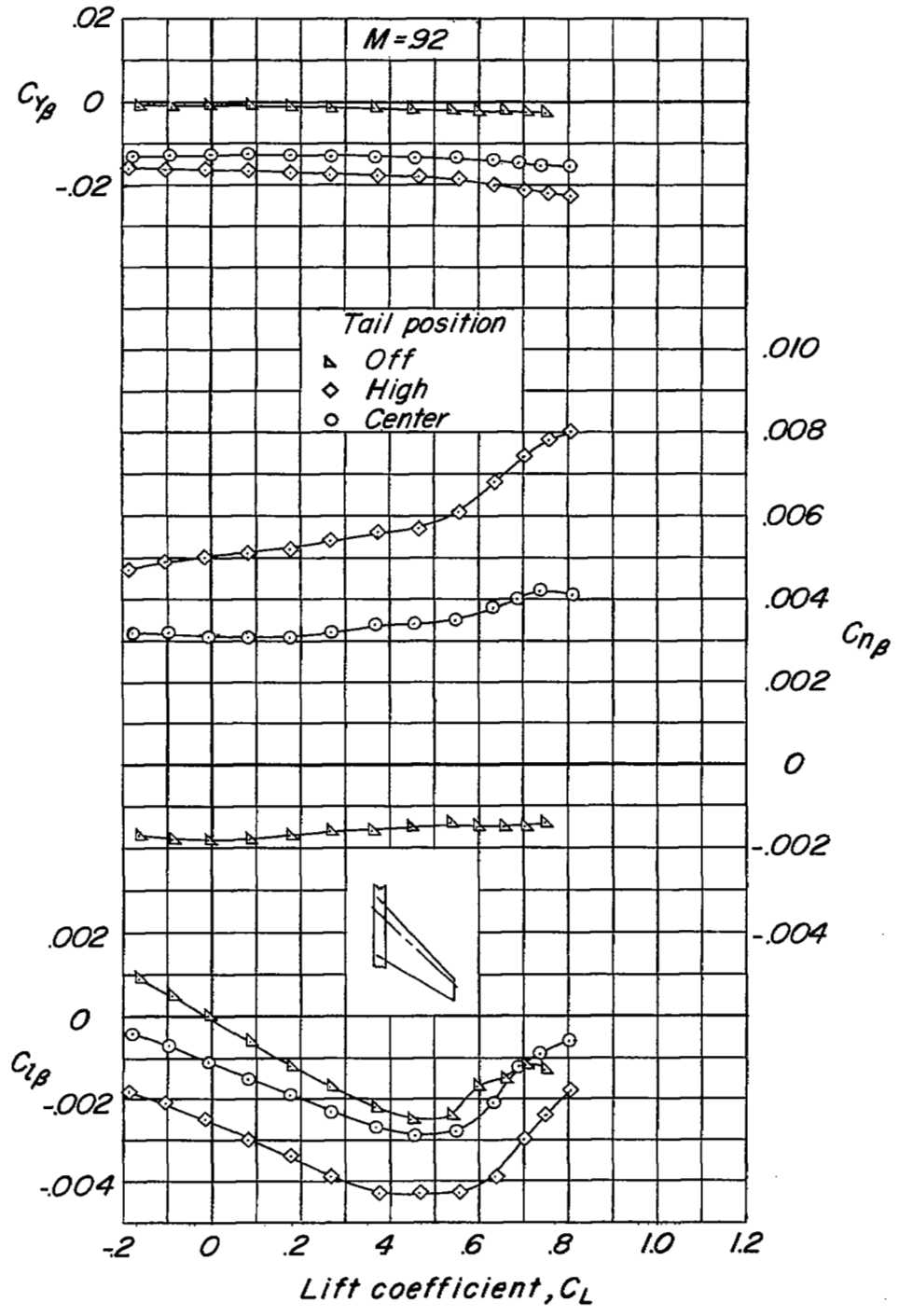

(d) M = 0.92.

Figure 15.- Concluded.

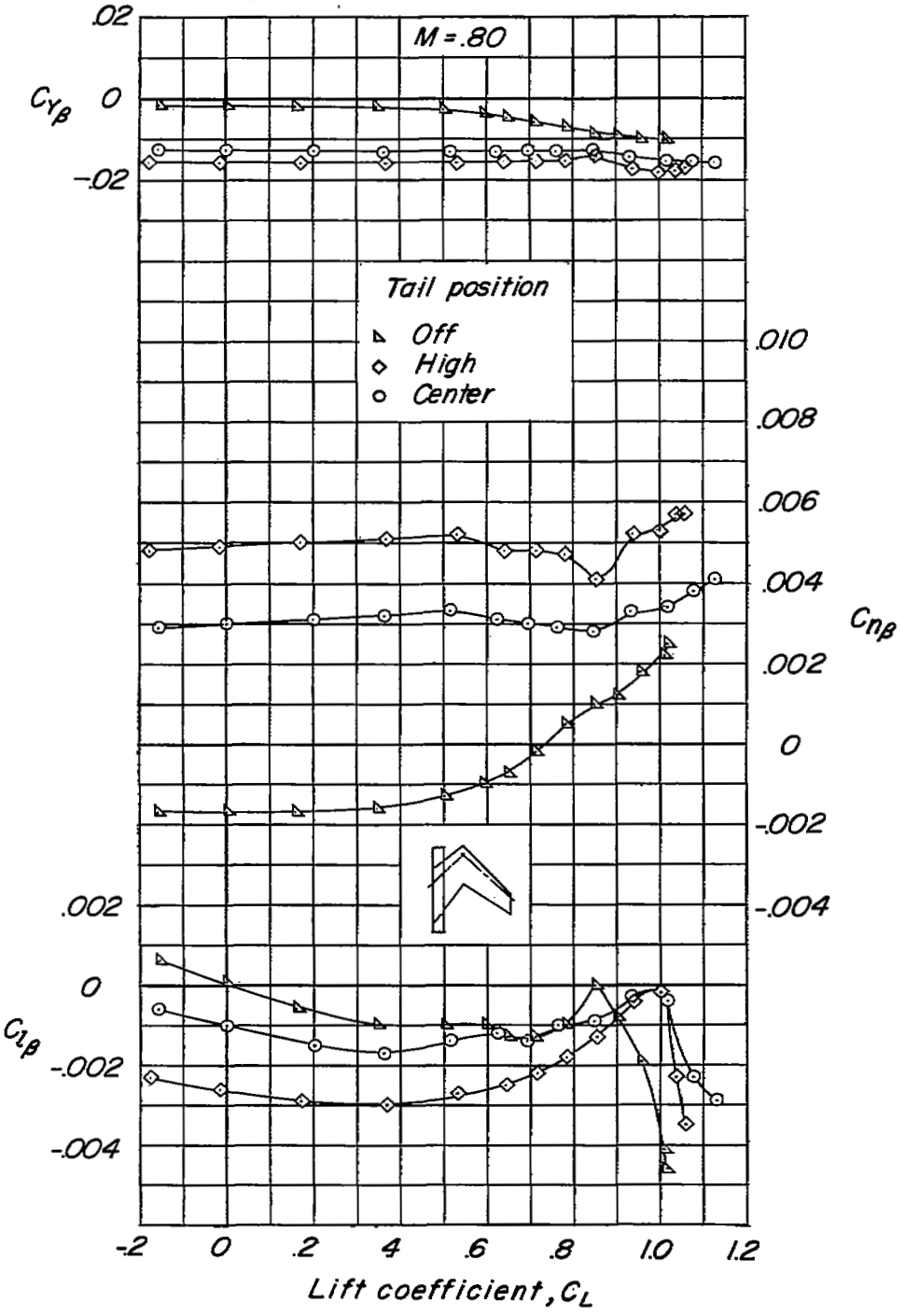

(a) M = 0.80.

Figure 16.- Lateral parameter characteristics of the M-wing model.

[redacted]

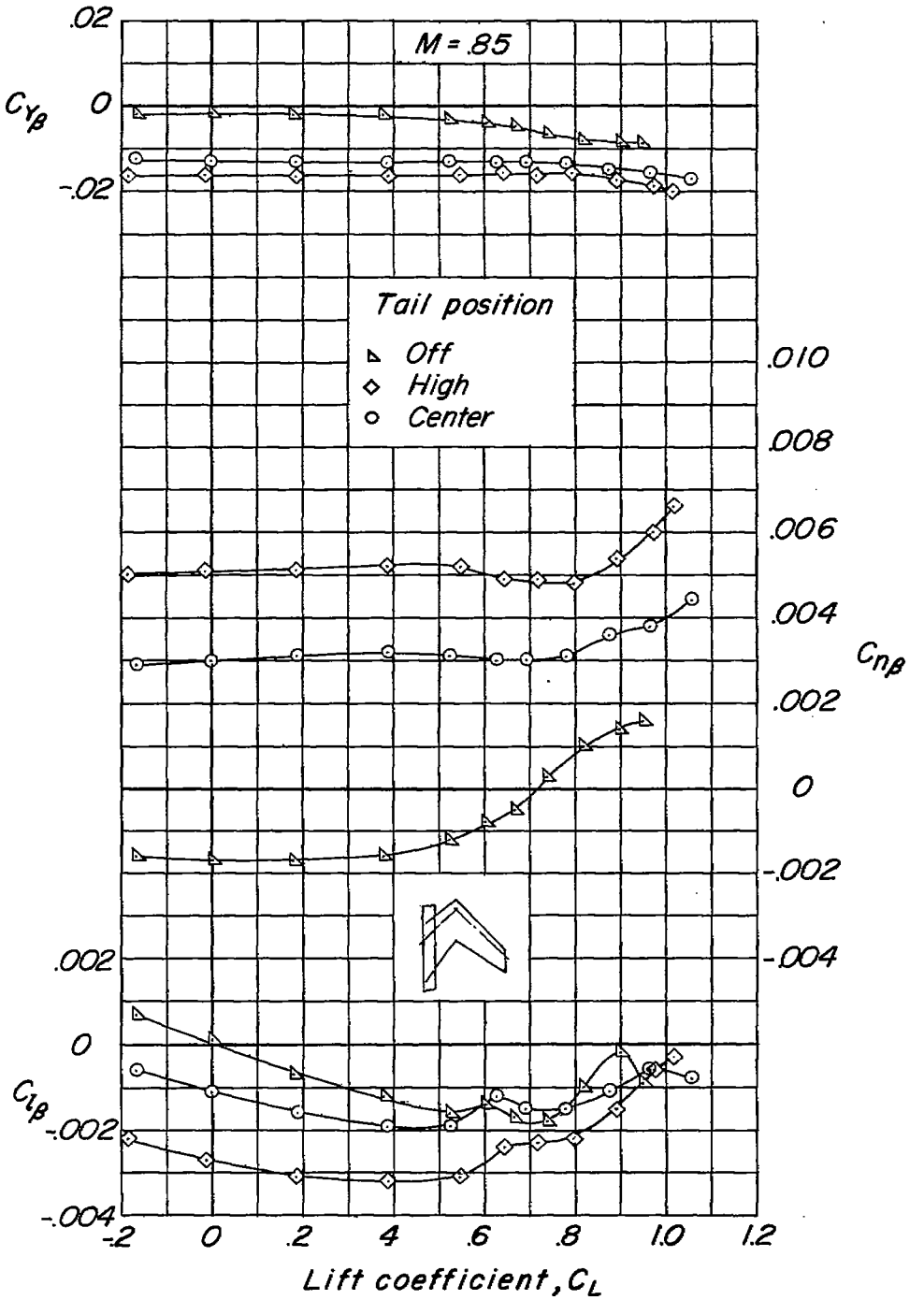

(b) M = 0.85.

Figure 16.- Continued.

[redacted]

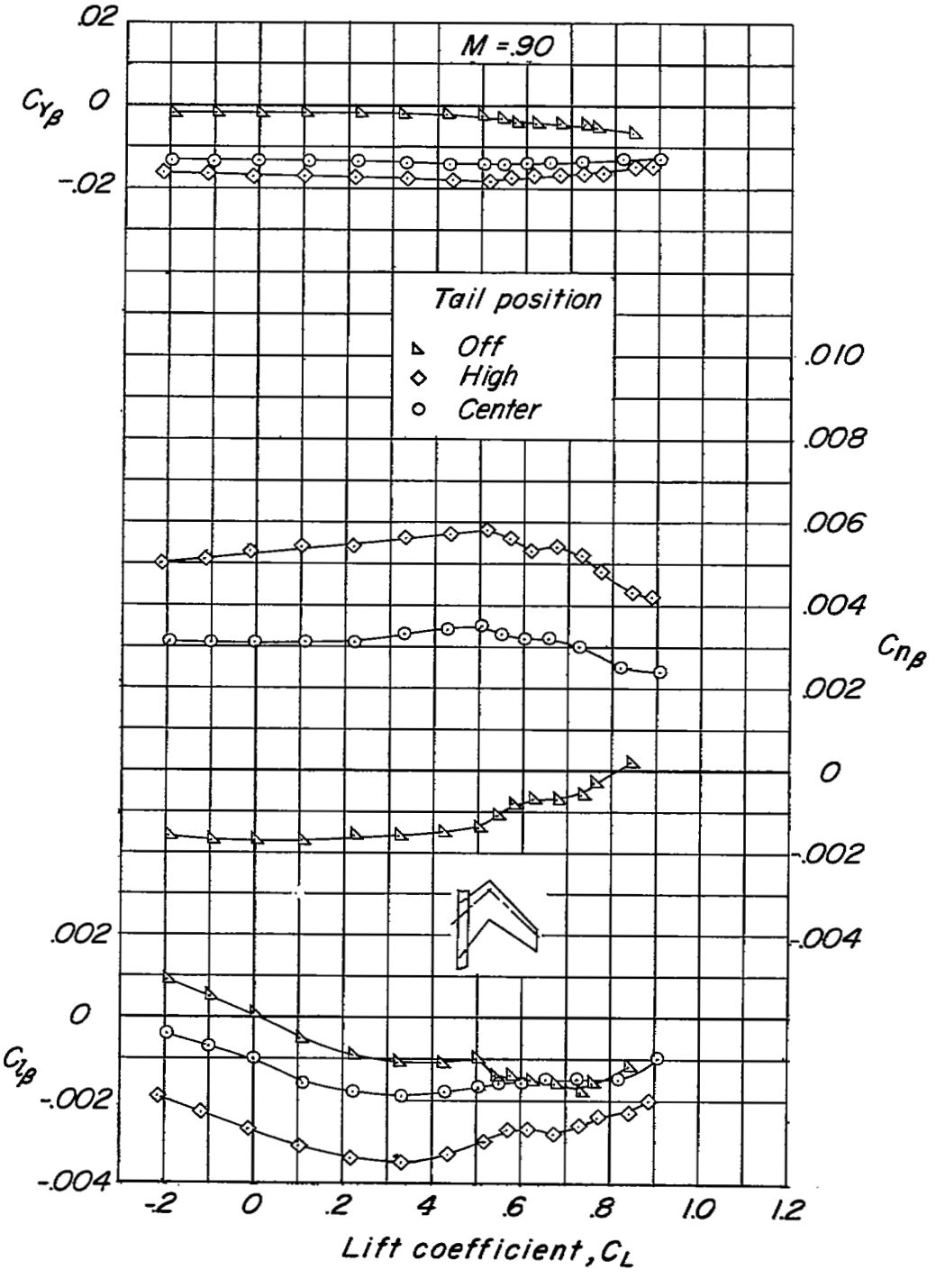

(c) M = 0.90.

Figure 16.- Continued.

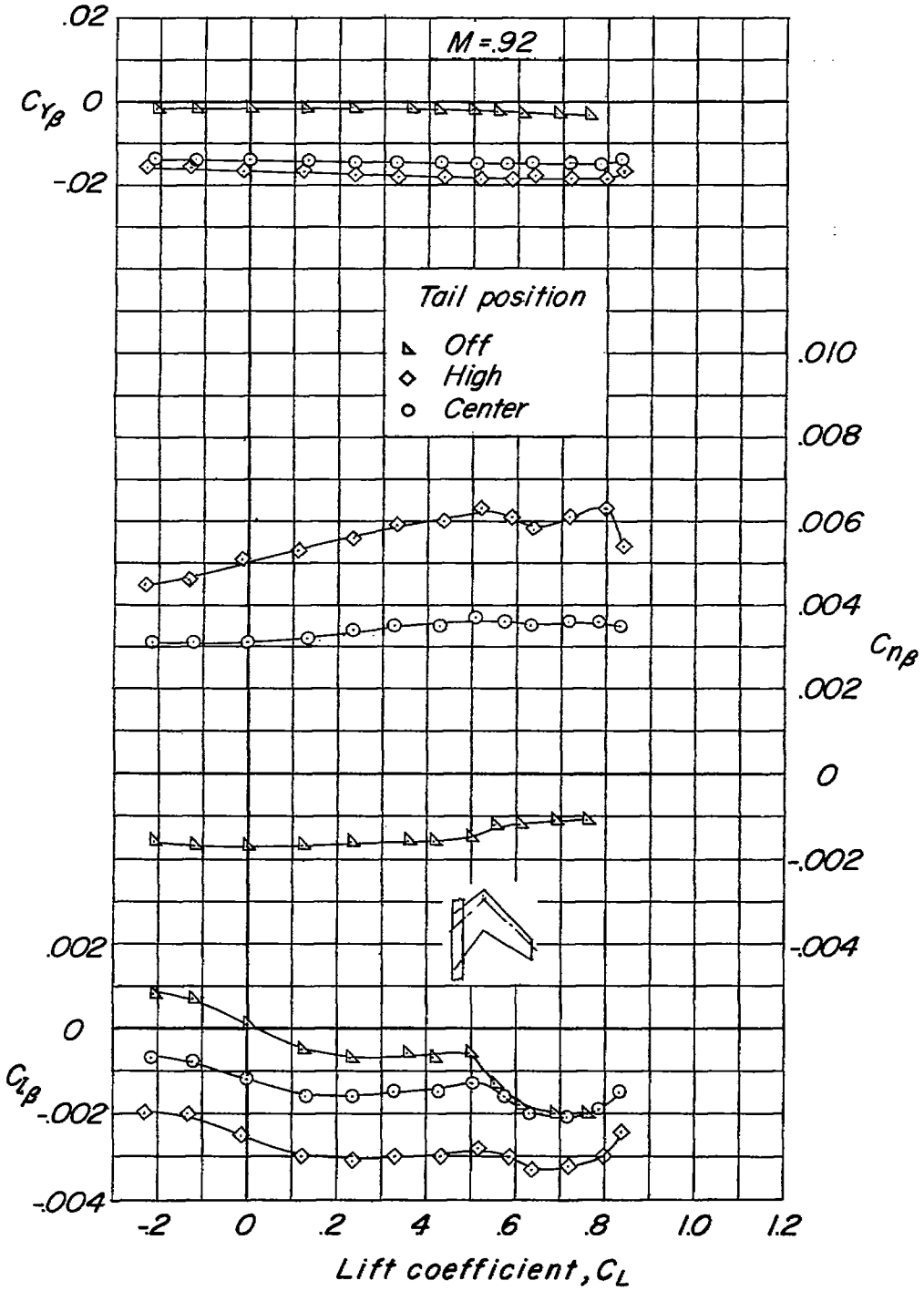

(d) M = 0.92.

Figure 16.- Concluded.

NACA-Langley - 5-14-54 - 350